University of California
Los Angeles

Measurement of ϕ Meson Production and Searches for Pentaquark Particles from the STAR Experiment at RHIC

A dissertation submitted in partial satisfaction
of the requirements for the degree
Doctor of Philosophy in Physics

by

Jingguo Ma

2006

The dissertation of Jingguo Ma is approved.

Ronald Miech

Graciela Gelmini

Charles A. Whitten Jr.

Huan Z. Huang, Committee Chair

University of California, Los Angeles

2006

To my dear mom . . .

who—passed away eight years ago,

but will always be remembered in my heart.

Table of Contents

List of Figures

List of Tables

Acknowledgments

Members of the nuclear experiment group at UCLA have provided me with an excellent research and study environment and tremendous amount of support. I benefit the most from their visions and values in both academic and daily life through out my PhD study. I would like to thank all of them for their kind help.

I feel strongly thankful to my supervisor professor Huan Z. Huang for his guidance and support in the past few years, without them it would have been impossible for me to go this far. I would like to thank professor Charles J. Whitten for his generous help. I would also like to thank Dr. Eugene Yamamoto for his help on data analysis. My many thanks also go to Dr. An Tai for the many valuable discussions we had. I would like to thank other students in the group for the joyful time we had together.

I would like to give my special thank you to my lovely wife Xiaohong Wang and other family members. Their endless love, support and encouragement have always been the most important part of my life.

Vita

1975	Born, Hunan Province, P.R. China.
1998	B.S. (Physics), Peking University, Beijing, P.R. China.
2001	M.S. (Physics), Peking University, Beijing, P.R. China.
2001–present	PhD student, University of California at Los Angeles, Los Angeles, USA.

Publications and Presentations

Jingguo Ma *et al.*
Construction and performance test of a large area RPC module.
High Energy Physics and Nuclear Physics-Chinese Edition, Vol. **25**, No. 9, 898 902, 2001

J. Ying *et al.*
Beam test results of a resistive plate chamber made of Chinese bakelites.
Nucl. Instr. Meth. In Phys. Res. **A459**, 513, 2001.

Y. Ye *et al.*
Resistive plate chambers for muon detection at LHC.
Science in China Series A, ISSN:1006-9283, Vol. **45**, No. 11, 1446-1451, 2002

Jingguo Ma

ϕ meson production in $\sqrt{s_{NN}} = 200$ GeV $Au + Au$ and $p + p$ collisions at RHIC.

J. Phys. G: Nucl. Part. Phys. **30**, S543-S547, 2004.

Jingguo Ma

Mid-rapidity ϕ meson production at $\sqrt{s_{NN}} = 200$ GeV $Au + Au$ and $p + p$ collisions from STAR.

Acta. Phys. Hung. **A21**, 179, 2004.

J. Adams *et al.* [STAR Collaboration].

Forward neutral pion production in $p + p$ and $d + Au$ collisions at $\sqrt{s_{NN}} = 200$ GeV.

nucl-ex/0602011.

J. Adams *et al.* [STAR Collaboration].

Proton - lambda correlations in central $Au + Au$ collisions at $\sqrt{s_{NN}} = 200$ GeV.

nucl-ex/0511003.

J. Adams *et al.* [STAR Collaboration].

Multiplicity and pseudorapidity distributions of charged particles and photons at forward pseudorapidity in $Au + Au$ collisions at $\sqrt{s_{NN}} = 62.4$ GeV.

Phys. Rev. **C73**, 034906, 2006, nucl-ex/0511026.

J. Adams *et al.* [STAR Collaboration].

Strangelet search at RHIC.

nucl-ex/0511047.

J. Adams *et al.* [STAR Collaboration].
Directed flow in $Au + Au$ collisions at $\sqrt{s_{_{NN}}} = 62$ GeV.
Phys. Rev. **C73**, 034903, 2006, nucl-ex/0510053.

J. Adams *et al.* [STAR Collaboration].
Transverse-momentum p_t correlations on $(\eta,\ \phi)$ from mean-p_t fluctuations in $Au - Au$ collisions at $\sqrt{s_{_{NN}}} = 200$ GeV.
nucl-ex/0509030.

J. Adams *et al.* [STAR Collaboration].
Multi-strange baryon elliptic flow in $Au + Au$ collisions at $\sqrt{s_{_{NN}}} = 200$ GeV.
Phys. Rev. Lett. **95**, 122301, 2005, nucl-ex/0504022

J. Adams *et al.* [STAR Collaboration].
Incident energy dependence of pt correlations at RHIC.
Phys. Rev. **C72**, 044902, 2005, nucl-ex/0504031.

J. Adams *et al.* [STAR Collaboration].
Multiplicity and pseudorapidity distributions of photons in $Au + Au$ collisions at $\sqrt{s_{_{NN}}} = 62.4$ GeV.
Phys. Rev. Lett. **95**, 062301, 2005, nucl-ex/0502008.

J. Adams *et al.* [STAR Collaboration].
Experimental and theoretical challenges in the search for the quark gluon plasma, The STAR Collaboration's critical assessment of the evidence from RHIC collisions.

Nucl. Phys. **A757**, 102-183, 2005, nucl-ex/0501009.

J. Adams *et al.* [STAR Collaboration].
Distributions of charged hadrons associated with high transverse momentum particles in pp and $Au + Au$ collisions at $\sqrt{s_{NN}} = 200$ GeV.
Phys. Rev. Lett. **95**, 152301, 2005, nucl-ex/0501016.

J. Adams *et al.* [STAR Collaboration].
$K^*(892)$ resonance production in $Au+Au$ and $p+p$ collisions at $\sqrt{s_{NN}} = 200$ GeV at STAR.
Phys. Rev. **C71**, 064902, 2005, nucl-ex/0412019.

J. Adams *et al.* [STAR Collaboration].
Minijet deformation and charge-independent two-particle correlations on momentum subspace (η, ϕ) in $Au - Au$ collisions at $\sqrt{s_{NN}} = 130$ GeV.
nucl-ex/0411003.

J. Adams *et al.* [STAR Collaboration].
Pion interferometry in $Au + Au$ collisions at $\sqrt{s_{NN}} = 200$ GeV.
Phys. Rev. **C71**, 044906, 2005, nucl-ex/0411036.

J. Adams *et al.* [STAR Collaboration].
Azimuthal anisotropy in $Au + Au$ collisions at $\sqrt{s_{NN}} = 200$ GeV.
nucl-ex/0409033.

J. Adams *et al.* [STAR Collaboration].
Transverse momentum correlations and minijet dissipation in $Au - Au$ collisions

at $\sqrt{s_{NN}} = 130$ GeV.
nucl-ex/0408012.

J. Adams *et al.* [STAR Collaboration].
Pseudorapidity asymmetry and centrality dependence of charged hadron spectra in $d + Au$ collisions at $\sqrt{s_{NN}} = 200$ GeV.
Phys. Rev. **C70**, 064907, 2004, nucl-ex/0408016.

J. Adams *et al.* [STAR Collaboration].
Transverse-momentum dependent modification of dynamic texture in central $Au + Au$ collisions at $\sqrt{s_{NN}} = 200$ GeV.
Phys. Rev. **C71**, 031901, 2005, nucl-ex/0407001.

J. Adams *et al.* [STAR Collaboration].
Measurements of transverse energy distributions in $Au+Au$ collisions at $\sqrt{s_{NN}} = 200$ GeV.
Phys. Rev. **C70**, 054907, 2004, nucl-ex/0407003.

J. Adams *et al.* [STAR Collaboration].
Open charm yields in $d + Au$ collisions at $\sqrt{s_{NN}} = 200$ GeV.
Phys. Rev. Lett. **94**, 062301, 2005, nucl-ex/0407006.

J. Adams *et al.* [STAR Collaboration].
Azimuthal anisotropy and correlations at large transverse momenta in $p + p$ and $Au + Au$ collisions at $\sqrt{s_{NN}} = 200$ GeV.
Phys. Rev. Lett. **93**, 252301, 2004, nucl-ex/0407007.

J. Adams *et al.* [STAR Collaboration].

ϕ meson production in $Au + Au$ and $p + p$ collisions at $\sqrt{s_{NN}} = 200$ GeV.

Phys. Lett. **B612**, 181-189, 2005, nucl-ex/0406003.

J. Adams *et al.* [STAR Collaboration].

Hadronization geometry and charge-dependent number autocorrelations on axial momentum space in $Au - Au$ collisions at $\sqrt{s_{NN}} = 130$ GeV.

Phys. Lett. **B634**, 347-355, 2006, nucl-ex/0406035.

J. Adams *et al.* [STAR Collaboration].

Production of e^+e^- pairs accompanied by nuclear dissociation in ultra-peripheral heavy ion collision.

Phys. Rev. **C70**, 031902, 2004, nucl-ex/0404012.

J. Adams *et al.* [STAR Collaboration].

Centrality and pseudorapidity dependence of charged hadron production at intermediate p_T in $Au + Au$ collisions at $\sqrt{s_{NN}} = 130$ GeV.

Phys. Rev. **C70**, 044901, 2004, nucl-ex/0404020.

J. Adams *et al.* [STAR Collaboration].

Photon and neutral pion production in $Au + Au$ collisions at $\sqrt{s_{NN}} = 130$ GeV.

Phys. Rev. **C70**, 044902, 2004, nucl-ex/0401008.

J. Adams *et al.* [STAR Collaboration].

Azimuthally sensitive HBT in $Au + Au$ collisions at $\sqrt{s_{NN}} = 200$ GeV.

Phys. Rev. Lett. **93**, 012301, 2004, nucl-ex/0312009.

J. Adams *et al.* [STAR Collaboration].

Production of charged pions and hadrons in $Au + Au$ collisions at $\sqrt{s_{NN}} =$ 130 GeV.

nucl-ex/0311017.

J. Adams *et al.* [STAR Collaboration].

Identified particle distributions in pp and $Au+Au$ collisions at $\sqrt{s_{NN}} = 200$ GeV.

Phys. Rev. Lett. **92**, 112301, 2004, nucl-ex/0310004.

J. Adams *et al.* [STAR Collaboration].

Azimuthal anisotropy at RHIC, the first and fourth harmonics.

Phys. Rev. Lett. **92**, 062301, 2004, nucl-ex/0310029.

J. Adams *et al.* [STAR Collaboration].

Cross-sections and transverse single spin asymmetries in forward neutral pion production from proton collisions at $\sqrt{s_{NN}} = 200$ GeV.

Phys. Rev. Lett. **92**, 171801, 2004, hep-ex/0310058.

J. Adams *et al.* [STAR Collaboration].

Pion, kaon, proton and anti-proton transverse momentum distributions from $p+p$ and $d + Au$ collisions at $\sqrt{s_{NN}} = 200$ GeV.

Phys. Lett. **B616**, 8-16, 2005, nucl-ex/0309012.

J. Adams *et al.* [STAR Collaboration].

Event by event $\langle p_t \rangle$ fluctuations in $Au - Au$ collisions at $\sqrt{s_{NN}} = 130$ GeV.

Phys. Rev. **C71**, 064906, 2005, nucl-ex/0308033.

J. Adams *et al.* [STAR Collaboration].

Multiplicity fluctuations in $Au + Au$ collisions at $\sqrt{s_{NN}} = 130$ GeV.

Phys. Rev. **C68**, 044905, 2003, nucl-ex/0307007.

J. Adams *et al.* [STAR Collaboration].

ρ^0 production and possible modification in $Au{+}Au$ and $p{+}p$ collisions at $\sqrt{s_{NN}} =$ 200 GeV.

Phys. Rev. Lett. **92**, 092301, 2004, nucl-ex/0307023.

J. Adams *et al.* [STAR Collaboration].

Multistrange baryon production in $Au - Au$ collisions at $\sqrt{s_{NN}} = 130$ GeV.

Phys. Rev. Lett. **92**, 182301, 2004, nucl-ex/0307024.

J. Adams *et al.* [STAR Collaboration].

Pion kaon correlations in $Au + Au$ collisions at $\sqrt{s_{NN}} = 130$ GeV.

Phys. Rev. Lett. **91**, 262302, 2003, nucl-ex/0307025.

J. Adams *et al.* [STAR Collaboration].

Particle type dependence of azimuthal anisotropy and nuclear modification of particle production in $Au + Au$ collisions at $\sqrt{s_{NN}} = 200$ GeV.

Phys. Rev. Lett. **92**, 052302, 2004, nucl-ex/0306007.

J. Adams *et al.* [STAR Collaboration].

Evidence from $d{+}Au$ measurements for final state suppression of high p_T hadrons in $Au + Au$ collisions at RHIC.

Phys. Rev. Lett. **91**, 072304, 2003, nucl-ex/0306024.

J. Adams *et al.* [STAR Collaboration].

Three pion HBT correlations in relativistic heavy ion collisions from the STAR experiment.

Phys. Rev. Lett. **91**, 262301, 2003, nucl-ex/0306028.

J. Adams *et al.* [STAR Collaboration].

Rapidity and centrality dependence of proton and anti-proton production from $^{197}Au + {}^{197}Au$ collisions at $\sqrt{s_{NN}} = 130$ GeV.

Phys. Rev. **C70**, 041901, 2004, nucl-ex/0306029.

J. Adams *et al.* [STAR Collaboration].

Transverse momentum and collision energy dependence of high p_T hadron suppression in $Au + Au$ collisions at ultrarelativistic energies.

Phys. Rev. Lett. **91**, 172302, 2003, nucl-ex/0305015.

J. Adams *et al.* [STAR Collaboration].

Narrowing of the balance function with centrality in $Au+Au$ collisions at $\sqrt{s_{NN}} = 130$ GeV.

Phys. Rev. Lett. **90**, 172301, 2003, nucl-ex/0301014.

J. Adams *et al.* [STAR Collaboration].

Strange anti-particle to particle ratios at mid-rapidity in $\sqrt{s_{NN}} = 130$ GeV $Au + Au$ collisions.

Phys. Lett. **B567**, 167-174, 2003, nucl-ex/0211024.

C. Adler *et al.* [STAR Collaboration].

Disappearance of back-to-back high p_T hadron correlations in central $Au + Au$

collisions at $\sqrt{s_{NN}} = 200$ GeV.

Phys. Rev. Lett. **90**, 082302, 2003, nucl-ex/0210033.

C. Adler *et al.* [STAR Collaboration].

Elliptic flow from two and four particle correlations in $Au + Au$ collisions at $\sqrt{s_{NN}} = 130$ GeV.

Phys. Rev. **C66**, 034904, 2002, nucl-ex/0206001.

C. Adler *et al.* [STAR Collaboration].

Coherent ρ^0 production in ultraperipheral heavy ion collisions.

Phys. Rev. Lett. **89**, 272302, 2002, nucl-ex/0206004.

C. Adler *et al.* [STAR Collaboration].

Azimuthal anisotropy and correlations in the hard scattering regime at RHIC.

Phys. Rev. Lett. **90**, 032301, 2003, nucl-ex/0206006.

C. Adler *et al.* [STAR Collaboration].

Kaon production and kaon to pion ratio in $Au{+}Au$ collisions at $\sqrt{s_{NN}} = 130$ GeV.

Phys. Lett. **B595**, 143-150, 2004, nucl-ex/0206008.

C. Adler *et al.* [STAR Collaboration].

Centrality dependence of high p_T hadron suppression in $Au + Au$ collisions at $\sqrt{s_{NN}} = 130$ GeV.

Phys. Rev. Lett. **89**, 202301, 2002, nucl-ex/0206011.

C. Adler *et al.* [STAR Collaboration].

Azimuthal anisotropy of K_S^0 and $\Lambda + \bar{\Lambda}$ production at mid-rapidity from $Au + Au$

collisions at $\sqrt{s_{NN}} = 130$ GeV.

Phys. Rev. Lett. **89**, 132301, 2002, hep-ex/0205072.

C. Adler *et al.* [STAR Collaboration].

$K^{*0}(892)$ production in relativistic heavy ion collisions at $\sqrt{s_{NN}} = 130$ GeV.

Phys. Rev. **C66**, 061901, 2002, nucl-ex/0205015.

C. Adler *et al.* [STAR Collaboration].

Midrapidity Λ and $\bar{\Lambda}$ production in $Au + Au$ collisions at $\sqrt{s_{NN}} = 130$ GeV.

Phys. Rev. Lett. **89**, 092301, 2002, nucl-ex/0203016.

Jingguo Ma

Mid-rapidity Phi meson production at 200 GeV from STAR.

The 19th Winter Workshop on Nuclear Dynamics, Breckenridge, Colorado 2003

Jingguo Ma

Phi meson production at 200 GeV from STAR

The 7th International Conference on Strangeness in Quark Matter, Atlantic Beach, North Carolina, 2003.

Jingguo Ma

Phi meson production at 200 GeV pp and $AuAu$ collisions from STAR.

The 17th International Conference on Ultra-Relativistic Nucleus-Nucleus Collisions, Oakland, California, 2004.

Jingguo Ma

Search for exotic particles with the STAR detector at RHIC.

American Physical Society April Meeting, Denver, Colorado, 2004.

Jingguo Ma

Search for Pentaquark particles at RHIC.

American Physical Society April Meeting, Tampa, Florida, 2005.

Abstract of the Dissertation

Measurement of ϕ Meson Production and Searches for Pentaquark Particles from the STAR Experiment at RHIC

by

Jingguo Ma

Doctor of Philosophy in Physics

University of California, Los Angeles, 2006

Professor Huan Z. Huang, Chair

We present results for the measurement of ϕ meson production at mid-rapidity in $\sqrt{s_{NN}} = 200$ GeV $p + p$ and $Au + Au$ collisions from the STAR experiment at RHIC, and results for searches of pentaquark particles Θ^{++}, Ξ^{--} and their corresponding anti-particles in several data sets recorded by STAR. Event mixing and topological techniques are used in these measurements.

The ϕ meson mass and width measured in this work are found to be consistent with the Particle Data Group (PDG) values. No significant modifications of these properties are found in our measurement. The measured transverse mass spectra of ϕ are found to be different in shape between $p + p$ and $Au + Au$ data. The $Au + Au$ data are well represented by a single exponential distribution while the $p + p$ data can only be represented by a double exponential distribution due to the power law tail at high p_t.

The ϕ/K^- yield ratio is found to be constant as a function of both collision energy and collision centrality. The $\langle p_t \rangle$ of ϕ is found to increase as a function

of collision energy and does not change significantly as a function of centrality in $Au+Au$ collisions at RHIC. A comparison of the measured ϕ/K^- yield ratio and of the ϕ $\langle p_t \rangle$ with model calculations exclude kaon coalescence as the dominant mechanism for ϕ production in heavy ion collisions at RHIC.

The integrated yield of ϕ meson is found to be consistent with thermal statistical model fits which assume an equilibrated partonic state has been reached. A hydrodynamic model inspired blast wave fit to the ϕ spectra indicates that the ϕ freezes out earlier than the π, K and p in heavy ion collisions at RHIC. The constant ϕ $\langle p_t \rangle$ as a function of centrality is also consistent with earlier freeze out of the ϕ than the π, K and p.

The measured R_{AA} for the ϕ is consistent with unity in the region of intermediate p_t, either due to the OZI rule suppression of ϕ production in $p+p$ collisions or the enhancement of strangeness production in $Au + Au$ collisions. On the other hand, the value of R_{CP} is found to be suppressed (< 1) and consistent with that for the K^0_S, instead of that for the Λ at intermediate p_t. The hadron production at intermediate p_t region at RHIC is determined by particle type rather than by particle mass, consistent with quark recombination/coalescence model calculations.

The measured v_2 for the ϕ in MinBias $Au+Au$ collisions indicates that significant amount of flow has been built up for the ϕ. Since the ϕ does not participate in the final hadronic interaction, this flow must have been built up in the early partonic stage.

A peak structure with significance of about 4.2 σ is observed for the $\Theta^{++} \rightarrow p + K^+$ and its anti-particle in $\sqrt{s_{_{NN}}} = 200$ GeV $d + Au$ collisions at RHIC. If confirmed as a real particle, it would be explicitly a pentaquark particle. However, only much weaker signals are seen in other collision systems. It is found that the production rate of Θ^{++} across all systems is consistent with each other and future high statistics data are needed to confirm or exclude the observed peak structure. A search for the $\Xi^{--} \rightarrow \Xi^{-} + \pi^{-}$ and its anti-particle yields null results. Future directions of study will be discussed.

CHAPTER 1

Introduction and Physics Topics

Scientists' query of the world around us is driven by the human passion for discovery. The purpose of nuclear and particle physics is to gain knowledge of the matter that has formed the universe by asking what this matter is formed of and how do these constituents interact with each other. It is believed that leptons and quarks are the building blocks of matter and that these most elemental particles interact with each by exchanging force mediators.

The main goal of relativistic heavy ion collision program is to search for a predicted new state of matter, and study the equation of state of nuclear matter at extremely high temperature and energy density. It has been suggested that in heavy ion collisions at very high energies protons and neutrons will melt, producing a system with free quarks over a large volume (much larger than the size of the nucleon), namely the Quark Gluon Plasma (QGP) [HM96]. Searching for its existence and measuring its properties will greatly enrich our knowledge about the force that has governed the formation of our Universe.

Quantum Chromodynamics (QCD) is the modern theory of the strong interaction. In this chapter we will review some important features of QCD and introduce the physics topics that will be investigated and discussed in this thesis. An outline for the subsequent chapters will be given at the end of this chapter.

1.1 Quantum Chromodynamics

The most elementary building blocks of matter are leptons and quarks, which interact among themselves by exchanging force mediators (photon, gluon. . .). QCD, the theory of strong interactions, is a $SU(3)$ gauge field theory of quarks and gluons. QCD is an analogy of the theory for electromagnetic interactions, the Quantum Electrodynamics (QED). However, unlike QED, QCD's non-Abelian character requires gluons to carry color charge and self-interact, resulting in more astonishing and fascinating phenomena in strong interactions.

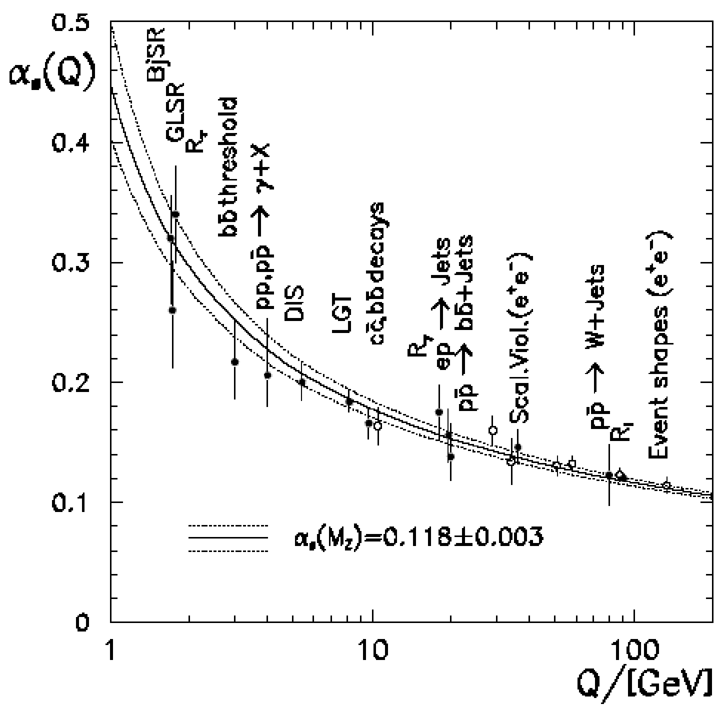

Figure 1.1: Running of the strong coupling constant established by various types of measurements at different scales, compared to the QCD prediction [Sch96].

Due to the gluon-gluon self-interaction, the effective coupling constant of strong interaction (α_s) becomes smaller at shorter distances (larger momentum transfer (Q^2)). This is known as asymptotic freedom in the strong interaction. The strong coupling constant has been experimentally measured to be a strongly varying function of distance or Q^2 of the form

$$\alpha_s(Q^2) = \frac{12\pi}{\beta_0 \ln(Q^2/\Lambda_{QCD})}, \tag{1.1}$$

where Q^2 is the momentum transfer, β_0 and Λ_{QCD} are constants. The experimentally measured strong coupling constant α_s as well as the QCD calculation are shown in figure 1.1. The figure shows that the measured value of α_s decreases monotonously with increasing momentum transfer for the interaction, consistent with the QCD calculations.

No free quarks have ever been observed in any experiment. This means that quarks are always confined in color-neutral objects (hadrons). This is known as quark/color confinement and can be explained by the running coupling constant of strong interaction. When two quarks are separated to large distance, the coupling becomes stronger, thus more and more self-coupled gluons hold the quarks together. As a result, no single quark can be extracted from a hadron and it can only exist in color neutral objects.

QCD is a precise and beautiful theory [Wil00]. However, it cannot be used to analytically calculate processes that dominate the hadronic world around us due to the non-linear nature of the strong force.

Physicists have developed Monte Carlo methods using numerical path integrals of the QCD Lagrangian on a discrete Euclidian space time grid (LQCD) to study QCD matter. Since no new parameters or field variables are introduced in this discretization, LQCD retains the fundamental characters of QCD. The only tunable input parameters in LQCD simulations are the strong coupling constant and the bare masses of quarks. LQCD has been used to provide the framework for investigation of non-perturbative phenomena in the regime of strong interaction.

There is one kind of processes that QCD can be directly used to calculate, the regime where the strong coupling constant is small (large momentum transfer). Perturbation theory can be applied in these QCD processes and physics quantities can be calculated in a power series as leading order, next-to-leading order etc (pQCD). In fact, pQCD has been proven to describe a large set of high energy, large momentum transfer processes with outstanding accuracy.

1.2 QCD phase diagram and relativistic heavy ion collisions

When the density and/or the temperature of matter gets higher and higher (like continue squeezing and heating nuclear matter), QCD predicts that eventually nucleons will not be able to hold their constituents together and quarks and gluons will be liberated from nucleons. These quarks and gluons are not limited in nucleons any more (called deconfinement), they are free to move in a much larger phase space and able to interact with multiple partons at high density. The color degree of freedom becomes the effective degree of freedom for the system, and this new state of matter is called the Quark Gluon Plasma (QGP). In QGP matter the broken chiral symmetry in normal nuclear matter may also be (partially) restored (there is speculation that this happens at a higher temperature than deconfinement) as the quark mass diminishes and the masses of scalar and vector mesons will decrease [Kar02].

At extremely high energy densities and/or temperature, QCD theory does predict a phase transition from normal nuclear matter to a new form of matter, which consists of an extended volume of interacting quarks, antiquarks, and gluons (QGP). QGP is predicted to come into existence at a critical temperature

(T_c) and/or a density approximately 10 times the normal nuclear matter.

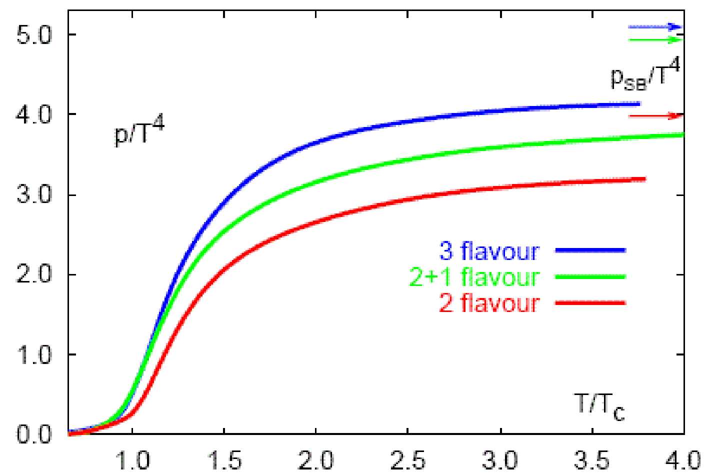

Figure 1.2: LQCD results of P/T^4 as a function of temperature showing QCD phase transition. Different lines are for several different choices of number of dynamical quark flavors. The arrows are the corresponding Stefan-Boltzmann pressures for the same quark flavor configurations.

Figure 1.2 shows one LQCD calculation [KLP00] of the nuclear matter pressure as a function of the temperature of the system. It shows that the pressure divided by T^4 (P/T^4) increases rapidly above T_c and then begins to saturate by about $2T_c$. The rapid rise of P/T^4 indicates a phase transition from hadronic matter to QGP, when the color degree of freedom takes control of the matter, resulting in a rapid rise of entropy and thus pressure. The predicted critical temperature for the phase transition is $T_c \approx 160$ MeV. The saturated values of P/T^4 are lower than that for an idea gas (Stefan-Boltzmann limit), in which quarks and gluons are non-interacting and quarks are massless. And this means that there are still substantial remaining interactions among the quarks and gluons in the QGP phase.

The evolution of a heavy ion collision with the formation of the QGP can be depicted by the following: After the two colliding nuclei pass each other, a huge amount of energy is deposited in the interaction region. A phase transition occurs and the QGP is formed if the temperature of the fireball exceeds the critical temperature T_c. Then the system immediately starts expanding and cooling down, and the temperature decreases and passes T_c again and reaching a chemical freeze out temperature T_{ch}, at which inelastic scattering ceases and relative abundance for hadron species stabilizes. When the system continues expanding and cooling, the temperature finally reaches the kinetic freeze out temperature T_{fo} where elastic scattering between hadrons ceases. The produced particles escape from the interaction region and eventually stream into detectors.

The extreme conditions needed for the formation of QGP are thought to have existed a few microseconds after the Big Bang (high temperature) and might exist in neutron stars (high density). It has been proposed that this extreme condition can be reached by smashing heavy ions together with very high energies in the laboratory. The Relativistic Heavy Ion Collider (RHIC) at the Brookhaven National Laboratory (BNL) has been built to create such conditions for the creation of the QGP in the laboratory. The primary goal at RHIC is to create the QGP in the highest-energy collisions of heavy nuclei ever achieved under laboratory conditions and to measure the properties of this new state of matter. The scrutiny of this new state of matter promises to answer some of the key questions of nuclear and particle physics.

Early results from the RHIC experiments reveal new nuclear phenomena at temperatures and densities well into the range where quarks and gluons–rather than nucleons and mesons–are expected to define the relevant degrees of freedom. The first measurements of head-on collisions at RHIC energies, with nuclei as heavy as gold, have already taken us a major step toward the long-sought quark-gluon plasma. It has been found that different regions reveal dramatically different dynamics at RHIC. In the soft sector ($p_t \lesssim 1.5$ GeV/c), soft processes dominate and the multiplicities, yield, momentum spectra and correlations of hadrons reflect the properties of the bulk, for example its initial conditions, its degree of thermalization and its equation of state. In the sector of hard processes ($p_t \gtrsim 5$ GeV/c), the interaction of energetic particles produced in initial hard scattering processes with the medium provides a unique, penetrating probes for the matter produced at RHIC. In the intermediate p_t region, where soft processes interplay with hard processes, the study of hadron production explores the hadronization processes in heavy ion collisions and provide important information of the system evolution. A comprehensive summaries of the RHIC physics results can be found in [Ada05b].

1.3 ϕ meson production in heavy ion collisions

The ϕ, a vector meson with spin = 1, is composed of a strange and an anti-strange quark and thus has hidden strangeness. Table 1.1 lists the quantum numbers, mass, full width and some of the decay modes of the ϕ meson as listed by the Particle Data Group [Eid04].

ϕ meson production has always been of great interest from elementary collisions up to heavy ion collisions. Due to its valence quark structure, ϕ meson decay and production is thought to be suppressed by the OZI rule (also known as the quark-line rule) [Oku63, Zwe64, IOS66]. For example, the ϕ decays more often to two kaons rather than three pions, although the later is more favorable in energy and phase space. The OZI rule is directly related to the asymptotic freedom of the strong interaction. In a process involving the strong interaction,

$I^G(J^{PC})$	$0^-(1^{--})$
Mass	1019.417±0.014 MeV/c^2
Full width Γ	4.458±0.032 MeV/c^2
Decay mode	Branching ratio
$\phi \rightarrow K^+ + K^-$	49.2±0.7%
$\phi \rightarrow e^+ + e^-$	(2.91±0.07)×10^{-4}
$\phi \rightarrow \mu^+ + \mu^-$	(3.7±0.5)×10^{-4}

Table 1.1: List of ϕ properties taken from the Particle Data Group (PDG).

when the initial state and final state are connected by gluons only, the gluons must carry enough energy to create a quark and anti-quark (for example $s\bar{s}$ quarks for the ϕ) pair. Asymptotic freedom tells us that the coupling constant for these gluons are small since they are relatively "energetic", especially for those gluons to produce heavier $s\bar{s}$ or even $c\bar{c}$ pairs. A small coupling constant means a small interaction magnitude, resulting in suppression for the ϕ decay and ϕ production in elementary collisions where no strangeness is available in the projectile/target.

In heavy ion collisions, ϕ meson production has been measured by several experiments from AGS up to RHIC energies. The E-802 experiment measured ϕ production from the kaon decay channel in central $Si + Au$ collisions at a beam energy of 14.6A GeV/c at the AGS [Aki96]. Their measured mass and width of the ϕ is consistent with those of free ϕ mesons, and the measured ϕ/K^- yield ratio is consistent with that in $p + p$ collisions. Another AGS experiment, the E-917 experiment, measured ϕ production from the kaon decay channel in several centrality bins in $Au + Au$ collisions at a beam energy of 11.7A GeV/c [Bac04a]. The measured ϕ meson yield per participant projectile nucleon increases strongly in central collisions in a manner similar to that observed for kaons. The yield ratio ϕ/K^- is observed to be approximately constant with collision centrality, but with large uncertainties. At the SPS, ϕ production has been measured by the NA49 experiment from the kaon decay channel [Afa00] and the NA50 experiment from the dimuon decay channel [Ale03] at a beam energy of 158A GeV/c. No mass shift or significant broadening of the ϕ peak is seen at the SPS. The ϕ/π yield ratio measured by the NA49 experiment is found to increase by a factor of 3 from inelastic $p + p$ to central $Pb + Pb$ collisions. The extracted ϕ yield from the NA50 experiment is about a factor 2-4 higher than that from the NA49 experiment, this difference has stimulated considerable interest.

If the QGP is formed in heavy ion collisions, strange quarks can be copiously produced by light quark-antiquark annihilation and gluon interactions [RM82, Raf84, KMR86]. In this system with copious strange quarks, the ϕ may be formed simply by coalescence of the strange quarks, bypassing the OZI rule, and thus the suppression of ϕ production observed in elementary collisions should not be prevalent in heavy ion collisions. There has been experimental observation of enhancement for ϕ production in $A + A$ collisions relative to $p + p$ collisions [Bac04b, Afa00, Adl02b, Ada05c]. In fact, an enhanced production of ϕ meson in heavy ion environment has been predicted to be a signal for QGP formation [Sho85]. A high statistic measurement of ϕ production at RHIC energies will address this question more precisely.

The ϕ meson is thought to have a very small cross section for interactions with non-strange hadrons [Sho85]. Whether the ϕ participates in the radial flow in heavy ion collisions as do the other ordinary hadrons has been a very interesting question. The ϕ life time is about 41 fm. This means that most of the ϕ mesons decay outside of the fireball in heavy ion collisions. So if ϕ keeps its properties in the hot medium, it will decouple earlier from the system and survive the late stage hadronic interaction, carrying more information about the early stages of heavy ion collisions and helping us understand the creation and evolution of the system [HSX98, DBB99, BD00]. If the ϕ meson does decouple earlier than normal hadrons, the ϕ will experience smaller radial flow during the expansion of the system and exhibit a different behavior comparing with the pion, kaon and proton.

Comparing to other hadrons, the ϕ meson has no feed-down from higher mass resonances, and this property makes it more appealing as a "clean" probe of heavy ion collisions. Further more, the ϕ dilepton decay channels are clean probes of the system since the decay products do not interact strongly in the hadronic stage and thus escape freely from the fireball.

On the other hand, transport models like RQMD, UrQMD and AMPT [Bas99, Ble99, Sor95, PKL02] have suggested that at low transverse momentum (p_t), the K^+K^- pair from ϕ decay is either dominantly rescattered or absorbed by the dense medium produced in heavy ion collisions. This results in a much lower ϕ yield at low p_t and a harder transverse mass ($m_t - m_\phi$) spectrum reconstructed from K^+K^- than that from dilepton channels (e^+e^- and $\mu^+\mu^-$). In these models, ϕ production from hadron scatterings includes baryon-baryon channels $BB \rightarrow \phi NN$, meson baryon channels $(\pi, \rho)B \rightarrow \phi B$ where $B \equiv N, \Delta, N^*$ and also reaction channels such as $K\Lambda \rightarrow \phi N$. The ϕ scattering with meson includes $\phi M \rightarrow (K, K^*)(K, K^*)$ and $\phi(K, K^*) \rightarrow M(K, K^*)$, where $M \equiv (\pi, \rho, \omega)$. As a consequence, these models predict the yield ratio ϕ/K^- increases with collision centrality. A comparison of the measurement with model predictions will distinguish between different production mechanisms for the ϕ.

Theoretical calculations show that possible in-medium effects of the kaon and the ϕ in nuclear matter can dramatically change the mass, decay width and decay branching ratios of ϕ meson [CV03, BGP97, Hag05, PKL02] because the ϕ meson mass is so close to the threshold for decay to two kaons. In these calculations, the ϕ meson mass decrease slightly with increasing temperature/density of the nuclear matter. The decay branching ratio and width can change dramatically at the same time. Experimentally, these effects can be measured and tested by study of the ϕ mass and width as a function of p_t and system size (centrality), and by measuring the ϕ simultaneously from both kaon and dilepton decay channels.

Nuclear modification factors (R_{AA} and R_{CP}), which are the yield ratio of $A + A$ collisions over $p + p$ collisions or central $A + A$ collisions over peripheral $A + A$ collisions normalized by number of binary collisions (N_{bin}), are used to study hadron production at RHIC. If $A+A$ collisions are the simple superposition of $p + p$ collisions, R_{AA} and R_{CP} will be 1. Any deviation from 1 would indicate nuclear effects or different hadron production mechanisms. Elliptic flow v_2, the second Fourier coefficient of the momentum distribution, has been proposed as a sensitive probe of the early stage in heavy ion collisions [Sto82, Sor99]. This anisotropy in momentum space is transferred from the initial coordinate space anisotropy by intensive interactions among constituents of the system. Thus it reflects the initial conditions of the collision and provides information of the system evolution.

It has been found that in relativistic heavy ion collisions, hadron production obeys certain scaling behaviors. For example, the STAR measurement of the nuclear modification factor (R_{CP}) and elliptic flow (v_2) of the K^0_S and Λ manifested a clear difference [Ada04d]. The measured v_2 for the K^0_S and Λ show mass hierarchy at $p_t < 1.5$ GeV/c, consistent with hydrodynamic model calculations [HKH01] under assumption that there is a common expansion in the early stage. However, at higher p_t, the measured v_2 deviate from the hydrodynamic model calculations and saturate at different values for the K_S^0 and Λ. The measured R_{CP} value is also different for the K_S^0 and Λ in the intermediate region, with the Λ R_{CP} being higher than that of the K_S^0. The proton to pion ratio at intermediate p_t measured by PHENIX experiment is also much higher than that expected from fragmentation mechanisms for hadron production [Adl03]. These observations, in disagreement with the traditional picture of hadron production, have stimulated considerable theoretical investigations.

Quark recombination/coalescence models [DH77, HY03, FMN03b, FMN03a] have been able to successfully explain the observed phenomena in the intermediate p_t region at RHIC. In quark recombination/coalescence models, hadron production proceeds via recombination of lower p_t partons instead of via fragmentation of higher p_t partons. At low p_t, the parton distribution is exponential in shape and recombination/coalescence wins over fragmentation in the intermediate p_t region. One characteristic prediction of this model is that hadron production is dominated only by number of constituent quarks of the hadron, and this manifests a meson-baryon difference as illustrated by the K_S^0 and Λ v_2 and R_{CP} measurements. Nonaka and collaborators [NFB04] studied elliptic flow v_2 for the ϕ and other multi-strange hadrons (Ξ, Ω) in the framework of recombination and fragmentation. Their study shows that measurement of the ϕ and Ω v_2 allows unambiguous distinction between parton recombination and statistical hydronization for hadron production in the intermediate p_t region. In this approach, they find that the behavior of v_2 as a function of p_t is dominated by the number of valence quarks of the respective hadron, leading to very similar values of the elliptic flow for all mesons and likewise for all baryons, nearly independent of the hadron mass, as opposed to conventional statistical hadronization in hydrodynamic calculations. The calculated v_2 for the ϕ meson is nearly identical to that of kaon above a p_t of 2 GeV/c, while at high p_t the elliptic flow is dominated by fragmentation, leading to a universal curve above 6 GeV/c for all hadrons.

The experimentally observed particle type dependence of R_{CP} and v_2 needs much more data from other hadrons to be fully established since there is a big mass difference between the K_S^0 and Λ (or π and proton). The ϕ meson plays a very important roles here due to its unique properties. The ϕ is a meson yet it is as heavy as a Λ, making it perfect for differentiating between mass or particle type (meson or baryon) ordering of the observed difference in v_2 and R_{CP} between the K_S^0 and Λ. In other words, precise measurement of ϕ meson nuclear modification factors R_{AA}, R_{CP} and elliptic flow v_2 will provide more detailed very important insights into hadron production mechanisms and the evolution of the heavy ion collisions at RHIC.

1.4 The search for pentaquark particles

Physicists have long been wondering why nature prefers hadron to be made of two or three quarks instead of four or five or even more. Quantum Chromodynamics (QCD), which is believed to be the underlying theory of strong interaction, does not exclude the existence of nonconventional multi-quark states such as $qq\bar{q}\bar{q}$, $qqqq\bar{q}$ etc. The real question is only what should be the mass and width of such states if they really exist. However, QCD is highly non-perturbative when dealing with hadron spectra, and thus most theoretical calculations rely on phenomenological models that are inspired by QCD theory, yet not precisely QCD.

In early 2003 the LEPS experiment announced the observation of a baryon resonance state with mass 1.54±0.01 GeV/c^2 and width less than 25 MeV/c^2 [Nak03]. The observed state is consistent with the five-quark state (pentaquark Θ^+) predicted by the Chiral Soliton Model [DPP97]. The claim of the discovery has motivated a lot of experimental and theoretical investigations on the possible existence of five-quark systems. More than 50 experimental papers and more than 500 theoretical/phenomenological papers have appeared since then.

Following the first claim of the pentaquark sighting, more than ten experiments [Bar03a, Ste03, Kub04, Bar03b, ADK04, Ale05, Air04, Abd04, AER05, Che04, Tro] have reported evidence supporting the existence of such a state. These experiments report the observation of a peak structure consistent with the production of the Θ^+ pentaquark particle from various interactions and energies, but all with low statistical significance. The NA49 and the H1 experiment also reported the evidence for possible heavier pentaquark states [Alt04, Akt04]. However, more experiments have reported null results in their searches of pentaquark particles [Bai04, Aub04a, Abe06, Abe04, KZZ04, Abt04, Sch04, Ant04, Lon04, Lit05, Gor04, Ste05, Pin04, Arm05, NCW04, Ada04a]. Among these experimental results, most experiments with positive evidences were reported from early 2003 to mid-2004, while experiments with negative results overwhelmed after mid-2004.

The evidence of pentaquark states has motivated a lot of debate since its birth. The experiments reporting positive results all suffer from low statistics (significance of a few σ) and inconsistency between experiments (For example, the reported values of mass span a region more than 20 MeV/c^2). On the other hand, those experiments reporting negative results usually come from very different reaction channels thus making comparisons difficult. So the fate of the pentaquark relies on dedicated high-statistics experiments. The recent repetitions [Bat06, Hic05a] of some of the previous experiments that claim positive evidence of pentaquark state yielded null results and overruled the previous observations.

After mining the old KN scattering data, no resonance structure has been seen and the Θ^+ width has been constrained to be less than a few MeV [Nus03, ASW03, HK03, CT04]. Detailed summary of the experimental situation on pentaquark searches can be found in the following references: [Hic05b, Bur05, Dan05]. Overall, the positive evidence for the existence of pentaquark particles is diminishing and the remaining positive results need to be tested.

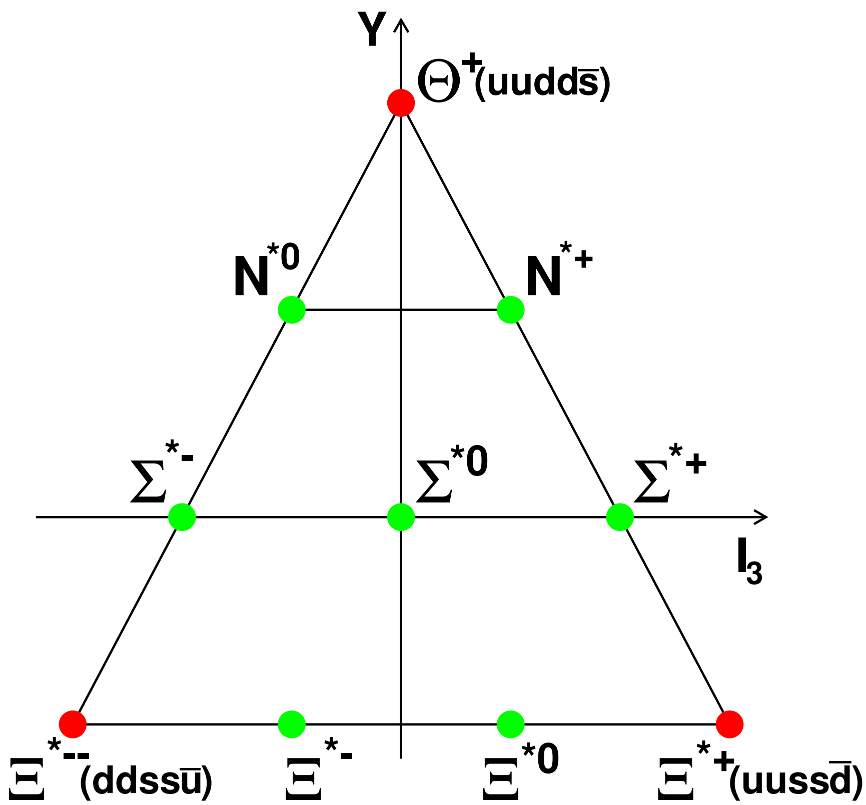

Figure 1.3: The $\overline{10}$ pentaquarks predicted by Chiral Soliton Model. x axis is the third component of isospin (I_3) while y axis is the hypercharge $Y = B + S$.

In 1997, Diakonov et al. proposed the possible existence of a $S = 1$, $J^P = \frac{1}{2}^+$ resonance (the Θ^+) at 1530 MeV with a width less than 15 MeV by using the chiral soliton model [DPP97], which partly motivated the recent experimental search of this particle. The Chiral Soliton Model is based on the Skyrme soliton (Skyrmion) model of the baryon, which utilizes a topological soliton solution in the $SU(3) \times SU(3)$ chiral symmetric nonlinear sigma model. Their model has specific $SU(3)$ breaking terms, indicated by the chiral quark model, but the strengths of the individual terms of the effective Lagrangian are determined phenomenologically [Oka04]. According to this model calculation, the Θ^+ is the lightest member of the anti-decuplet multiplet ($\overline{10}$) in the third rotational state. The anti-decuplet members are shown in figure 1.3. In this figure, the three members lie in the corner have explicit exotic quantum numbers and thus are explicit exotic particles, i.e. they can not be explained by conventional two or three quark states.

After the Chiral Soliton Model prediction by Diakonov et al. and the subsequent reported observation by various experiments, there have appeared numerous theoretical models trying to explain the low mass and narrow width of the observed Θ^+. These model calculations includes the diquark model [JW03], clustered quark model [KL03], constituent quark model [SR03], QCD sum rules [Zhu03] etc. These theoretical calculations are nicely summarized in a few papers [JM04, Zhu04, Oka04].

In the diquark model, Θ^+ is composed of two diquarks and a strange antiquark, where the diquark is a strongly correlated quark pair. In all quark models, including conventional quark model, clustered quark models and diquark model, a small decay width for the Θ^+ is hard to be accommodated, due to the fall-apart decay mode of five quark system. In this decay mode, no extra quark antiquark pair needs to be created for pentaquark to decay into a meson and a baryon since there are already four quarks and an antiquark around.

People are also trying to look for pentaquark structures in Monte-Carlo lattice

QCD simulations (see [LM05] and references therein). Similar to the experimental situation, several LQCD calculations found positive evidence for the pentaquark while others reported null results. Among those positive results, there is disagreements regarding the spin and parity of the ground state.

S. Capstick et al. [CPR03] have raised the possibility for the Θ^+ to be an isotensor ($I = 2$) state. There will be an isospin multiplet containing $\Theta^-(dddd\bar{s})$, $\Theta^0(uddd\bar{s})$, $\Theta^+(uudd\bar{s})$, $\Theta^{++}(uuud\bar{s})$ and $\Theta^{+++}(uuuu\bar{s})$ if this hypothesis is true. Of course, the Θ^+ isospin can also possibly be one thus the multiplet contains only three members $\Theta^0(uddd\bar{s})$, $\Theta^+(uudd\bar{s})$ and $\Theta^{++}(uuud\bar{s})$. Besides the Θ^+, the proposed decay channel $\Theta^{++} \rightarrow p + K^+$ is very well suited for experimental investigations since the decayed daughters are easily to be detected and identified. However, several experiments [Sch04, Aub04b, Kar04, Bar03b, Jue05, Air04] reported null results on searches of Θ^{++} through decay channel $\Theta^{++} \rightarrow p + K^+$ and concluded that the Θ^+ state should be isosinglet.

In relativistic heavy ion collisions, it has been found that the production of hadron in the intermediate p_t region can be explained nicely by quark recombination/coalescence models (see [Ada05b]). If this scenario is true and the pentaquark particles really exist, then heavy ion collisions at RHIC may be a good environment that favors the production of pentaquark particles by just combining the available copious constituent quarks together. It is therefore very important that at RHIC we perform the search for pentaquark particles to help clarify the experimental situation.

Based on its design, STAR is well suited for the search of pentaquark particles. The large acceptance and the tracking capability of the TPC have made STAR able to identify various short-living particles such as the ϕ, K^*, Λ^*, K_S^0, Λ, Ξ^- and Ω by utilizing either event mixing techniques or reconstruction of displaced decay vertices. Stable particles such as $\pi^{\pm}$, $K^{\pm}$ and $p(\bar{p})$ can be identified as well by measuring their ionization energy loss in the TPC gas.

Here we present the results for the search of $\Theta^{++} \rightarrow p + K^{+}$, its anti-particle $\bar{\Theta}^{--} \rightarrow \bar{p} + K^{-}$, and also $\Xi^{--} \rightarrow \Xi^{-} + \pi^{-}$ and its anti-particle $\bar{\Xi}^{++} \rightarrow \bar{\Xi}^{+} + \pi^{+}$ from the STAR experiment at RHIC. Charged hadrons $\pi^{\pm}K^{\pm}p\bar{p}$ are identified by their ionization energy loss in the TPC gas. The pK invariant mass is calculated to search for the $\Theta^{++} \rightarrow p + K^{+}$ signal. For the $\Xi^{--} \rightarrow \Xi^{-} + \pi^{-}$ pentaquark, the Ξ^{-} and Λ are reconstructed by finding their displaced decay vertices from the decay channel $\Xi^{-} \rightarrow \Lambda + \pi^{-}$ and $\Lambda \rightarrow p + \pi^{-}$ respectively.

From now on, we shall refer to the Θ^{++} and Ξ^{--} as implicitly including their anti-particles unless specified otherwise. It's also worth keeping in mind that the names used for pentaquarks in this thesis are for convenience only, and the names do not imply that we claim the existence of these particles.

1.5 Thesis outline

In this thesis we present the measurement of ϕ meson production as well as the results for the searches of pentaquark particles at RHIC from the STAR experiment. In chapter 2 we will briefly introduce the experimental facilities. This is followed in chapter 3 by the description of the analysis methods and by the presentation of results for the ϕ meson measurements. In chapter 4 we will present the analysis details and results for the searches of pentaquark particles from STAR. Finally, in chapter 5 we will conclude and talk about further measurements that are needed for both the ϕ and the pentaquark particles.

CHAPTER 2

Experimental Facilities

In this chapter the facilities built for the heavy ion program are briefly described. We will describe the collider complex, the STAR experiment and the main tracking device–the TPC for STAR.

2.1 RHIC collider

The Relativistic Heavy Ion Collider (RHIC) at Brookhaven National Laboratory (BNL) is a world-class scientific research facility that was built to create and investigate strongly interacting matter at energy densities unprecedented in a laboratory setting. It is the first machine that can bring heavy ions to head-on collisions. The purpose of this extraordinary new accelerator is to seek out and explore new high-energy forms of matter and thus continue the centuries-old quest to understand the nature and origins of matter at its most basic level. Hundreds of physicists from around the world use RHIC to study what the universe may have looked like in the first few moments after its creation. RHIC drives two intersecting beams of gold ions head-on, in a subatomic collision. What physicists learn from these collisions may help us understand more about why the physical world works the way it does, from the smallest subatomic particles, to the largest stars [RHI].

Figure 2.1 shows the components of RHIC complex. Some designed param-

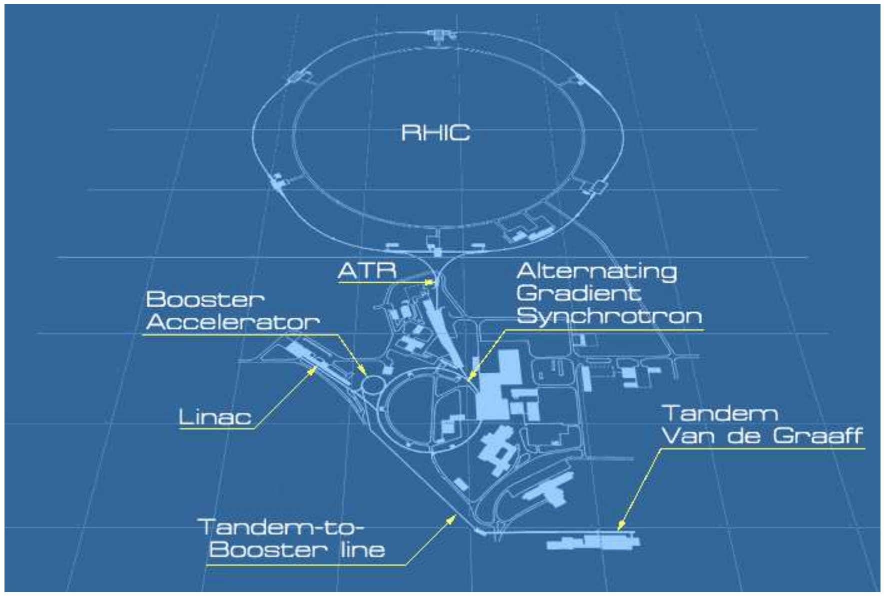

Figure 2.1: The RHIC complex.

eters of RHIC are listed in table 2.1. RHIC is designed to accelerate and clash heavy ions and also (polarized) protons. Its two counter-circulating superconducting storage rings are arbitrarily denoted as blue and yellow. The RHIC double storage ring is itself hexagonally shaped and 3834 m long in circumference, with curved edges in which stored particles are deflected by 1,740 superconducting niobium titanium magnets. The six interaction points are at the middle of the six relatively straight sections, where the two rings cross, allowing the particles to collide. The interaction points are enumerated by clock positions, with the injection point at 6 o'clock. Four interaction points are occupied by experimental detector systems, STAR at 6 o'clock, PHENIX at 8 o'clock, PHOBOS at 10 o'clock and BRAHMS at 2 o'clock, respectively. The four experimental programs complement each other with emphasis on different physics goals. Two interaction points are unused and left for further expansion.

A particle passes through several stages of boosters before it reaches the RHIC

Parameter	Value
Luminosity ($Au + Au$)	2×10^{26} cm^{-2}sec^{-1}
Luminosity ($p + p$)	4×10^{30} cm^{-2}sec^{-1}
Top beam energy (Au)	100 GeV/u
Top beam energy (proton)	250 GeV/u
# of bunches per ring	60
Revolution frequency	78 kHz
Ions per bunch (Au)	10^9
Ions per bunch (proton)	10^{11}
# of interaction points	6
Beam life time	~10 hours
Ring circumference	3833.845 m

Table 2.1: List of some design parameters for RHIC.

storage ring. The first stage for ions is the Tandem Van de Graaff accelerator, while for protons, the 200 MeV linear accelerator (Linac) is used. As an example, Au nuclei with charge $Q = -1e$ are produced by the Pulsed Sputter Ion Source. They are then accelerated by Van de Graaff and some of their electrons are knocked off by stripping foils. Au nuclei leaving the Tandem Van de Graaff have an energy of about 1 MeV per nucleon and have an approximate average electric charge $Q = +32e$ (32 electrons stripped from the Au atom). The selected $Q = +32e$ particles are then accelerated to 95 MeV per nucleon by the Booster Synchrotron. At the exit of the Booster Synchrotron the nuclei pass through another stripping foil and Au nuclei with $Q = +77e$ are selected for injection into the Alternating Gradient Synchrontron (AGS). In the AGS they finally reach 8.86 GeV per nucleon and after passing through a final stripping foil, fully stripped $Q = +79e$ Au nuclei are injected into the RHIC storage ring over the AGS-To-RHIC Transfer Line (ATR) sitting at the 6 o'clock position. In proton beam operations, protons are injected from Linac to the Booster Synchrotron and then accelerated and stored in the AGS and RHIC. In RHIC, ions reach their top energy and can be stored up to 10 hours. Since the first physics running in year 2000, RHIC has successfully run $Au + Au$ and $Cu + Cu$ collisions at several beam energies and also $d + Au$ and (polarized) $p + p$ collisions at $\sqrt{s_{NN}} = 200$ GeV.

2.2 STAR detector

The Solenoidal Tracker at RHIC (STAR) [Ack03b] shown in figure 2.2 is a composite detector system which was constructed to study the behavior of strongly interacting matter at high energy density and search for signatures of the formation of the Quark Gluon Plasma (QGP). STAR is designed to simultaneously measure many observables in an investigation of the space-time evolution for relativistic heavy ion collisions and searching for the possible phase transition in this process.

To meet its physics goals, STAR is primarily designed to measure hadron production over a very large solid angle, featuring detector systems for high precision tracking, momentum analysis and particle identification. Figure 2.2 shows a layout of the STAR detector, with cutaway showing the inner components. The whole detector is placed in a uniform magnetic field with a maximum field strength of 0.5 T. The magnetic field allows momentum analysis for charged particles by measuring the bend of their trajectories.

The Silicon Vertex Tracker (SVT) [Bel03] provides particle tracking close to the interaction region. The main tracker Time Projection Chamber (TPC) [And03]

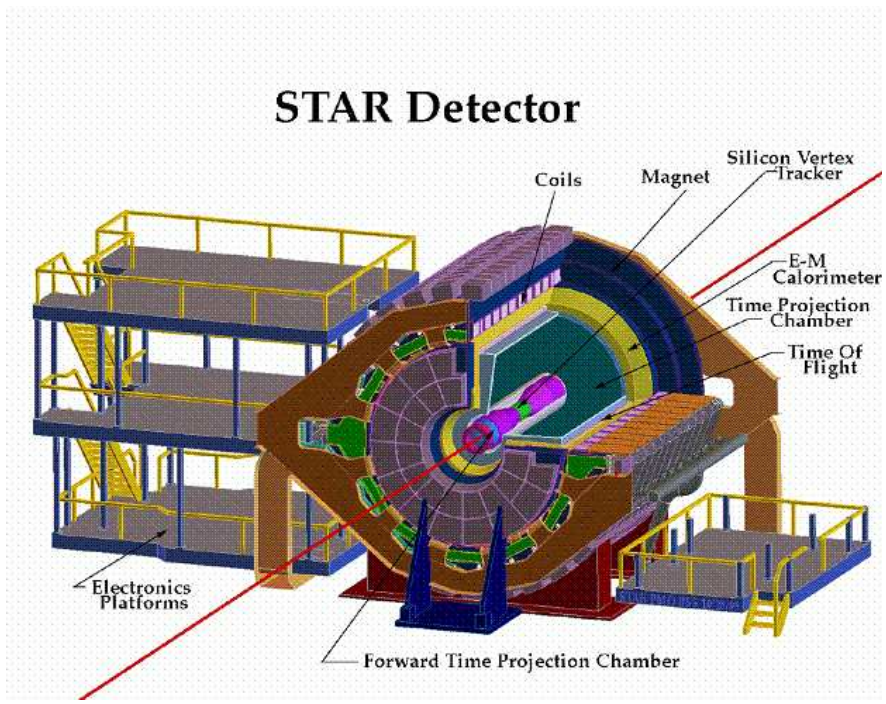

Figure 2.2: Layout of the STAR detector with cutaway showing the inner components.

is 4.2 meters long and 0.5 to 2 meters in radius. It covers a pseudo-rapidity range $\eta \leq 1.8$ for tracking with complete azimuthal coverage ($\Delta\phi = 2\pi$). A radial-drift TPC (FTPC) [Ack03a] is also installed to extend particle tracking into forward region ($2.5 < \eta < 4.0$). To extend particle identification in STAR to larger momenta , a ring imaging Cherenkov detector [Bra03] and a time-of-flight (TOF) patch are installed. The barrel and endcap Electromagnetic Calorimeters (EMC) [Bed03, All03] allow measurement of the event transverse energy, and trigger on and measure high transverse momentum photons, electrons and electromagnetically decaying hadrons.

2.2.1 DAQ and trigger

STAR has a fast data acquisition system (DAQ) [Lan03]. It receives data from various detectors having a wide range of readout rates. $Au + Au$ collision events are ~200 MB in size and are processed at input rates up to 100 Hz.

The trigger system for STAR [Bie03] is a 10 MHz pipelined system which is based on input from fast detectors to control the event selection for the much slower tracking detectors. The trigger system is functionally divided into different layers with level 0 being the fastest while level 1 and 2 are slower but they apply more sophisticated constraints on the event selection.

Fast detectors that provide input to the trigger system are a Central Trigger Barrel (CTB) at $|\eta| < 1$ and two Zero Degree Calorimeters (ZDC) located in the forward direction at $\theta < 2$ mrad, at ±18 meters from the TPC center. The ZDCs measure the total energy of neutrons which originate from the break-up of the nuclei colliding in the interaction region at the center of the STAR detector. A coincident signal of the ZDCs is the only requirement for the minimum bias $Au + Au$ trigger. The CTB provides a good estimate of number of charged particles produced in the mid-rapidity region. The central $Au + Au$ data is triggered by requiring coincidence in the ZDCs and a CTB signal which exceeds a certain predetermined threshold. For $p + p$ data taking, a coincident signal of two Beam-Beam Counters (BBCs) is required for the minimum bias trigger.

2.2.2 Time Projection Chamber

The STAR TPC shown in figure 2.3 is the main tracker for STAR. It records the tracks of particles, measures their momenta and identifies the particles by measuring their ionization energy loss (dE/dx). Particles are identified over a momentum range from 100 MeV/c to greater than 1 GeV/c and momenta are measured over a range of 100 MeV/c to 30 GeV/c. The TPC is a three dimensional tracking device with about 70 million pixels from 136,608 channels of front end electronics (FEE).

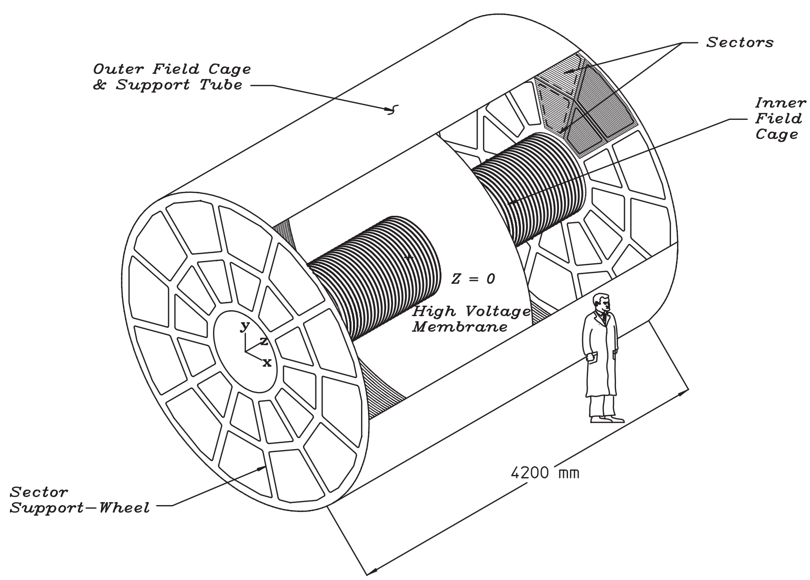

Figure 2.3: A cutaway view of the STAR TPC.

The TPC is a cylindrical large volume gaseous detector which is put in a uniform magnetic field. A uniform electric field of $\sim$ 135 V/cm is well defined by a thin conductive Central Membrane (CM) at the center of the TPC, concentric field cage cylinders and the read out end caps. The paths of primary ionizing particles passing through the gas volume are reconstructed with high precision from the released secondary electrons which drift to the readout end caps at the ends of the chamber.

The TPC uses Multi Wire Proportional Chambers (MWPC) with readout pads as the readout device. The drifting electrons avalanche in the high fields at the 20 μm anode wires providing an amplification of 1000 to 3000. The image charge produced on the pads is measured by a preamplifier/shaper/waveform digitizer system. Usually the image charge is shared by several adjacent pads, so the original track position can be reconstructed to a small fraction of a pad width.

P10 (10% methane, 90% argon) has been chosen as the working gas for the TPC. The gas pressure is maintained at 2 mbar above atmospheric pressure. The P10 gas has a fast drift velocity which peaks at a low electric field. The advantages are that operating on the peak velocity makes the drift velocity stable and insensitive to small variations in temperature and pressure. The low voltage also greatly simplifies the field cage design.

The TPC has been running stably and reliably for several years. It has produced many interesting and exciting physics results for STAR.

CHAPTER 3

Data Analysis and Results

In this chapter the methods used to select events and measure the ϕ meson production through its decay channel $\phi \rightarrow K^+K^-$ in the available data samples are presented. The event mixing technique which is used to measure ϕ meson and other resonances has been developed in the STAR experiment and many details can be found in Eugene Yamamoto's PhD thesis [Yam01].

We start this chapter by describing the data sets that are used in the analysis, followed by description of the detailed analysis procedure. We end this chapter by presenting the results from the analysis. We will describe the methods that are used to calculate the ϕ meson spectra, the elliptic flow v_2 parameter, and the vertex finding efficiency for $p+p$ events. We will present the results for the ϕ meson invariant multiplicity distribution, the calculated particle ratios, the nuclear modification factor R_{CP} and the ϕ meson v_2.

3.1 Data

The data sets used in this measurement were taken by the STAR detector in the year 2001 RHIC run for $Au + Au$ and $p + p$ collisions at $\sqrt{s_{NN}} = 200$ GeV. Information on these data sets are listed in table 3.1. At the time of writing this thesis, there has been much more data from STAR that have been used for ϕ analyses, but these new data will not be discussed here.

Data Set	Centrality Selection	Vertex Z Cut	Usable Events (M)
MinBias $Au + Au$	(0-80%)	$\|Z\| \leq 25$	2.13
Central $Au + Au$	(0-5%)	$\|Z\| \leq 25$	1.06
MinBias $p + p$	MinBias	$\|Z\| \leq 50$	6.54

Table 3.1: List of data sets used for the ϕ meson measurement. The centrality and vertex position (Z direction) selection are also listed. The number of usable events is the final number of events after these selections.

The complete data sets include minimum bias (MinBias) triggered and central triggered $Au + Au$ collision events and minimum bias triggered $p + p$ collision events, all at $\sqrt{s_{NN}} = 200$ GeV. The MinBias trigger for $Au + Au$ collisions requires a coincidence between the two ZDCs and the central trigger for the $Au + Au$ additionally requires a high energy deposition in the CTB, while the MinBias trigger for $p+p$ collisions requires a coincidence between the two BBCs. Note that this $p + p$ trigger configuration only triggers Non-Singly Diffractive (NSD) $p+p$ events at RHIC so what we are measuring is actually ϕ yield in NSD $p + p$ collisions.

An online cut on the vertex Z is set to only record events around the center of the TPC when the detector is taking data. A cut on the vertex Z is applied to avoid bias of this online vertex cut and also to select events around the center of the TPC.

The centrality of $Au + Au$ collisions is defined by slicing the uncorrected number of charged hadron (N_{ch}) distribution into several bins, where each bin corresponds to a certain fraction of the total inelastic cross section. Figure 3.1 shows the uncorrected charged hadron distributions in both $Au + Au$ and $p + p$ collisions. The $Au + Au$ data are divided into 9 centrality bins from the most

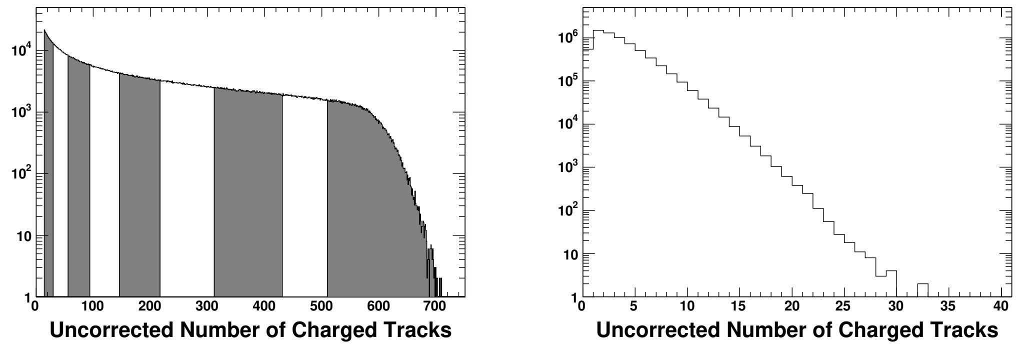

Figure 3.1: Left plot: Distribution of uncorrected number of charged tracks (N_{ch}) within $|\eta| < 0.5$ in 200 GeV $Au + Au$ collisions. The distribution is sliced into 9 centrality bins according to the fraction to the total inelastic cross section as indicated in the plot. Right plot: N_{ch} distribution within $|\eta| < 0.5$ in 200 GeV $p + p$ collisions. The $p + p$ data are divided into two multiplicity bins for study of multiplicity dependence.

central bin toward the most peripheral bin (from right to left in the left plot of figure 3.1): 0-5%, 5-10%, 10-20%, 20-30%, 30-40%, 40-50%, 50-60%, 60-70% and 70-80%. The 80-100% most peripheral bin is not used in the analysis due to quickly decreasing vertex finding efficiency and triggering efficiency when the multiplicity is low.

For the analysis of the ϕ meson, several centrality bins are combined together to increase statistics in each bin. These centrality bins used are 0-10%, 10-30%, 30-50% and 50-80%. To avoid trigger bias from the cut on CTB energy deposition, only events in the top 0-5% centrality bin are used for the central triggered $Au + Au$ data.

The $p+p$ data are divided into two multiplicity bins to study the multiplicity dependence of ϕ meson production. The low multiplicity bin is defined as $N_{ch} <$

5 and the high multiplicity bin is defined as $N_{ch} \geq 5$. The final numbers of events which passed all event selection criteria are listed in the final column of table 3.1.

3.2 Analysis

3.2.1 Applied cuts

For the reconstruction of the ϕ meson, we need to identify the two decay daughters K^+ and K^-. Besides the cuts used to select events, there are several track cuts applied to ensure the selection of desired and good tracks. Table 3.2 lists the applied cuts used in the data analysis. Since the ϕ meson has a decay distance of only 41 fm, the decay kaons should originate from the collision vertex, thus only primary tracks (tracks which have a distance of closest approach (dca) to the collision vertex less than 3 cm) are used for the ϕ meson analysis.

Applied Cuts for ϕ	
Primary Track	Yes
Track Fitting Flag	flag > 0
Track Number of Fit Points	nFit ≥ 15
Track Fit Points to Maximum Points Ratio	nFit / nMax > 0.55
Track Pseudo-Rapidity	$\|\eta\| < 1.0$
Track Momentum	0.1 GeV/c $\leq p \leq$ 4.0 GeV/c
Track Transverse Momentum	0.1 GeV/c $\leq p_t \leq$ 4.0 GeV/c
Track PID by dE/dx	$-2.0 < n\sigma_{kaon} < 2.0$
Track Pair δ–$DipAngle$	δ–$DipAngle > 0.04$ Radian

Table 3.2: List of cuts used for the ϕ meson measurement.

Some track quality cuts are applied to ensure that we get the good tracks.

The flag of a track is used to record the status of the track fitting at the stage of track reconstruction. It is required to be greater than 0 to avoid tracks with bad fitting. Number of fit points of the track is required to be nFit $\geq$ 15 and nFit / nMax $>$ 0.55 to reject short tracks and splitting tracks. The pseudo-rapidity (η) of the track is required to be within $|\eta| < 1.0$ to make sure selected tracks are well within the TPC acceptance. Both the momentum (p) and transverse momentum (p_t) are required to be within [0.1 GeV/c, 4.0 GeV/c]. Tracks with $p_t < 0.1$ GeV/c are usually very short and not usable, while the high momentum cut is used to reduce combinatorial background.

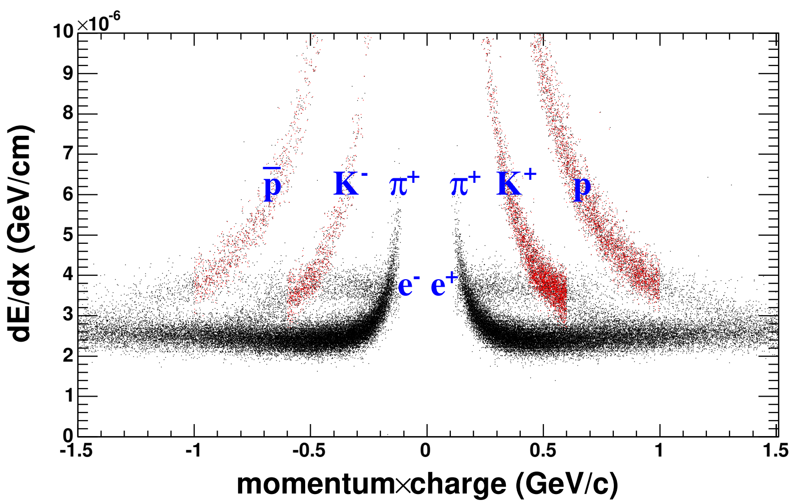

Figure 3.2: The mean ionization energy loss ($\langle dE/dx \rangle$) (in GeV/cm) of charged track in the TPC gas vs. rigidity ($p \times charge$) of the track. Black points are for all of the charged tracks and red points are for the selected kaons and protons.

Charged tracks in the TPC are identified by their ionization energy loss dE/dx in the TPC gas. The energy loss is calculated at each hit point and the mean is calculated after truncating the highest 30%. Figure 3.2 shows the mean ionization energy loss ($\langle dE/dx \rangle$) of charged tracks measured by the TPC vs. the rigidity of the track. Different bands correspond to different particle species as indicated by names in the figure. The electron/positron band crosses with the pion bands, kaon bands and proton bands in different p_t regions. Through the $\langle dE/dx \rangle$ measurement, kaons and pions can be separated by the TPC up to a momentum of about 0.6 GeV/c; And protons can be separated from kaons and pions up to a momentum of about 1.1 GeV/c. The red dots in the figure are kaon and proton (anti-proton) bands in certain momentum range by a 2 σ cut on $\langle dE/dx \rangle$ for kaons and protons respectively. For the ϕ meson analysis, a cut $-2.0 < n\sigma_{kaon} < 2.0$ is applied to select the kaon sample. As we can see from the figure, the kaon sample is contaminated by electrons around $p = 0.5$ GeV/c, pions at $p \gtrapprox 0.6$ GeV/c and protons at $p \gtrapprox 1.0$ GeV/c.

Due to the electron contamination in the kaon sample, the K^+K^- pair we used to calculate the ϕ meson invariant mass may be actually an e^+e^- pair. This brings the e^+e^- pairs from photon conversion in the materials of the detector into our data. The result is that a huge photon conversion peak, which may affect the extraction of ϕ meson yield, appears near the threshold of two kaons' invariant mass. It is therefor necessary to eliminate or at least reduce the contamination from photon conversion.

Fortunately, the e^+ and e^- from photon conversion are found to have a small δ–$DipAngle$ distribution, so a δ–$DipAngle > 0.04$ radian cut is applied to remove contamination from photon conversion. A layout of $\delta-DipAngle$ between two tracks is shown in figure 3.3 and defined by

$$\delta\text{–}DipAngle = \arccos(\frac{p_{t1}p_{t2} + p_{z1}p_{z2}}{p_1 p_2}). \tag{3.1}$$

Most of the contamination from photon conversion can be removed by applying this cut. The effect of this $\delta-DipAngle$ cut on the ϕ meson reconstruction efficiency is found to be small, lowerring the efficiency by $< 5\%$ at $p_t < 1.0$ GeV/c

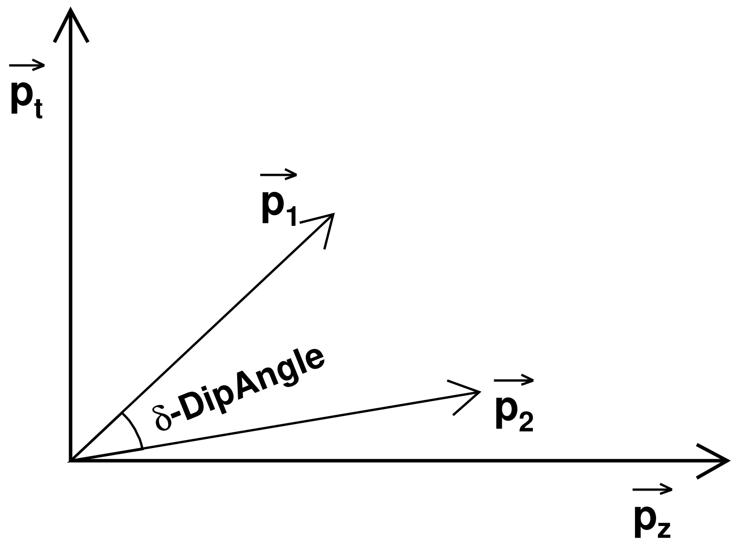

Figure 3.3: δ–*DipAngle* between two tracks.

and $\sim$ 10% at $p_t > 2.0$ GeV/c.

3.2.2 ϕ meson signal building and yield extraction

After selecting the K^+ and K^- samples, the ϕ meson invariant mass (m_{inv}) is calculated for every permutation of K^+K^- pair and accumulated in each transverse momentum, rapidity and invariant mass ((p_t, y, m_{inv})) bin (same event). The resulting invariant mass distribution consists of a ϕ meson peak on top of a combinatorial background. For the calculation of the background, the event mixing technique as described in [Yam01, DFN84, LH94] is used. To get the best description of the background shape, the two events to mix with each other should have similar geometric shape, i.e. similar track number, similar track space and momentum distributions etc. In our data analysis, the two events that mix with each other is required to have a similar vertex position (they belong to the same vertex Z bin, each bin is 10 cm wide for $p+p$ events and 5 cm wide for $Au + Au$ events) and charged hadron multiplicity to make sure the two events have similar geometric shape. To increase statistics for the mixed event and at the same time lower the memory consumption of computing, each event is mixed with 10 other events for $p + p$ data and 4 other events for $Au + Au$ data. The resulting invariant mass distribution from both same event and mixed event in the measured p_t range 0.4 GeV/c $< p_t <$ 4.0 GeV/c and rapidity range $|y| < 0.5$ are shown in figure 3.4 and 3.5.

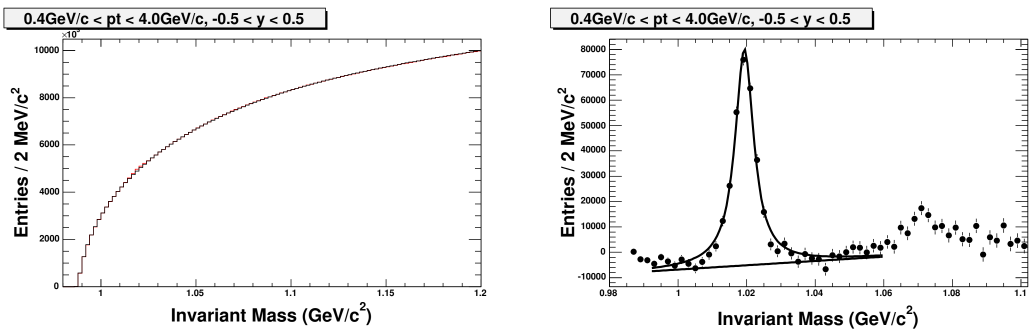

Figure 3.4: ϕ meson invariant mass distribution from MinBias $Au+Au$ collisions at 200 GeV. Left plot: Red histogram represents the invariant mass distribution from same event while the black histogram is from mixed event. The two distributions almost overlap with each other. The ϕ meson peak is not visible from the same event invariant mass distribution without background substraction. Right plot: ϕ meson invariant mass distribution after background subtraction from event mixing. The fit to the invariant mass is a Breit-Wigner function for the ϕ peak plus a linear function for the residual background.

The red histograms in the left plots of figure 3.4 and 3.5 are the same event invariant mass distribution while the black histograms are the background distribution calculated by event mixing. We can see from the left plot of figure 3.4 that the event mixing background matches the same event distribution well. The

ϕ meson peak is not visible due to the overwhelming combinatorial background. However, for the invariant mass distribution in $p+p$ collisions from the left plot of figure 3.5, we can clearly see a peak for the ϕ meson at $m \sim 1.019$ GeV/c^2 from the same event. There are also excesses over the event mixing background at $m > 1.06$ GeV/c^2 which are mainly due to the contaminations from other particles. For example, from the study of simulation the invariant masses of $K_S^0 \rightarrow \pi^+\pi^-$ and $\Lambda \rightarrow p+\pi^-$ will show up in this region when the pion daughters are misidentified as kaons, as shown in both $Au + Au$ and $p + p$ data.

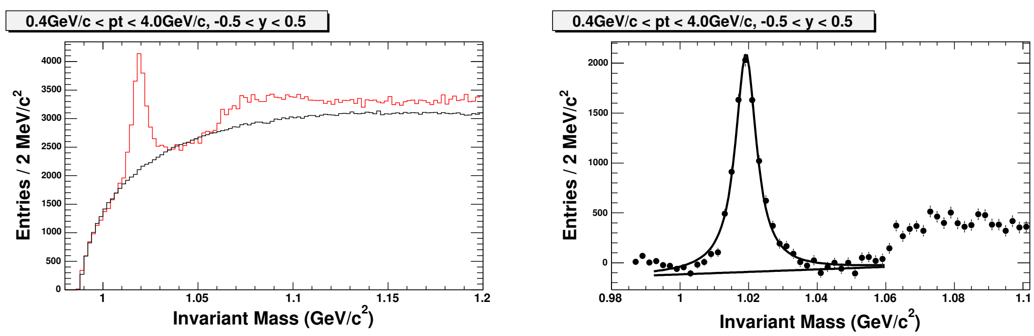

Figure 3.5: ϕ meson invariant mass distribution from $p+p$ collisions at 200 GeV. Left plot: Red histogram represents the invariant mass distribution from same event while black histogram is from mixed event. The large peak at invariant mass around 1.019 GeV/c^2 is the ϕ meson peak, while the excesses at invariant mass greater than 1.06 GeV/c^2 are mainly from particle misidentification. Right plot: ϕ meson invariant mass distribution after background subtraction from event mixing. The fit to the peak is a Breit-Wigner plus a linear function.

The event mixing background is normalized to the same event distribution in the mass region 1.04 GeV/c^2 $< m_{inv} <$ 1.06 GeV/c^2, and then subtracted from the same event distribution. The results are presented in the two right plots of figure 3.4 and 3.5. The fit to the peak is a Breit-Wigner plus a linear background function:

$$
\begin{aligned}
&\frac{n}{1000}\frac{1}{2\pi}\frac{Y\Gamma}{(m_{inv}-m_0)^2+\Gamma^2/4}+B \\
&n = \text{Invariant mass bin width in unit of MeV/c}^2 \\
&m_{inv} = \text{Mass peak position in GeV/c}^2 \\
&Y = \text{Resonance raw count} \\
&\Gamma = \text{Full width half maximum (FWHM) in GeV/c}^2 \\
&m_0 = \text{Resonance mass in GeV/c}^2 \\
&B = p_1 m_{inv} + p_0, \text{background function}
\end{aligned} \tag{3.2}
$$

The fit parameters from 200 GeV $p+p$ and $Au+Au$ collisions are listed in table 3.3. The measured mass and width are consistent with that from the embedding study, thus consistent with the values in PDG for the ϕ.

	$Au+Au$	$p+p$
mass (GeV/c^2)	1.0193± 0.0001	1.0192± 0.0001
FWHM (MeV/c^2)	6.8± 0.3	7.2± 0.3

Table 3.3: Extracted mass and width of the ϕ meson from a Breit-Wigner plus a linear function fit to the invariant mass distribution in $p+p$ and $Au+Au$ collisions. Errors are statistical only.

The ϕ meson raw yield is extracted in each p_t and rapidity bin by fitting the invariant mass distributions. The extracted raw yield is then corrected by acceptance and tracking efficiency to calculate the invariant multiplicity distribution as a function of transverse mass and rapidity.

3.2.3 Acceptance and tracking efficiency correction

The acceptance and tracking efficiency are studied by embedding techniques. Simulated ϕ mesons with flat p_t and rapidity distribution (input ϕ mesons) are generated and then allowed to decay in the GEANT program. Input ϕ mesons are called Monte-Carlo ϕ mesons if both of the decayed kaons leave a Monte-Carlo track in the TPC. Simulated responses of GEANT for the generated ϕ are embedded into raw real events and then go through the track and event reconstruction software as used for real data production.

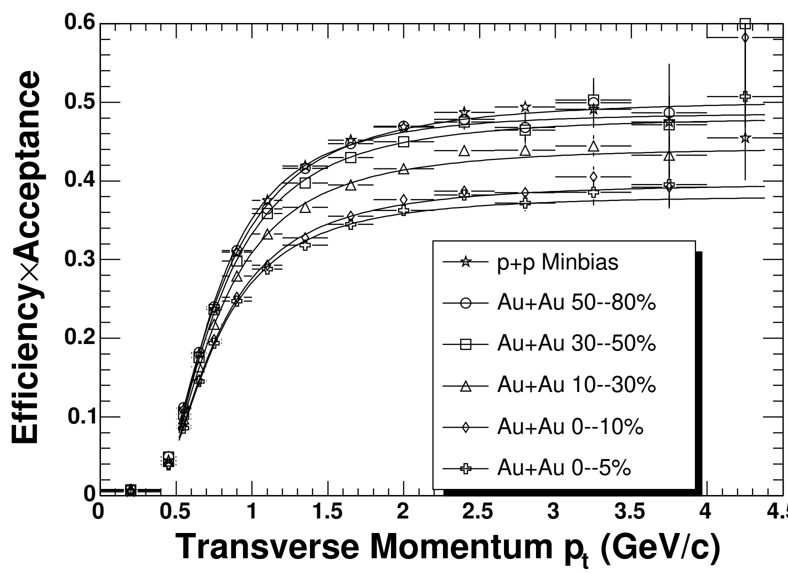

Figure 3.6: The total correction factor (Detector acceptance × tracking efficiency) for the ϕ meson in p+p and different centralities of Au+Au collisions as calculated by embedding technique.

Reconstructed ϕ mesons are counted if both decay daughters (K^+K^-) are reconstructed tracks after all cuts used in the real data analysis are applied. Detector acceptance is calculated by dividing the number of Monte-Carlo ϕ mesons by the number of input ϕ mesons, while the tracking efficiency is calculated by dividing the number of reconstructed ϕ mesons by the number of Monte-Carlo ϕ mesons. The total correction factor is calculated as the product of these two.

Figure 3.6 shows the correction factor for the ϕ meson as a function of p_t in $p+p$ collisions and in 5 centrality bins of $Au+Au$ collisions. The correction factor rises quickly from about 5% at 0.5 GeV/c to about 40% at 2.0 GeV/c, and stays almost flat up to 4.5 GeV/c. The correction factor in $p+p$ collisions is similar to that of peripheral $Au+Au$ collisions, and decreases from $p+p$ and peripheral $Au+Au$ to central $Au+Au$ collisions due to increasing occupancy in the TPC.

3.2.4 Vertex finding efficiency for $p+p$

The collision vertex finding efficiency drops quickly for low multiplicity events. If the vertex of an event is not reconstructed (called lost event) or reconstructed at a wrong place (called fake event), the ϕ meson will not be reconstructed. Those lost events will not be counted in the final number of events either. Since for $p+p$ collisions at 200 GeV, the mean number of charged hadrons at mid-rapidity is only $dN/d\eta \sim 2.65$, it is therefore necessary to study the vertex finding efficiency and make the necessary corrections to get accurate measurement of ϕ meson spectra in $p+p$ collisions. If the vertex finding inefficiency affects the ϕ spectra shape, correction as a function of p_t will be needed. Only a normalization factor needs to be applied if the vertex finding inefficiency does not affect the spectra shape.

There are two kinds of vertex finding inefficiencies as listed below.

1. Lost events. Events that have no vertex reconstructed.

2. Fake events. Events that have the vertex reconstructed at the wrong place, $|V_Z^{reconstructed} - V_Z^{real}| > 2.0$ cm.

By embedding Hijing $p+p$ events into abort-gap events (events that are triggered by the time of beam bucket), we are able to study these vertex finding inefficiencies. Figure 3.7 shows the vertex reconstruction efficiency (left plot) and the fraction of fake events (right plot) as a function of the number of good global tracks, where good global tracks are defined in table 3.4.

Criteria for good global tracks
flag > 0
nFit ≥ 15

Table 3.4: Criteria for good global tracks.

We can see that the vertex finding efficiency increases quickly at low number of good global tracks and nearly saturates at 1 when number of good global tracks is greater than 5. The fraction of fake events drops very quickly when number of good global tracks increases. The total fraction of lost events is 14.35% and the fraction of fake events is 9.32% of the total Hijing events respectively.

To study the possible effects of vertex finding inefficiencies on the measured ϕ spectra, we also need to look at these inefficiencies for events with at least one ϕ decaying to two kaons. The vertex inefficiencies may be very different for these events with ϕ. To get the vertex finding efficiency correction for resonances such as the ϕ meson, we need to study the number of lost ϕ mesons due to vertex finding inefficiencies.

Figure 3.8 shows the number of produced ϕ mesons as a function of number of good global tracks in Hijing $p+p$ events. We can see that most ϕ are produced in events that have number of good global tracks greater than 5. This means

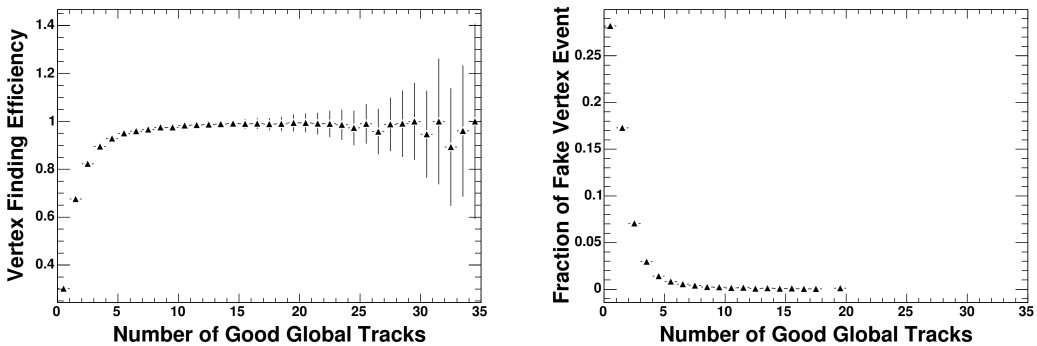

Figure 3.7: Left plot: Vertex reconstruction efficiency as a function of number of good global tracks for Hijing $p+p$ events embedded into abort-gap events. Right plot: Fraction of events with a fake vertex to the total simulated Hijing events as a function of number of good global tracks in the same $p+p$ data.

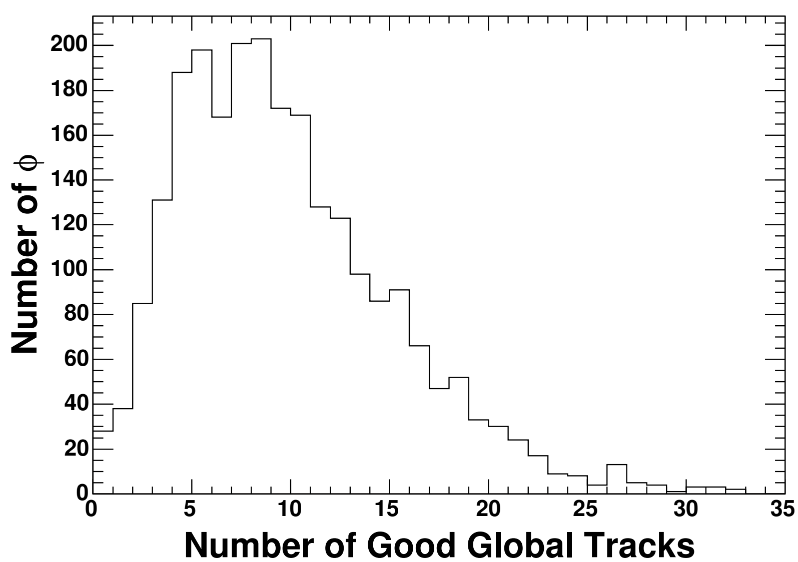

Figure 3.8: Number of produced ϕ meson as a function of number of good global tracks in Hijing $p+p$ events.

the number of lost ϕ due to vertex inefficiencies is small since the vertex finding efficiency is very high and the fraction of fake events is very low for events that have a number of good global tracks greater than 5. By requiring Hijing events to have at least one ϕ decaying to kaons at mid-rapidity (satisfy criteria listed in table 3.5), it is calculated that the vertex finding efficiency is 98.8% and the fraction of fake events is 2.59%. The conclusion is that the lost of ϕ due to vertex finding inefficiencies is very small and thus negligible. Only the total number of events due to lost events (14.35%) needs to be corrected, that is, the number of events used to calculate the spectra needs to be scaled by $1/(1-0.1435)$.

Hijing events with ϕ
At least one ϕ in $\lvert y \rvert$ <0.5
Daughter track K^+K^- flag > 0
Daughter track K^+K^- $\lvert\eta\rvert < 1.0$
Daughter track K^+K^- nFit ≥ 15
Daughter track K^+K^- nFit / nMax > 0.55

Table 3.5: Definition of Hijing events with ϕ.

3.2.5 Nuclear modification factors

Nuclear modification factors are defined by

$$R_{AA}(p_t) = \frac{[(d^2N/dp_t)/N_{bin}]^{AA}}{[(\sigma_{NSD}/\sigma_{inel})d^2N/dp_t]^{NN}} \tag{3.3}$$

and

$$R_{CP}(p_t) = \frac{[(d^2N/dp_t)/N_{bin}]^{Central}}{[(d^2N/dp_t)/N_{bin}]^{Peripheral}}, \tag{3.4}$$

where R_{AA} is the yield ratio of $A+A$ collisions to inelastic $N+N$ collisions and R_{CP} is the yield ratio of central $A+A$ collisions to peripheral $A+A$ collisions, both normalized by number of equivalent nucleon-nucleon collisions (N_{bin}). N_{bin} in the formula is derived from a Monte-Carlo Glauber model calculation [Adl02a]. The total inelastic cross section for $p+p$ collisions at 200 GeV used here is $\sigma_{inel}^{NN} = 42$ mb. However, the STAR only measures $p+p$ Non-Singly Diffractive (NSD) cross section which is $\sigma_{NSD}^{NN} = 30.0 \pm 3.5$ mb. So the ratio $\sigma_{NSD}^{NN}/\sigma_{inel}^{NN}$ is used to scale our measured yield in NSD $p+p$ collisions to inelastic $p+p$ collisions. This is reasonable since singly diffractive interactions contribute predominantly to low p_t part, thus its impact on our measured ϕ yield is negligible and the only correction needed is the overall normalization of the total cross section.

3.2.6 Elliptic flow v_2 measurement

In this section we present the method used to measure the anisotropic flow parameter v_2 of the ϕ meson. We employ the standard reaction plane method as described by Poskanzer and Voloshin [PV98] using a Fourier expansion to describe particle emission with respect to the reaction plane angle

$$E\frac{d^3N}{d^3p} = \frac{1}{2\pi}\frac{d^2N}{p_t dp_t dy}\left(1 + \sum_{n=1}^{\infty} 2v_n \cos[n(\varphi - \Psi_r)]\right), \tag{3.5}$$

where Ψ_r is the real reaction plane angle and φ is the ϕ meson azimuthal angle. The coefficient in the second order term of the expansion is the dominant part called the anisotropic flow parameter v_2.

The real reaction plane angle Ψ_r is not known, but it can be estimated experimentally. The estimated event plane angle from the second order harmonic (Ψ_2) is used, which has a finite resolution due to limited number of particles available for the estimation. The reaction plane resolution is estimated by dividing the whole event into two sub-events and it is used to correct the observed v_2^{obs} to get the final determination of v_2 for the ϕ meson.

Applied Cuts	
Primary Track	Yes
Track Fitting Flag	flag > 0
Track Number of Fit Points	nFit $\geq$ 15
Track Fit Points to Maximum Points Ratio	nFit / nMax > 0.55
Track Pseudo-Rapidity	$\|\eta\| < 1.0$
Track Momentum	p >0.1 GeV/c
Track Transverse Momentum	p_t >0.1 GeV/c

Table 3.6: List of cuts for reaction plane angle calculation.

Selected tracks (cuts are shown in table 3.6) are used to calculated the two components (X_n and Y_n) of the flow vector Q_2 and the reaction plane angle Ψ_2 by the following equations

$$\begin{aligned} X_2 &= Q_2 \cos(2\Psi_2) = \sum_i [w_i \cos(2\varphi_i)] \\ Y_2 &= Q_2 \sin(2\Psi_2) = \sum_i [w_i \sin(2\varphi_i)] \\ \Psi_2 &= \left(\arctan \frac{Y_2}{X_2} \right) /2. \end{aligned} \tag{3.6}$$

The weight used here includes both p_t-weight and φ-weight. The p_t-weight is taken to be p_t up to 2.0 GeV/c and constant above that. φ-weight is taken to be the reciprocal of all selected tracks' φ distribution. In order to make φ-weight represents different run conditions and gets enough statistics at the same time, some runs are combined together to calculate the φ-weight. The whole event is randomly divided into two sub-events a and b with equal multiplicity to calculate the reaction plane resolution. The event plane resolution is calculated by

$$\langle \cos[2(\Psi_2 - \Psi_r)] \rangle = \sqrt{2} \sqrt{\langle \cos[2(\Psi_2^a - \Psi_2^b)] \rangle}, \tag{3.7}$$

where Ψ_2^a and Ψ_2^b are the event plane angles of the two sub-events respectively. For the MinBias 0-80% $Au+Au$ data, the calculated reaction plane resolution is 0.69.

It has been found that strong auto-correlations exist when tracks used to calculate ϕ invariant mass are also used to calculate the reaction plane angle. These auto-correlations are eliminated by excluding those tracks that are used for the ϕ invariant mass calculation from the reaction plane angle estimation.

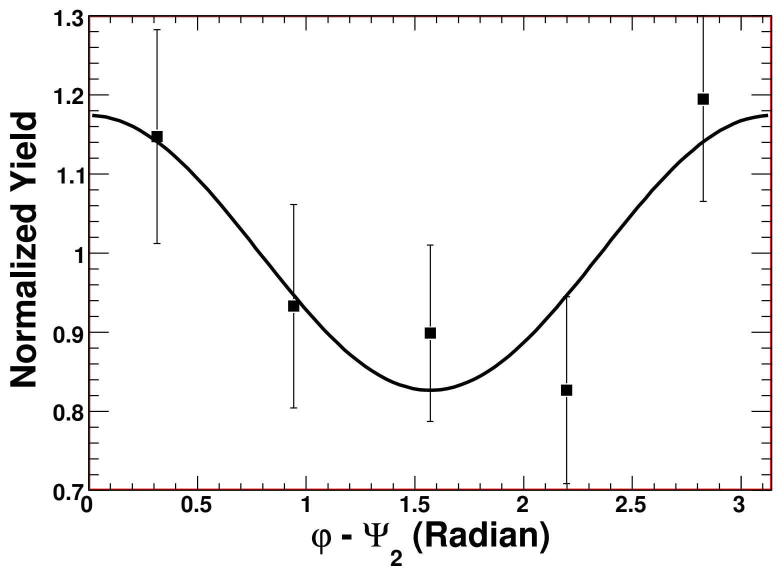

Figure 3.9: Normalized ϕ meson yield distribution as a function of $\varphi - \Psi_2$. $\varphi - \Psi_2$ represents the azimuthal angle of ϕ meson with respect to the azimuthal angle of the estimated reaction plane. A function is used to fit the data points and extract the v_2^{obs} parameter.

In order to calculate the observed v_2^{obs}, the ϕ meson yield is extracted in each $(p_t, \varphi - \Psi_2)$ bin. The extracted yield distribution as a function of $\varphi - \Psi_2$ is then fitted by function

$$A[1 + 2v_2^{obs} \cos 2(\varphi - \Psi_2)], \tag{3.8}$$

where A is a constant, to extract the v_2^{obs} value as shown in figure 3.9.

The yield in the figure is normalized by the mean yield in each $\varphi - \Psi_2$ bin to make the data points reside around 1. The extracted v_2^{obs} is divided by the reaction plane resolution to get the final v_2 of the ϕ meson.

From simulation studies, it has been found that due to limited number of $\varphi - \Psi_2$ bins (only 5 bins for the ϕ meson) and limited statistics in each bin, the measured v_2 is usually about 7% lower than real v_2. The limited statistics in each bin also introduces extra systematical uncertainty for the measured v_2, especially in the low p_t region where it can be the dominant component of the total uncertainties.

3.3 Results and discussions

3.3.1 Mass and width

It has been proposed to search for a signature of (partial) chiral symmetry restoration and/or in-medium effects by looking for possible modification of the ϕ meson mass and width in heavy ion collision.

A comparison of the measured width after de-convolution of detector resolution with the PDG value in 130 GeV $Au + Au$ collisions has been discussed in detail in Section 6.1 of Yamamoto's PhD thesis [Yam01]. No obvious broadening of the ϕ meson width was observed. The situation is similar in 200 GeV $Au + Au$ and $p + p$ collisions and thus will not be discussed here.

Figure 3.10 shows the ϕ meson mass measured from real data (filled circles) and from embedding (filled triangles) as a function of p_t. The lines in the plots indicate the ϕ mass value from the PDG. The left plot is from $p+p$ data while the right plot is from top 5% central $Au+Au$ data. It is seen that the measured ϕ mass

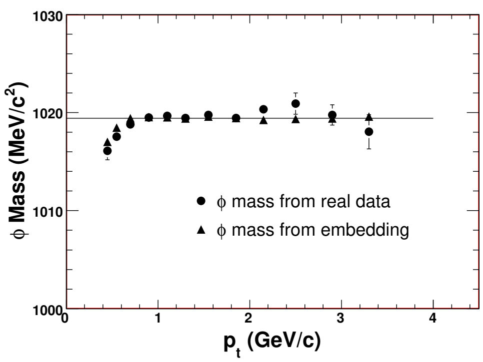

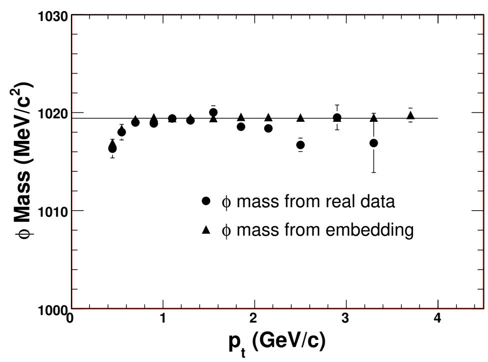

Figure 3.10: ϕ meson mass measured from real data (filled circles) and embedding (filled triangles) as a function of transverse momentum p_t. The left plot is from $p+p$ data and the right plot is from top 5% central $Au+Au$ data. Error bars are statistical errors only.

is lower than the PDG value for the low p_t region (0.4 GeV/c $< p_t <$0.6 GeV/c) and consistent with the PDG value in the higher p_t region ($p_t >$0.6 GeV/c) for both data sets. The same trend is also seen from the simulations as shown by filled triangles in the figure. Within the uncertainties the measured mass from real data is consistent with that from simulations. Therefore the low p_t deviation of the measured ϕ mass from the PDG value is understood as due to the energy loss of decayed daughter kaons in the detector materials as shown by the simulation results.

The conclusion from the mass and width measurement is that no obvious modification of the ϕ mass and width is seen in both $p+p$ and $Au+Au$ collisions at 200 GeV in the measured transverse momentum region $p_t > 0.4$ GeV/c. Further tests would need to extend the ϕ measurement to a much lower p_t region and have a precise measurement of charged track energy loss in the detector material.

3.3.2 Transverse mass spectra

After taking into account the acceptance and tracking efficiency correction for both $Au + Au$ and $p + p$ data and the additional vertex finding efficiency for $p + p$ data, the ϕ invariant yield $\frac{1}{N_{events}} \frac{1}{2\pi m_t} \frac{d^2N}{dm_t dy}$ is calculated as a function of transverse mass $m_t - m_\phi$. The results are shown in figure 3.11, which presents the transverse mass spectra in 5 centrality bins for $Au + Au$ collisions and in 3 multiplicity bins for $p + p$ collisions. Some distributions in the figure are scaled by different factors to guide eyes. The top 5 % $Au + Au$ data are from the central triggered data set while the other centrality bins of $Au + Au$ data are from MinBias triggered data set. The $p + p$ MinBias data set is divided into two extra multiplicity bins ($N_{ch} < 5$ and $N_{ch} \geq 5$).

The lines in the figure are fit results using a single exponential function

$$\frac{1}{N_{events}} \frac{1}{2\pi m_t} \frac{d^2N}{dm_t dy} = \frac{1}{2\pi} \frac{dN/dy}{T(m_\phi + T)} e^{-(m_t - m_\phi)/T}, \tag{3.9}$$

where dN/dy and T are fit parameters, for $Au+Au$ data and a double exponential function

$$\frac{1}{N_{events}} \frac{1}{2\pi m_t} \frac{d^2N}{dm_t dy} = A_1 e^{-(m_t - m_\phi)/T_1} + A_2 e^{-(m_t - m_\phi)/T_2}, \tag{3.10}$$

where A_1, T_1, A_2 and T_2 are fit parameters, for $p + p$ data.

It can be seen that the spectra in $Au + Au$ collisions can be well fit by a single exponential function. However, the spectra in $p + p$ collisions exhibit a power law shape at high p_t and thus can not be described well by a single exponential function. A double exponential function is used to fit the $p + p$ results and it can represent the data well. The inverse slope T, $\langle p_t \rangle$ and yield dN/dy values are extracted from the fits to the spectra and are listed in table 3.7.

Only statistical uncertainties are shown in the figure. The main contributions to the systematic uncertainty come from fitting to the K^+K^- invariant-mass

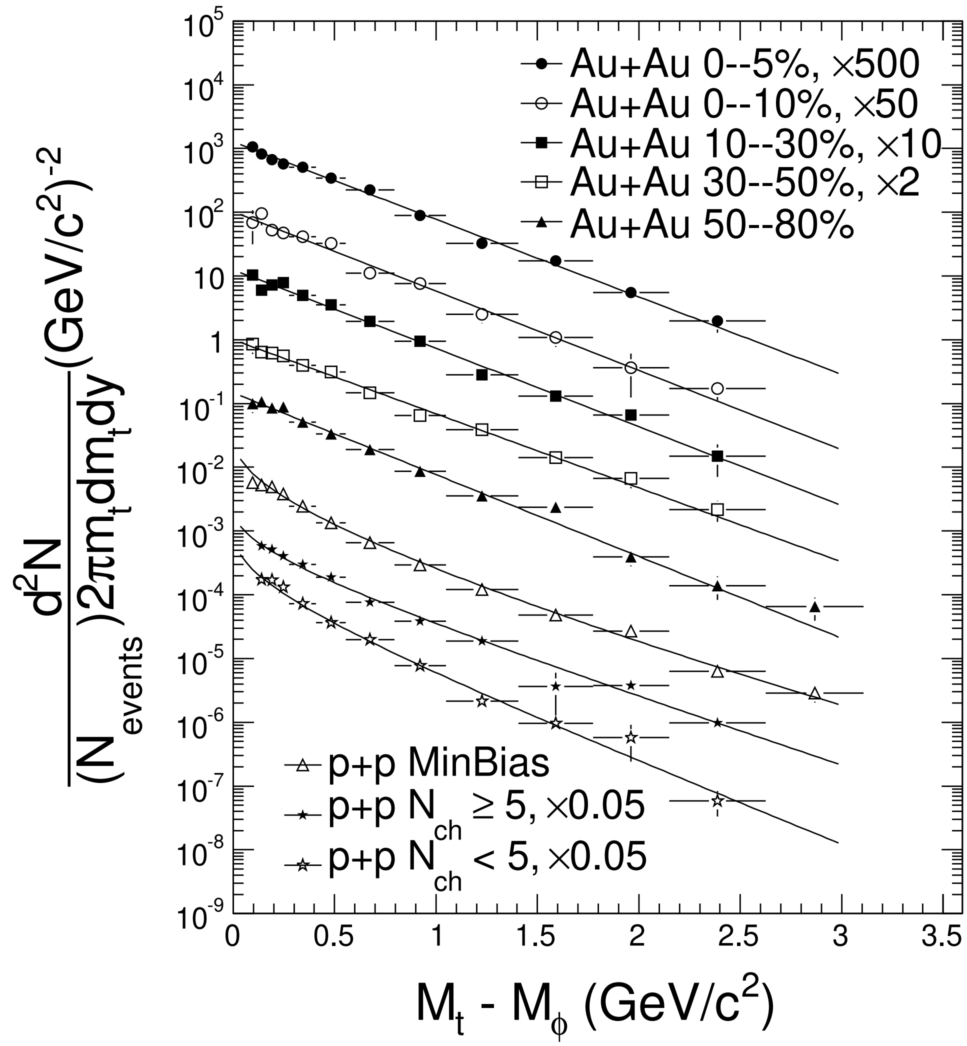

Figure 3.11: The ϕ meson transverse mass distributions from 5 centrality bins in $Au{+}Au$ collisions and 3 multiplicity bins in $p{+}p$ collisions at 200 GeV. For clarity, some distributions are scaled by factors as indicated in the figure. The top 5% data are obtained from the central triggered data set. All other distributions are obtained from the minimum-bias triggered data set. Lines in the figure represent fit to the distributions. The fit is a single exponential function for $Au + Au$ collisions and a double exponential function for $p + p$ collisions. Error bars are statistical errors only.

distribution, tracking and the PID efficiency calculation. Different background functions and normalization factors for the mixed-event background were used to determine the uncertainty in the fitting to the invariant-mass distribution and is estimated to be about 5%. The uncertainty from tracking and PID efficiency is estimated, by varying the tracking and PID cuts on the daughter tracks, to be 8%. The overall systematic uncertainty for the yield, dN/dy and $\langle p_t \rangle$ in $Au+Au$ collisions is estimated to be 11%, and includes an additional contribution from fitting the transverse momentum distributions. The systematic uncertainty is $\sim 15\%$ in the overall normalization and $\leq 5\%$ in mean p_t for the $p+p$ data, including uncertainties in the vertex efficiency for very low multiplicity events.

Centrality	Slope (MeV)	$\langle p_t \rangle$ (GeV/c)	dN/dy
$Au+Au$ 0–5%	363 ± 8	0.97 ± 0.02	7.70 ± 0.30
$Au+Au$ 0–10%	357 ± 14	0.95 ± 0.03	6.65 ± 0.35
$Au+Au$ 10–30%	353 ± 8	0.97 ± 0.02	3.82 ± 0.19
$Au+Au$ 30–50%	383 ± 10	1.02 ± 0.03	1.72 ± 0.06
$Au+Au$ 50–80%	344 ± 9	0.94 ± 0.02	0.48 ± 0.02
$p+p$ minbias	$--$	0.82 ± 0.03	0.018 ± 0.001
$p+p$ $N_{ch} < 5$	$--$	0.75 ± 0.04	0.011 ± 0.001
$p+p$ $N_{ch} \geq 5$	$--$	0.91 ± 0.05	0.040 ± 0.003

Table 3.7: Determinations of the ϕ meson inverse slope parameter T, $\langle p_t \rangle$, and yield dN/dy from 5 centrality bins of $Au+Au$ collisions and three multiplicity bins of NSD $p+p$ collisions at RHIC. A single exponential function is used to fit the $Au+Au$ data while a double-exponential function is used to fit the $p+p$ data. All values are for $|y| < 0.5$ and only statistical errors are quoted.

It's interesting to see that the $p+p$ spectra have a power law tail at high p_t while the $Au+Au$ data are represented well by a single exponential function. This difference of the spectrum shape is likely due to the suppression of ϕ production at high p_t in $Au + Au$ collisions. Future higher statistics data will allow the ϕ spectra to be measured in finer centrality bins and up to higher p_t, and will explore in more detail the changing of the spectrum shape with system-size, from $p + p$ to peripheral and central $Au + Au$ collisions.

The integrated yields for hadrons measured at RHIC, including the ϕ yield, are found to agree surprisingly well with statistical models under the assumption that the system has reached thermal and chemical equilibrium (see figure 12 in reference [Ada05b]). This observation suggests that thermal and chemical equilibration is at least approximately achieved in heavy ion collisions at RHIC.

Hydrodynamics motivated blast wave fits to the measured spectra have been done and the freeze out temperature and flow velocity are extracted as a function of centrality (see figure 14 in reference [Ada05b]). For the copiously produced π, K and p, the fitted freeze out temperature decreases from $p + p$ and peripheral $Au + Au$ collisions toward central $Au + Au$ collisions, while the flow velocity increases at the same time. This is understood as the result of smaller interaction volume in $p+p$ and peripheral $Au+Au$ collisions and an extended system volume in central $Au + Au$ collisions. For the multi-strange hadrons ϕ and Ω, the fitted results indicate that they freeze out earlier (at higher temperature, consistent with the chemical freeze out temperature) and that the flow velocity is lower than for the π, K and p. This suggests diminished hadronic interactions with the expanding bulk matter after chemical freeze out for the ϕ and Ω. The substantial radial flow velocity for ϕ and Ω would have to be accumulated prior to chemical freeze out, giving the multi-strange hadrons greater sensitivity to collective behavior during earlier partonic stages of the system evolution. However, the fits for ϕ and Ω have quite large uncertainties, and firm conclusions will be drawn only after the analyses of the coming high statistics data.

3.3.3 $\langle p_t \rangle$ and particle ratios

The system-size and beam-energy dependence of $\langle p_t \rangle$, the yield ratio ϕ/K^- and the yield ratio ϕ/h^- are shown in figure 3.12. Plot (a) shows the ϕ $\langle p_t \rangle$ distribution as a function of number of charged hadrons. For comparison, the $\langle p_t \rangle$ of the $\bar{p}$, K^- and π^- [Ada04b] are also shown.

The ϕ/h^- yield ratio at 200 GeV shows no significant dependence on centrality for $Au + Au$ collisions, but decreases by about 30% for $p + p$ collisions, see open symbols in plot (b). As a function of beam energy, see plots (c) and open circles in plot (d), both the values of ϕ $\langle p_t \rangle$ and the ϕ/h^- yield ratio increase. This indicates that the production of ϕ mesons is sensitive to the initial conditions of the collision. In $p + p$ collisions, ϕ $\langle p_t \rangle$ is found to increase with increasing multiplicity as seen in table 3.7, possibly due to increasing contribution from mini-jet production in high multiplicity $p + p$ events.

From plot (a) it can be seen that the general trend for $\bar{p}$, K^- and π^- is an increase in $\langle p_t \rangle$ as a function of centrality, which is indicative of an increased transverse radial flow velocity component to these particles' momentum distributions toward central $Au+Au$ collisions. The ϕ $\langle p_t \rangle$, however, shows no significant centrality dependence. This indicates that the ϕ does not participate in the transverse radial flow as does the $\bar{p}$, K^- and π^-. This is expected if the ϕ decouples early on in the collision before transverse radial flow is completely built up. If the ϕ hadronic scattering cross section is much smaller than that of other particles, one would not expect the ϕ $\langle p_t \rangle$ distribution to be appreciably affected by any final state hadronic rescatterings. In contrast to these observations, the RQMD predictions of $\langle p_t \rangle$ for the kaon, proton and ϕ all increase as functions of centrality

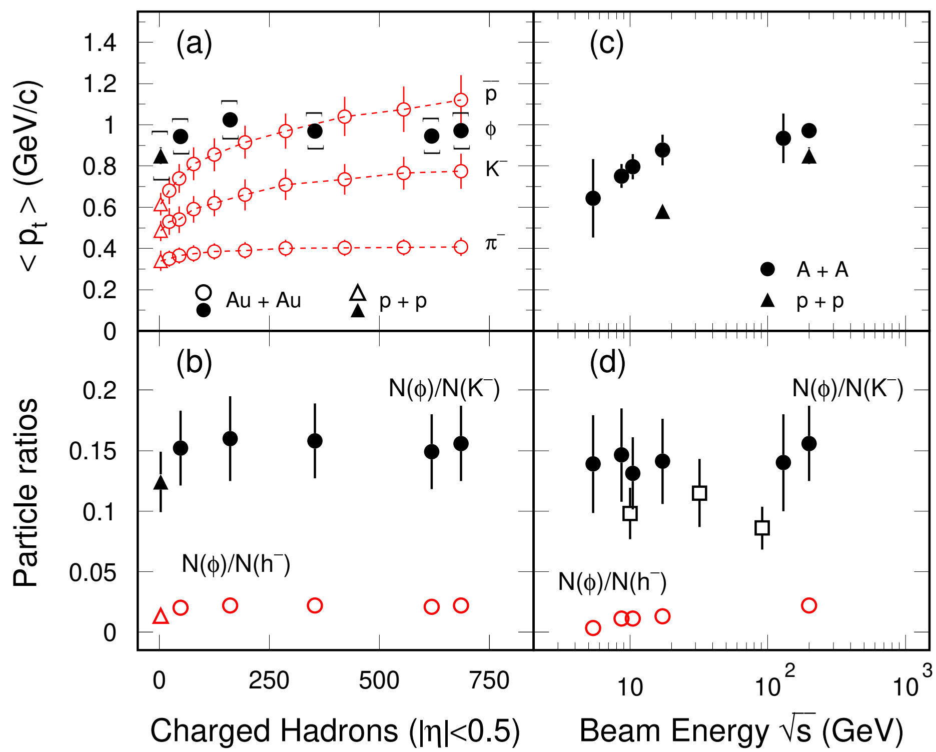

Figure 3.12: (a) ϕ meson $\langle p_t \rangle$ vs. measured number of charged hadrons (N_{ch}) within $|\eta| \leq 0.5$ at 200 GeV. For comparison, the values of $\langle p_t \rangle$ for negative pions, kaons, and anti-protons are also shown (dashed lines are used to connect data points and guide eyes); (b) Ratios of N(ϕ)/N(K^-), filled symbols, and N(ϕ)/N(h^-), open symbols, vs. N_{ch}; (c) $\langle p_t \rangle$ vs. center-of-mass beam energy from central nucleus-nucleus (filled circles) and $p + p$ collisions (filled triangles); (d) Ratios of N(ϕ)/N(K^-) from central nucleus-nucleus collisions, filled circles, and N(ϕ)/N(h^-), open circles, vs. center-of-mass beam energy. N(ϕ)/N(K^-) ratio from e^+e^- collisions (open squares) are also shown. Note: All plots are from mid-rapidity. Both the statistical and systematic errors are shown for the 200 GeV STAR data, while only statistical errors are shown for the energy dependence of the particle ratios.

[Sor95, CLL03].

The yield ratio ϕ/K^- from this analysis is constant as a function of centrality and collision system species ($p+p$ or $Au+Au$). In fact, for collisions above the threshold for ϕ production, the ϕ/K^- ratio is essentially independent of system size, $e^+ + e^-$ to nucleus-nucleus, and energy from a few GeV up to 200 GeV (figure 3.12 (d)) [Bac04a, Ahl98, Afa00, Afa02, Adl02b, Adl04, Ada05c, Eid04]. This is remarkable, considering that the initial conditions of an $e^+ + e^-$ collision are so drastically different from $Au+Au$ collisions. This observation may indicate that the ratio is dominated by the hadronization process.

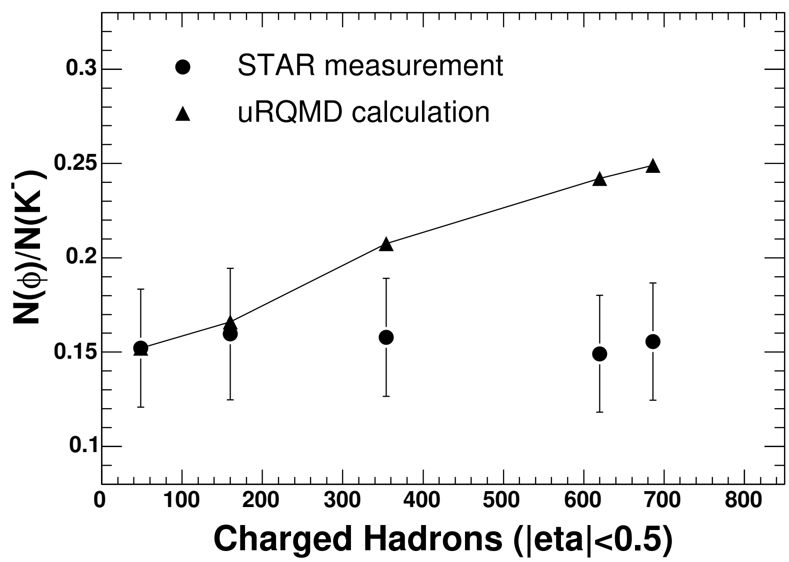

Figure 3.13: ϕ/K^- yield ratio calculated by UrQMD model as a function of number of charged hadrons within $|\eta| < 0.5$ (triangles) as well as the measured ratio (circles). The ratio from UrQMD is scaled to the measurement in the most peripheral bin.

Rescattering models (RQMD [Sor95], UrQMD [Ble99, Bas99]) predict that about 2/3 of ϕ mesons come from kaon coalescence in the final state. The centrality dependence of the ϕ/K^- ratio alone provides a serious test of the current rescattering models. In these models, such as UrQMD, rescattering channels for ϕ production includes $K\bar{K}$ and K-Hyperon modes and predicts an increasing ϕ/K^- ratio vs. centrality as can be seen in figure 3.13. These models also predict an increase in $\langle p_t \rangle$ for the proton, kaon, and ϕ of 40 to 50% from peripheral to central collisions. A comparison of the data to these models does not support the kaon coalescence production mechanism for ϕ mesons.

3.3.4 Nuclear modification factors R_{CP} and R_{AA}

A comparison of the R_{CP} for the ϕ, K_S^0 and Λ is shown in figure 3.14 (a). Both statistical and systematic errors are included in the figure. The ratio R_{AA} for central (top 5%) and peripheral (60-80%) $Au + Au$ data are shown in figure 3.14 (b) and (c), respectively. R_{AA} for charged hadrons [Ada03] is also shown as a reference. The charged hadron and ϕ peripheral R_{AA} both go above the binary scaling limit, but are consistent with unity within the systematic uncertainties. The ϕ central R_{AA} approaches unity and point to point is higher than R_{CP}. With the systematic uncertainty on the normalization of the ratio, however, both R_{AA} and R_{CP} are consistent. Note that a R_{AA} ratio that is higher than the R_{CP} ratio would be consistent with OZI suppression of ϕ production in $p + p$ [Oku63, Zwe64, IOS66] and/or strangeness enhancement in $Au + Au$ collisions. A measurement of R_{AA} vs. system size may be sensitive to the system size at which OZI becomes irrelevant to ϕ production.

The ϕ R_{CP} result is consistent with partonic recombination models [DH77, HY03, FMN03b, FMN03a]. In these models, hadronization proceeds by recombining 2 (3) quarks to form mesons (baryons) up to intermediate p_t region. Thus the centrality dependence of the yield at intermediate p_t depends on the number

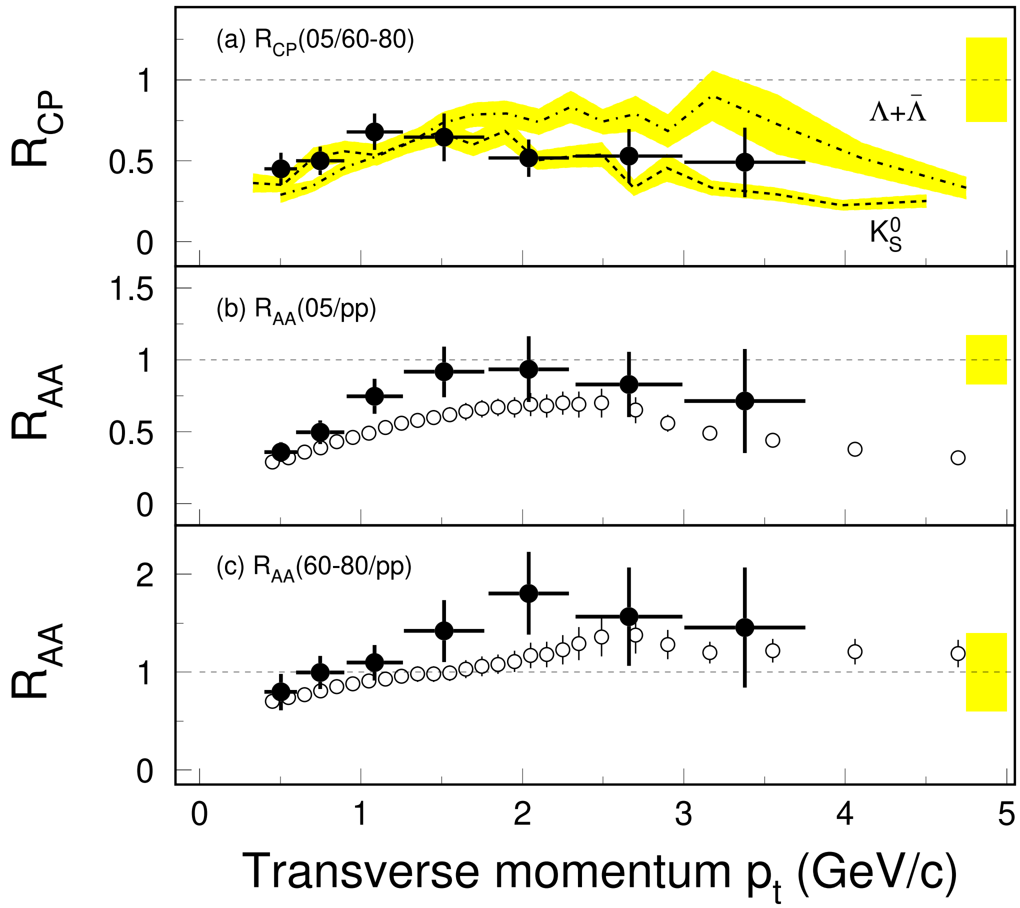

Figure 3.14: R_{CP} (a): The ratio of central (top 5%) over peripheral (60-80%) (R_{CP}) normalized by $\langle N_{bin} \rangle$. The ratios for the Λ and K^0_S, shown by dotted-dashed and dashed lines, are taken from [Ada04d]; R_{AA} (b) and (c) are the ratios of central $Au + Au$ (top 5%) to $p + p$ and peripheral $Au + Au$ (60-80%) to $p + p$, respectively. The values of R_{AA} for charged hadrons are shown as open circles [Adl02a]. The width of the gray bands represent the uncertainties in the estimation of $\langle N_{bin} \rangle$ summed in quadrature with the normalization uncertainties of the spectra. Errors on the ϕ meson data points are the statistical plus 15% systematic errors.

of constituent quarks rather than on the particle mass. The STAR measurement of R_{CP} for various hadrons supports the prediction from recombination models (see figure 15 in [Ada05b]). Further high statistics data for the ϕ are needed to draw a solid conclusion on whether ϕ follows number of constituent quark scaling or particle mass scaling and provide in detail the scaling behavior.

3.3.5 Elliptic flow v_2

The measured ϕ meson elliptic flow v_2 as a function of p_t is shown by filled squares in figure 3.15. For comparison, v_2 values for the K_S^0 (filled triangles), $\Lambda+\bar{\Lambda}$ (filled circles) and charged hadrons (open diamonds) measured by STAR [Ada04d, Ada05a] are also shown. Lines represent π, K, p and Λ v_2 calculated by hydrodynamical model [HKH01]. The observed non zero v_2 value indicates that the ϕ has developed a significant amount of elliptic flow in $Au + Au$ collisions. Since the ϕ does not participate in the hadronic stage interactions, the non zero v_2 must have been built up in a pre-hadronic stage. This is consistent with the scenarios of recombination/coaslescence models where v_2 is assumed to have developed in partonic stage [NFB04, MV03, GKL03, LK02]. The v_2 scaled by number of constituent quarks as a function of p_t scaled by number of constituent is found to be consistent with one universal curve for several identified hadrons [Ada04d]. These results point directly to quark flow in the early partonic stages if this observation is further confirmed by more precise measurements.

The current measurements haven't been able to nail down whether the ϕ v_2 follows the mass hierarchy in the low p_t region ($p_t < 1.5$ GeV/c) as suggested by hydro models, and whether the ϕ follows the number of constituent quark scaling in the intermediate p_t region (2.0 GeV/c $< p_t <$ 5.0 GeV/c) as indicated by recombination/coalescence models. Precise measurement of the ϕ v_2 as a function of p_t and collision centrality will shed more insight into the hadronization processes in heavy ion collisions and help disentangle different models.

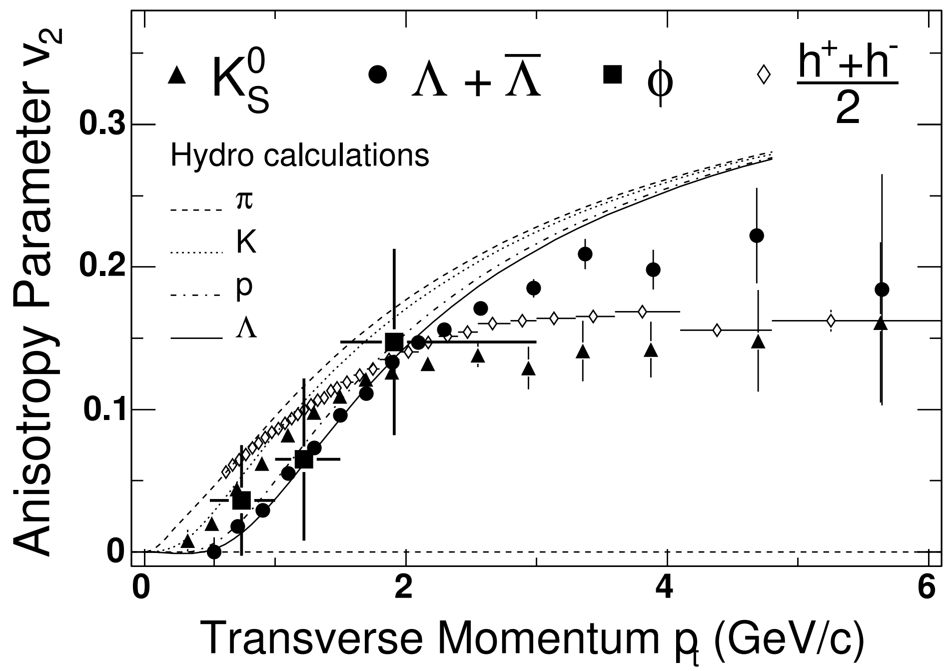

Figure 3.15: Measured ϕ meson v_2 as a function of transverse momentum (filled squares). The v_2 measured for K_S^0 (filled triangles), $\Lambda + \bar{\Lambda}$ (filled circles) and charged hadron (open diamonds) are also shown in the figure. Lines represent results of the calculation by hydrodynamic model for various particles as indicated in the figure. The error bars for the ϕ meson data points include statistical errors only.

CHAPTER 4

Searches for Pentaquark Particles at RHIC

In this chapter we describe the analysis procedures for the searches of the pentaquark particles Θ^{++}, Ξ^{--} and their anti-particles from the STAR experiment. The data samples that are used will be discussed first. Then we will present the analysis procedures and the results for the search of Θ^{++}. After that the search for the Ξ^{--} is presented in a separate section since the procedures are quite different from that of the Θ^{++}.

4.1 Data sets

During the first few years of RHIC running, STAR has accumulated several data samples which are of interest for searches of pentaquark particles. These data sets include minimum bias triggered $p + p$ events at $\sqrt{s_{NN}} = 200$ GeV which were collected in the year 2001 running, minimum bias triggered $d+Au$ events at $\sqrt{s_{NN}} = 200$ GeV which were collected in the year 2003 running, minimum bias triggered $Au + Au$ events at $\sqrt{s_{NN}} = 62.4$ GeV which were collected in the year 2004 running, minimum bias triggered $Cu+Cu$ events at $\sqrt{s_{NN}} = 62.4$ GeV which were collected in the year 2005 running and minimum bias triggered $Au + Au$ events at $\sqrt{s_{NN}} = 200$ GeV which were collected in the year 2004 running.

In relativistic heavy ion collisions at RHIC, the charged particle yield scales with the number of nucleon participant (N_{part}) in the collision. The combinatorial background is thus proportional to N^2_{part}. As a result, the resonance signal to background ratio (S/N) is much lower in central collisions than in peripheral collisions for $Au + Au$ collisions. The most central (top 20 %) collisions for the $Au + Au$ data sets are excluded for this reason.

The above data samples are taken by a minimum bias trigger setup. For the $p+p$ data, the BBC was used as the trigger detector while for the $d+Au$, $Au+Au$ and $Cu+Cu$ data the ZDC and CTB were used as the trigger detectors. Events are also selected so that they center around the TPC along the beam direction (Z direction). The actual cuts on the vertex Z are listed below: $|Z| < 50$ cm for $p + p$ at 200 GeV, $|Z| < 75$ cm for $d + Au$ at 200 GeV, $|Z| < 30$ cm for $Au+Au$ at 62.4 GeV, $|Z| < 30$ cm for $Cu+Cu$ at 62.4 GeV and $|Z| < 35$ cm for $Au + Au$ at 200 GeV. In table 4.1, the collision system, the year of data taking, the collision energy, the selected collision centrality, vertex Z and the total event number available for the pentaquark particle search are listed.

Collision	Year	$\sqrt{s_{NN}}$ (GeV)	Centrality	|VertexZ| (cm)	nEvent (M)
$p + p$	2001	200	MinBias	< 50	6.5
$d + Au$	2003	200	MinBias	< 75	18.6
$Au + Au$	2004	62.4	$20 - 80\%$	< 30	5.6
$Au + Au$	2004	200	$20 - 80\%$	< 35	10.7
$Cu + Cu$	2005	62.4	$0 - 70\%$	< 30	16.5

Table 4.1: List of data sets used in the search of pentaquark particle. All the listed data are used in the search for $\Theta^{++}(\bar{\Theta}^{--})$, while only the $d + Au$ data are used for the search of $\Xi^{--}(\bar{\Xi}^{++})$.

After the minimum bias trigger selection, the collision vertex Z cut and the centrality cut, 6.5 million $p + p$ events at 200 GeV, 18.6 million $d + Au$ events at

200 GeV, 5.6 million $Au + Au$ events in the 20-80% centrality bin at 62.4 GeV, 16.5 million $Cu+Cu$ events in the 0-70% centrality bin at 62.4 GeV and 10.7 million $Au + Au$ events in the 20-80% centrality bin at 200 GeV have been used for the results presented here. All these data sets are used for the search of the Θ^{++} pentaquark, while only the $d + Au$ data are used for the search of the Ξ^{--} pentaquark.

4.2 Analysis and results for the Θ^{++}

4.2.1 Analysis procedures

Some track quality cuts are applied to select the appropriate decay daughters, similar to that for ϕ meson measurement. Since the particle we are looking for is supposed to have a very short life time, the tracks from its decay should originate from the collision vertex. Thus each track is required to be a primary track, that is, it has a *dca* to the event vertex less than 3 cm. Tracks are required to have at least 15 hit points (nHit≥15) in the TPC, and the ratio of the actual number of hit points to the maximum possible number of hit points is required to be great than 0.55 (nHit/nMax>0.55) to ensure a good track and reject possible splitting tracks. A loose pseudo-rapidity cut ($|\eta| < 1.5$) is imposed to accept as many usable tracks as possible while avoiding the acceptance of tracks outside the TPC. A dE/dx cut on $n\sigma$ is used to select the corresponding track species (kaons and protons). Cuts on the momentum of the daughters are also used to limit the amount of contaminations from unwanted particles. These cuts used in the analysis are listed in table 4.2.

For the Θ^{++} search, the invariant mass of every pK^+ (or $\bar{p}K^-$) pair is calculated and accumulated in each transverse momentum (p_t), rapidity (y) and mass

Applied Cuts for Θ^{++}	
Primary Track	Yes
Track Fitting Flag	flag > 0
Track Number of Hit Points	nHit ≥ 15
Track Hit Points to Maximum Points Ratio	nHit / nMax > 0.55
Track Pseudo-Rapidity	$\lvert\eta\rvert < 1.5$
Kaon PID	$-2.0 < n\sigma_{kaon} < 2.0$
Kaon Momentum	0.2 GeV/c $\leq p\&p_t \leq$ 0.6 GeV/c
Proton PID	$-2.0 < n\sigma_{proton} < 2.0$
Proton Momentum	0.3 GeV/c $\leq p\&p_t \leq$ 1.0 GeV/c
Track Pair y	$\lvert y\rvert < 0.5$

Table 4.2: List of cuts used for the search of Θ^{++}.

(M) bin (the same event). Background is calculated using event mixing method (the mixed event). To minimize possible bias of the mixed background caused by different event geometrical shape, the two events chosen for the event mixing method are required to have a similar vertex Z position (in the same vertex Z bin of 10 cm interval). The two events are also required to have similar charged track multiplicities. To achieve this, the two events are required to be in the same centrality bin (in a 10 % interval) in $Cu + Cu$ and $Au + Au$ collisions. In these collisions the centrality is defined by the number of charged tracks in the pseudo-rapidity region $|\eta| < 0.5$.

For $d + Au$ collisions, the multiplicity is relatively small, so the two events to be mixed are grouped in only two bins according to the number of daughter candidates that have passed all cuts. Events with number of candidate daughters less than 3 are put in one group and the rest in another. Grouping in this way instead of collision centralities of $d + Au$ events has been found to be very useful, since this choice for grouping gives a much smaller residual background after background subtraction.

Further-more, to reduce the statistical uncertainty in the mixed background, each event is mixed with 15 other events for the $d + Au$ data and 6 for the $Cu + Cu$ and $Au + Au$ data. Memory demands and running time considerations of the analysis code make the number of mixed events smaller in $Cu + Cu$ and $Au + Au$.

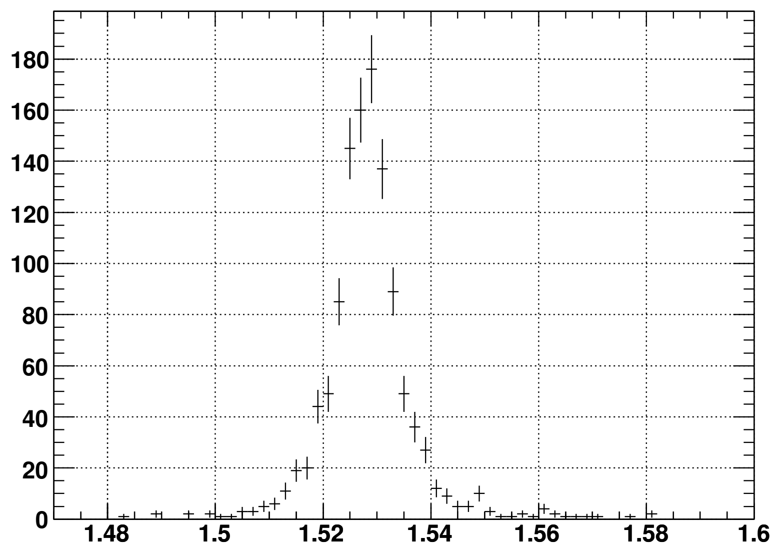

Figure 4.1: Simulated Θ^{++} invariant mass distribution with input Θ^{++} mass $m = 1.53$ GeV/c^2 and width = 0. The peak gaussian width $\sigma = 5.5$ MeV/c^2 represents the resolution of the detector.

To search for a pentaquark particle, the invariant mass distribution from the mixed background is normalized to that of the same event distribution in a certain region and subtracted from the same event distribution. The resulting invariant mass distribution is then searched for the signal of a resonance by looking for a peak structure.

4.2.2 Simulations

To check for consistency and to aid the searches of a pentaquark particle signal, simulations have been done for the Θ^{++} using embedding techniques. In GEANT Θ^{++} with flat p_t and rapidity distributions are generated with $m = 1.53$ GeV/c^2, width = 0 and then allowed to decay into a kaon and a proton. To produce embedding data the detector responses are simulated by GEANT and the information is embedded into real events for track and event reconstruction (the same process as used for real data production). The embedding data that includes the detector responses are then used to reconstruct the simulated Θ^{++}.

Figure 4.1 shows the reconstructed invariant mass of the simulated Θ^{++} from the STAR detector. The Gaussian width of the peak is $\sigma = 5.5$ MeV/c^2 from a fit by a Gaussian function. This width represents the resolution of the detector since the input width is 0. Similar to the ϕ meson, the reconstructed mass for the Θ^{++} is found to decrease by a few MeV due to the energy loss of kaons and protons. The embedding data is also used to calculate the acceptance and tracking efficiency for the pentaquark. More details will be discussed later in this chapter.

4.2.3 Results from $d + Au$ at 200 GeV

4.2.3.1 Invariant mass distributions

Figure 4.2 shows the invariant mass distribution of $pK^+ + \bar{p}K^-$ in $d+Au$ collisions at 200 GeV. The transverse momentum region is 0.5 GeV $< p_t <$ 1.2 GeV and the rapidity region is $|y| < 0.5$.

The plot on the left shows the invariant mass distribution before background subtraction, where the red data points are from the same event distribution while the histogram is from the mixed event distribution. The mixed event background distribution is normalized to the same event distribution in the mass region 1.6 GeV-1.65 GeV. The plot on the right is the mixed event background subtracted invariant mass distribution.

From the plot on the left, it can be seen that the event mixing method can represent well the invariant mass distribution of the same event except for some regions where excesses are obviously above the background. After the background subtraction, we can see clearly in the right plot that there appears to be a peak at an invariant mass near 1.53 GeV. The peak is fit by a Gaussian plus a 3rd order polynomial function. The peak mass position from the fit is 1528±2 MeV/c^2 and the σ of the gaussian is 6.5±0.5 MeV/c^2. The signal count from the fit is 1649±390, which indicates the significance of the peak to be 4.2 σ.

Is the peak a real particle? Is it an artifact of our data or data analysis? Is it a statistical fluctuation? These are some urgent and critical questions we need to address to identify the origin of this peak.

If this is confirmed as a real particle, it has to be manifestly a multi-quark state (at least and most likely five quarks), since the two decay daughters are $K^+(u\bar{s})$ and $p(uud)$. It naturally fits in as the isospin partner of the previously reported Θ^+. Since almost all theories claim the Θ^+ to be an isosinglet, this confirmation will place a serious challenge to these theoretical/model calculations.

It is very important that the excesses can already been seen without mixed event background subtraction, see the left plot of figure 4.2. This observation demonstrates that the peak structure is really in our data, not an artifact of the

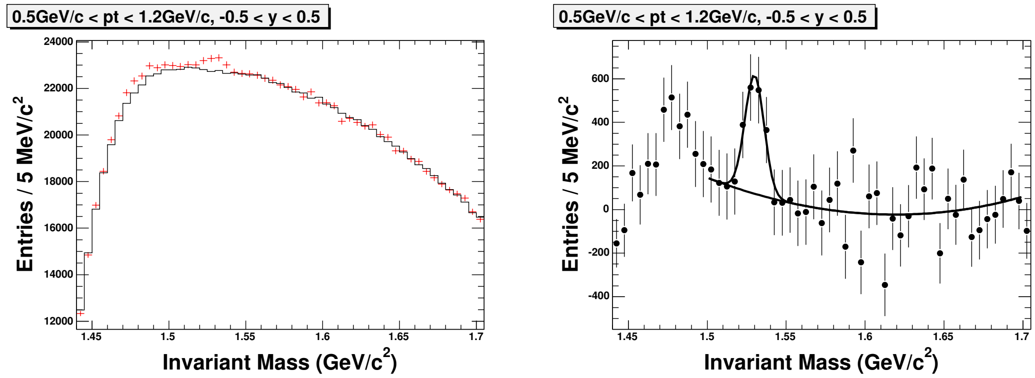

Figure 4.2: $pK^+ + \bar{p}K^-$ invariant mass distribution in 200 GeV $d + Au$ collisions. Left plot: Red data points are the $pK^+ + \bar{p}K^-$ invariant mass distribution from the same event. Black histogram is the $pK^+ + \bar{p}K^-$ invariant mass distribution from the mixed event. Right plot: $pK^+ + \bar{p}K^-$ invariant mass distribution after mixed event background subtraction. The fit in the plot is a gaussian plus a 3rd order polynomial function.

background subtraction in our data analysis. This peak structure is tested further by varying the cuts applied to look for any abnormal changes. For example, the daughter momentum cut, dE/dx cut, η cut, the event vertex Z cut etc. are varied and the results are found to be consistent with each other. The peak has also been examined in different rapidity regions and no anomaly has been found.

The $\Lambda(1520)$ particle has a very similar mass to the peak we see. The $\Lambda(1520) \rightarrow p + K^-$ decay channel is also very similar to $\Theta^{++} \rightarrow p + K^+$, thus they have similar decay kinematics, detection acceptance and efficiency. It's therefore natural to compare the $\Lambda(1520)$ production with that of the Θ^{++} to gain more information.

Figure 4.3 shows the $\Lambda(1520) + \bar{\Lambda}(1520)$ invariant mass distribution measured from the same $d + Au$ data sample using exactly the same cuts. The transverse

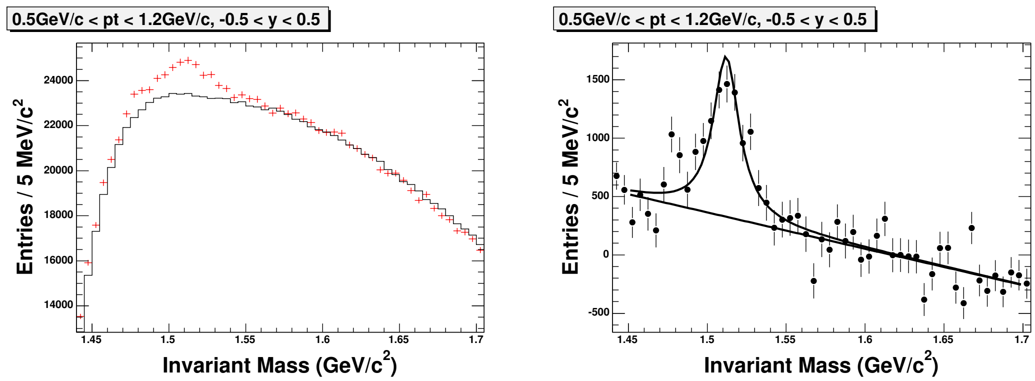

Figure 4.3: $\Lambda(1520) + \bar{\Lambda}(1520)$ invariant mass distribution in 200 GeV $d + Au$ collisions. Left plot: Red data points are the $\Lambda(1520) + \bar{\Lambda}(1520)$ invariant mass distribution from same event. Black histogram is the $\Lambda(1520)+\bar{\Lambda}(1520)$ invariant mass distribution from mixed event. Right plot: $\Lambda(1520)+\bar{\Lambda}(1520)$ invariant mass distribution after mixed event background subtraction. The fit in the plot is a Breit-Wigner plus a linear function.

momentum region is also 0.5 GeV $< p_t <$ 1.2 GeV and the rapidity region is also $|y|$ <0.5 for the measured $\Lambda(1520)$. In the plot on the left, the red data points are from the same event while the histogram is from event mixing. It can be seen clearly that there are excesses near the $\Lambda(1520)$ mass region from the same event invariant mass distribution. The plot on the right is the invariant mass distribution after mixed event background subtraction. The $\Lambda(1520)$ peak is fitted by a Breit-Wigner plus a linear function. The fitted mass is 1514$\pm$3 MeV/c^2 and the FWHM is 20$\pm$5 MeV/c^2.

4.2.3.2 Residual background from Δ

From both the Θ^{++} and the $\Lambda(1520)$ invariant mass plots in figure 4.2 and figure 4.3, we can see a peak at mass of 1.46-1.47 GeV/c^2. The offset of this peak in the $\Lambda(1520)$ invariant mass plot is suppressed because of a larger scale on the y axis, although its magnitude is actually similar to that in the Θ^{++} invariant mass plot.

The origin of this peak has been traced back to the $\Delta^{++} \rightarrow p + \pi^{+}$ and $\Delta^{0} \rightarrow p + \pi^{-}$ decays, where the pions are misidentified as kaons. The reason is that there is inevitably some $\pi^{\pm}$ contamination in the $K^{\pm}$ sample when particles are identified by the measurement of $< dE/dx >$ alone. Thus there should be some Δ^{++} contaminations in the Θ^{++} invariant mass distribution and some Δ^{0} in the $\Lambda(1520)$ invariant mass distribution. The Δ^{++} and Δ^{0} production rate is much higher, so a very small amount of contamination would result in a prominent peak in the Θ^{++} and $\Lambda(1520)$ invariant mass distribution.

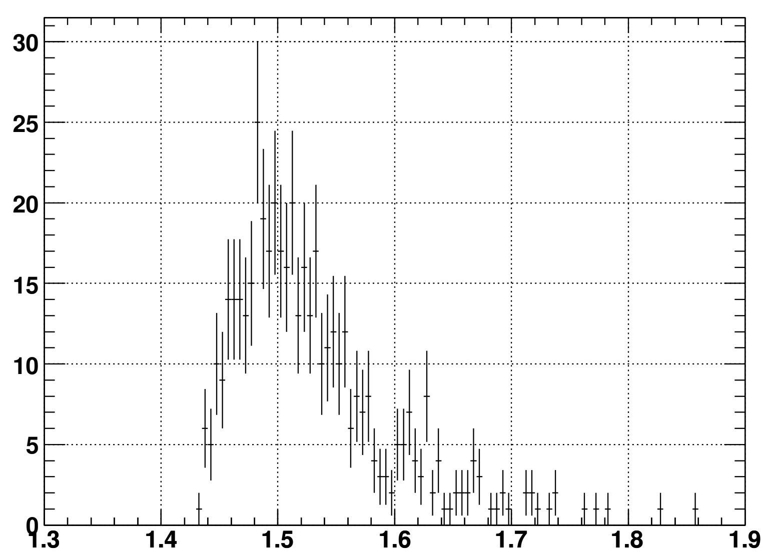

Figure 4.4: The simulated Δ^{++} invariant mass distribution when the decay daughter π^{+} is identified as K^{+}.

Figure 4.4 shows the Δ^{++} invariant mass distribution when the decay daughter π^+ is misidentified as K^+. Embedding data for the Δ^{++} is used here. The misidentified Δ^{++} mass peaks below 1.5 GeV. The peak position is consistent with the peak seen at 1.46-1.47 GeV/c^2 in the Θ^{++} and $\Lambda(1520)$ invariant mass distribution when the difference between the measured Δ^{++} mass and the simulated Δ^{++} mass is taken into account.

Other sources could also be responsible for the excesses in this region. Double photon conversion happens when the two photons from π^0 decay are both converted into a pair of $e^{\pm}$ in the detector materials. When two electrons (or two positrons) are misidentified as kaons and protons respectively (As we can see from dE/dx plot in chapter 3, the electron bands cross with the hadron bands.), the two electrons will end up in the Θ^{++} invariant mass plot. From simulation, we find that the two electrons' invariant mass is located at 1.46-1.47 GeV/c^2 when one electron is identified as a K^+ and the other is identified as a proton. This result confirms that there may be some contribution to the excesses at 1.46-1.47 GeV/c^2 in the Θ^{++} invariant mass from double photon conversion. However, the double photon conversion rate is low, so this contribution should be much smaller than that from misidentified Δ^{++}.

4.2.3.3 Anti-particle to particle ratio and other checks

In relativistic heavy ion collisions at RHIC energies, the anti-baryon to baryon ratio is pretty high. For example, the $\bar{p}/p$ yield ratio is found to be 0.81 ± 0.08 in $d + Au$ collisions at 200 GeV [STA]. To check whether the peak we are observing is a real resonance baryon state or not, it's necessary to separate the antiparticle from the particle.

Figure 4.5 shows the separated Θ^{++} and $\bar{\Theta}^{--}$ invariant mass distribution from the same $d + Au$ data sample with the same cuts as for figure 4.2. The plot on

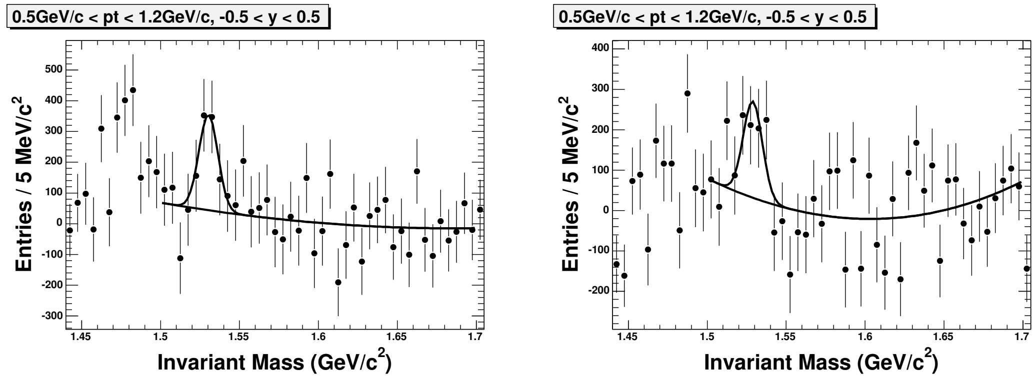

Figure 4.5: pK^+ (left plot) and $\bar{p}K^-$ (right plot) invariant mass distribution after mixed event background subtraction in 200 GeV $d + Au$ collisions. The fits in the plot are a gaussian plus a 3rd order polynomial function.

the left is for Θ^{++} and the plot on the right is for $\bar{\Theta}^{--}$. Both plots are event mixing background subtracted.

From these two plots we can see that there are excesses at about the same mass position. The significance is only 3-3.5 σ due to reduced statistics. The fit to the peak is a Gaussian plus a 3rd order polynomial function. The yield ratio is found to be $\bar{\Theta}^{--}/\Theta^{++} = 0.78 \pm 0.32$ (stat), which is in good agreement with the anti-baryon to baryon ratio in this collision system. This observation strengthens the significance of the signal we see in figure 4.2 and it's a very important check for the signal.

Energy loss of charged tracks in the TPC is corrected for that of pions. So for kaons and protons there could be potential problems caused by this approximate correction. For example, it is possible that a peak structure shows up in pK invariant mass distribution due to the energy loss correction. However, KK and pp invariant mass should also show a peak structure due to the same reason. To check for this possibility, both KK and pp invariant mass distribution are examined and no peak structures are found. This indicates that the Θ^{++} peak seen in $d + Au$ data is not due to energy loss corrections.

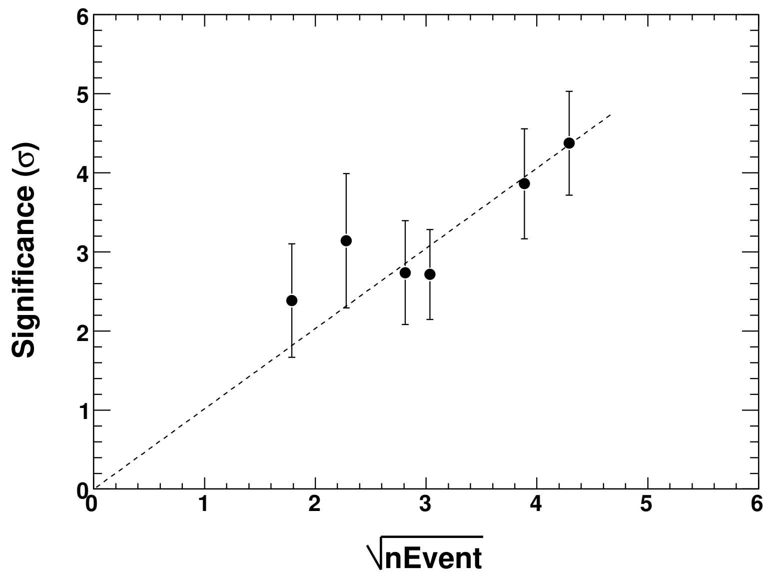

Figure 4.6: The measured significance σ of the peak as a function of the square root of number of events.

To check for possible anomaly of signal in certain set of data files, the $d + Au$ data is divided into several smaller data sets and the signal is looked for in these data sets. Figure 4.6 shows the significance of the Θ^{++} peak seen in each data set vs. the square root of number of events. The error bars on the data points are estimated by varying the fit to the peak. It can be seen that the significance increases with the number of events and that it is approximately proportional to the square root of number of events. This indicates the peak is not from some parts of the $d + Au$ data alone but from the whole data set.

4.2.4 Results from other collision systems

The same analysis procedures are applied to the 62.4 GeV $Au + Au$, 200 GeV $Au + Au$, 62.4 GeV $Cu + Cu$ and 200 GeV $p + p$ data samples by using the same cuts.

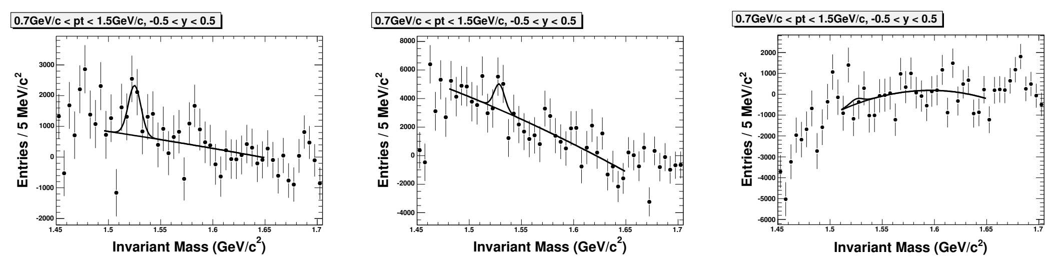

Figure 4.7: $pK^+ + \bar{p}K^-$ invariant mass distributions after mixed event background subtraction in 62.4 GeV $Au + Au$ collisions (left plot), 200 GeV $Au + Au$ collisions (middle plot), and 62.4 GeV $Cu + Cu$ collisions (right plot). The fits in the plots are Gaussian plus a 3rd order polynomial functions.

Figure 4.7 shows the $pK^+ + \bar{p}K^-$ invariant msss distribution from 62.4 GeV (left plot) and 200 GeV (middle plot) $Au + Au$ collisions and 62.4 GeV $Cu + Cu$ (right plot) collisions, where combinatorial background has been subtracted by event mixing as described before. The transverse momentum region is 0.7 GeV/c< p_t <1.5 GeV/c and the rapidity region is $|y| < 0.5$ for these plots. Curves are results of a Gaussian plus a 3rd order polynomial function fits to the invariant mass distributions. Data shown here are described in table 4.1 and all cuts used are described in table 4.2.

In figure 4.8 the invariant mass distribution of $pK^+ + \bar{p}K^-$ from $p + p$ collisions at 200 GeV is shown. The red histogram is from same event and the black histogram is from mixed event. It's found that mixed event describes the background shape pretty well. However, no signal for the Θ^{++} is seen in this data set.

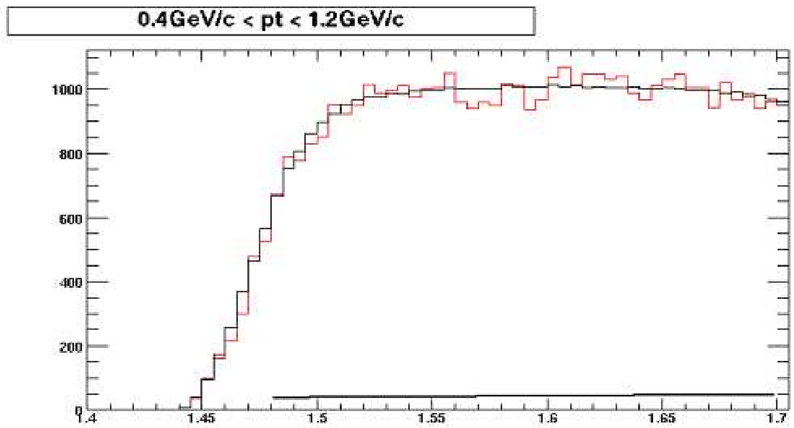

Figure 4.8: $pK^+ + \bar{p}K^-$ invariant mass distribution from same event (red histogram) and mixed event (black histogram) in 200 GeV $p+p$ collisions. No signal is seen for the Θ^{++} in this data set.

It is interesting to see that in 62.4 GeV and 200 GeV $Au+Au$ collisions there are some excesses at the same mass region of the peak seen in the $d+Au$ data. Extracted mass position and peak width are consistent with that in the $d+Au$ data. However, the significance is too low to really support the signal in $d+Au$. The estimated significance is only 2.7-3.7σ for the 62.4 GeV $Au+Au$ data and 2.5-3.3σ for the 200 GeV $Au+Au$. In 62.4 GeV $Cu+Cu$ data, no excesses are seen at the same mass region.

It has been found that in $Au+Au$ and $Cu+Cu$ collisions the signals are stronger when a different momentum cut on the decay daughters are applied. For example, the 62.4 GeV $Au+Au$ signal has a significance of 3.3-4.5σ when the momentum cuts are 0.2 GeV/c $< p(p_t) <$ 0.8 GeV/c for kaons and 0.3 GeV/c $< p(p_t) <$ 1.5 GeV/c for protons. The difference is reasonable if the Θ^{++} has a flatter transverse mass distribution in $Au+Au$ collisions.

The weak signal in these data sets could be due to several reasons. One explanation may be that the production rate per number of binary collisions or per number of participants in these collisions is lower than that in $d + Au$ collisions. It is a challenge to explain why the $d + Au$ collisions are favored for pentaquark production.

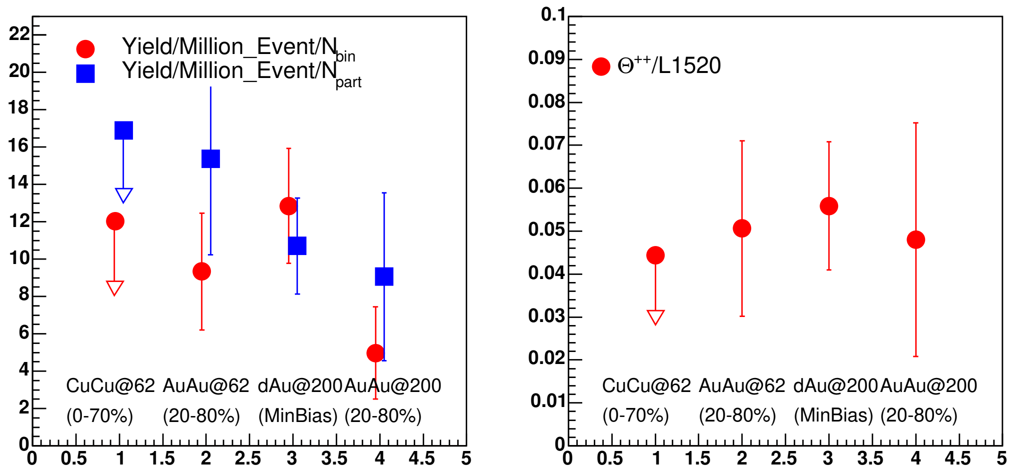

Figure 4.9: Θ^{++} production rate and $\Theta^{++}/\Lambda(1520)$ ratio in different systems. No efficiency corrections are applied since these corrections are consistent at $\sim$15% level in different systems and the Θ^{++} and $\Lambda(1520)$ efficiency should be similar due to similar mass, width and decay channel.

Another reason may be that the statistics of these data sets are not high enough. The yield per nucleon-nucleon collision per event is a useful way to look at the Θ^{++} production rate in different systems. Also since some of the $\Lambda(1520)$'s properties are very similar to that of Θ^{++}, the yield ratio $\Theta^{++}/\Lambda(1520)$ will provide more information on the production dynamics.

Figure 4.9 shows the number of observed signal for Θ^{++} divided by number of million events and number of binary collisions or number of participant nucleons in different systems (left plot) and the yield ratio $\Theta^{++}/\Lambda(1520)$ in these systems.

The data points for the 62.4 GeV $Cu + Cu$ data represent upper limits at 90% confidence level. From the left plot it's seen that the yield rate is consistent for different systems when scaled by number of participant nucleons and the 200 GeV $Au + Au$ yield rate is lower than the others when scaled by number of binary collisions. The yield ratio $\Theta^{++}/\Lambda(1520)$ is seen to be a constant at about 5% within different collision systems. Our conclusion is that due to unknown scaling behavior of Θ^{++} yield with system size (N_{bin} or N_{part} scaling) and the currently sizable error bars, the data are consistent with each other. Data sets with much more statistics are needed to check consistency between different systems.

4.2.5 Θ^{++} spectra and yield

The signals in 200 GeV $d + Au$ and 62.4 GeV $Au + Au$ data sets are divided into several p_t bins. Efficiency corrections are done in each p_t bin by using Θ^{++} embedding data and by assuming the branching ratio for the decay $\Theta^{++} \rightarrow p+K^{+}$ to be 100%. The calculated Θ^{++} invariant yield vs. transverse mass is plotted in figure 4.10. Filled circles represent results from 200 GeV $d + Au$ collisions while filled squares are from 62.4 GeV $Au + Au$ collisions. Dashed lines in the figure are fit results of a single exponential function.

The extracted dN/dy and inverse slopes from the fits to the spectra are listed in table 4.3. There is a huge systematic uncertainty on the extracted inverse slopes since there are only three data points for $d + Au$ data and two data points for $Au+Au$ data. The systematic uncertainties on the extracted yields are smaller and it is estimated that the yield ratio of Θ^{++}/ϕ is about 2% and $\Theta^{++}/\Lambda(1520)$ is about 5% in both 200 GeV $d + Au$ and 62.4 GeV $Au + Au$ collisions. The extracted yield for the Θ^{++} is so small from STAR that it's hard to imagine some of the low energy experiments can actually see the Θ^{+}, if Θ^{+} has the same yield

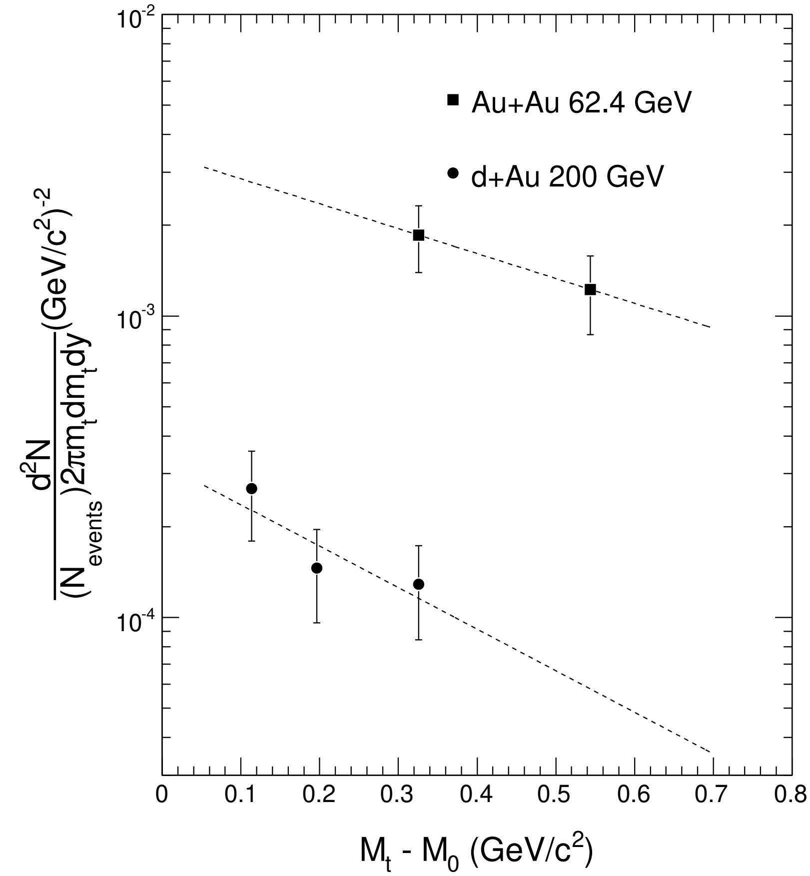

Figure 4.10: Θ^{++} spectra in 200 GeV $d+Au$ (filled circles) and 62.4 GeV $Au+Au$ (filled squares) collisions. The dashed lines are the result of a single exponential function fit to the spectra.

as Θ^{++}.

Data	Slope (MeV)	dN/dy
200 GeV $d + Au$ MinBias	315 ± 30	0.0012 ± 0.0006
62.4 GeV $Au + Au$ 20–80%	512 ± 49	0.022 ± 0.011

Table 4.3: Fit results of Θ^{++} spectra by a single exponential function. The error bars are statistical errors only.

4.2.6 The search for Ξ^{--} pentaquark

The $\Xi^{--}(\bar{\Xi}^{++})$ pentaquark is searched for from decay channel $\Xi^{--} \rightarrow \Xi^{-} + \pi^{-}$ and the subsequent decay of $\Xi^{-} \rightarrow \Lambda + \pi^{-}$ and $\Lambda \rightarrow p + \pi^{-}$. The decay of an excited Cascade state, the $\Xi(1530) \rightarrow \Xi^{-} + \pi^{+}$, is also analyzed for comparison with the Ξ^{--}.

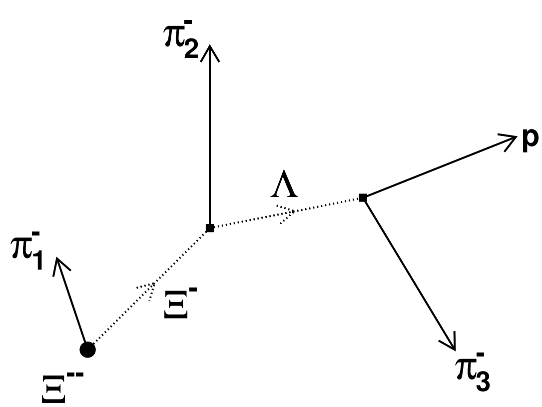

Figure 4.11: Schematic plot for the decay topology of Ξ^{--}. The decayed pions are numbered for convenience.

Figure 4.11 shows the topology for the Ξ^{--} decay. The Ξ^{--} is produced primordially from the collision and decays at the collision vertex to a Ξ^- and a π^-. The Ξ^- flies a certain distance before decaying into a Λ and a π^-. The Λ flies some further distance and decays into a p and a π^-. The Λ and Ξ^- are identified by reconstructing their displaced decay vertex from global tracks [Lon02, Ada04c]. The combinatorial background is greatly reduced by applying topological cuts to allow a relatively clean identification of these particles. Primary track pions are used to combine with identified Ξ^- to reconstruct the Ξ^{--} invariant mass. The combinatorial background is calculated by event mixing. Measurement of the $\Xi(1530)$ particle is done in a similar way.

There are three π^-s (as numbered in figure 4.11) in the final state of this decay chain. It is therefore crucial to make sure that one track is not used multiple times in the analysis. This is achieved by requiring the three π^-s have different track ID, which is unique for each track. A list of cuts used to select appropriate tracks and to reconstruct Ξ^- and Λ in the analysis are shown in table 4.4. Different sets of cuts are also used in the analysis to check the results.

Figure 4.12 shows the reconstructed Λ (left plot) and Ξ^- (right plot) invariant mass distributions in 200 GeV $d+Au$ collisions. It shows that the STAR detector has a very good capability of identifying these particles, with a signal to background ratio $S:N \sim 5:1$ for the Λ and $S:N \sim 9:1$ for the Ξ^- in the figure. The reconstructed mass for these particles are consistent with the values in PDG book. With the cuts listed in table 4.4, there are a total of $2.89\times10^5 \pm 750$ (stat) Λ, $2.27\times10^5 \pm 640$ (stat) $\bar{\Lambda}$, 14000 ± 140 (stat) Ξ^- and 11600 ± 126 (stat) $\bar{\Xi}^+$ reconstructed from the $d + Au$ data.

By combining every identified Ξ^- with every selected primary π^- to calculate the invariant mass, searches for the Ξ^{--} were performed in the $d + Au$ data. Invariant mass of $\Xi(1530)$ is calculated in a similar way. The resulting invariant

Applied cuts for Ξ^{--} search	
Track flag	> 0
Track nHits	≥ 15
Track nHits / nMax	≥ 0.55
π_1^- dE/dx	$-2.0 < n\sigma_\pi < 2.0$
π_2^-, π_3^- and proton dE/dx	$-4.0 < n\sigma < 4.0$
π_1^- global dca	≤ 1.5 cm
π_2^- global dca	≥ 1.0 cm
π_3^- global dca	≥ 2.5 cm
π_1^- momentum	0.1 GeV/c $\leq p\&p_t \leq$ 1.0 GeV/c
π_2^- momentum	0.1 GeV/c $\leq p\&p_t \leq$ 2.0 GeV/c
proton global dca	≥ 1.0 cm
Λ decay distance	≥ 5.0 cm
Λ dca to primary vertex	≥ 0.3 cm
Λ invariant mass	1.108 GeV/c^2 $\leq m_\Lambda \leq$ 1.122 GeV/c^2
Ξ^- invariant mass	1.31 GeV/c^2 $\leq m_{\Xi^-} \leq$ 1.33 GeV/c^2

Table 4.4: List of cuts used for the search of Ξ^{--}.

mass distributions are plotted in figure 4.13. Red histograms in the figure are from same event while black histograms are the background distributions calculated from event mixing. It can be seen that event mixing can represent the shape of the combinatorial background well.

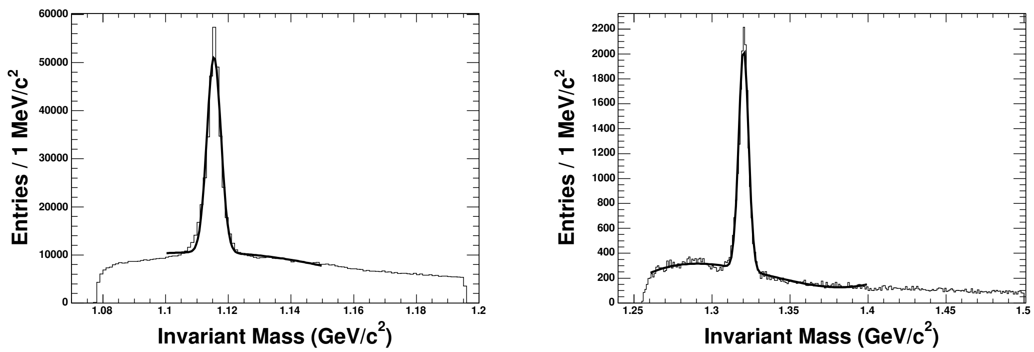

Figure 4.12: Λ (left plot) and Ξ^- (right plot) invariant mass distribution in $d+Au$ collisions.

The two left plots are the invariant mass distribution of $\Xi^-\pi^+$ and $\bar{\Xi}^+\pi^-$ respectively, where the $\Xi(1530)$ and $\bar{\Xi}(1530)$ peaks are clearly visible. There are 432 ± 87 (stat) $\Xi(1530)$ and 296 ± 83 (stat) $\bar{\Xi}(1530)$ identified from the $d + Au$ data. However, no signal is seen for the Ξ^{--} pentaquark at 1862 MeV/c^2, as seen in the $\Xi^-\pi^-$ and $\bar{\Xi}^+\pi^+$ invariant mass distributions in the two right plots.

We have not observed a siginificant Ξ^{--} pentaquark signal in our $d + Au$ collision data sample. However, the statistics are limited and a firm exclusion of Ξ^{--} production in $d + Au$ collisions at RHIC awaits a run with much higher statistics.

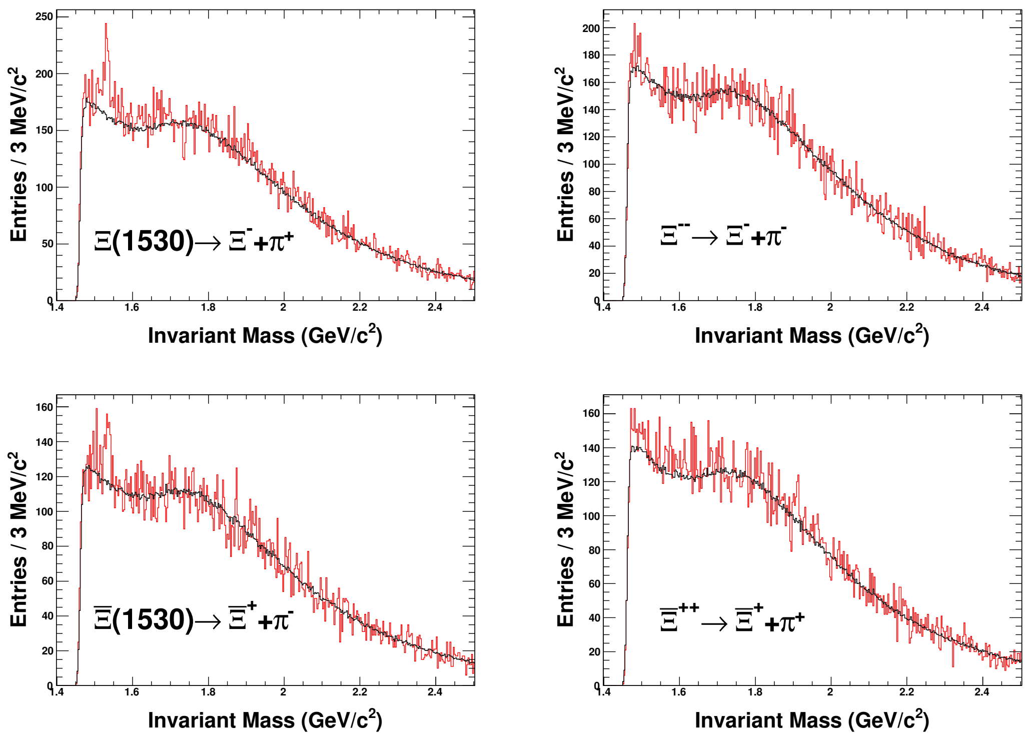

Figure 4.13: $\Xi\pi$ invariant mass distribution from both same event (red histograms) and mixed event (black histograms) in $d + Au$ collisions. Top left plot: $\Xi(1530)$ invariant mass distribution measured from the $\Xi^-\pi^+$ channel. Bottom left plot: $\bar{\Xi}(1530)$ invariant mass distribution measured from the $\bar{\Xi}^+\pi^-$ channel. Top right plot: Ξ^{--} invariant mass distribution measured from the $\Xi^-\pi^-$ channel. Bottom right plot: $\bar{\Xi}^{++}$ invariant mass distribution measured from the $\bar{\Xi}^+\pi^+$ channel.

CHAPTER 5

Conclusions and Outlooks

5.1 ϕ meson production at RHIC

We have successively measured ϕ meson production from its decay channel $\phi \rightarrow K^+K^-$ in $\sqrt{s_{NN}} = 200$ GeV $p+p$ and $Au+Au$ collisions from the STAR experiment at RHIC. Event mixing techniques have been used to calculate and subtract combinatorial background.

The measured mass and width of ϕ meson in 200 GeV $p+p$ and $Au+Au$ collisions are found to be consistent with the values listed by PDG. No obvious modification of the ϕ mass, width and line shape has been observed.

ϕ meson spectra are measured in 0-5%, 0-10%, 10-30%, 30-50%, 50-80% centrality bins of $Au+Au$ collisions and three multiplicity bins ($N_{ch} < 5$, $N_{ch} \geq 5$ and MinBias) of MinBias $p+p$ collisions. The spectra are found to be fitted well by a single exponential in $Au+Au$ collisions while in $p+p$ collisions, it's found that a double exponential function represents the data better. The change of spectra shape from $p+p$ to $Au+Au$ collisions may be due to the suppression of the high p_t tail in $Au+Au$ collisions.

The extracted yield for the ϕ meson increases with increasing multiplicity in $p+p$ collisions and collision centralities in $Au+Au$ collisions. The extracted ϕ yield agrees well with a thermal model fit, supporting the idea that a thermal equilibrated partonic stage has been reached in central $Au + Au$ collisions at RHIC.

The measured $\langle p_t \rangle$ of the ϕ meson is found to increase with increasing multiplicity in $p + p$ collisions, indicating increasing contributions from mini-jet in high multiplicity $p+p$ collisions. The $\langle p_t \rangle$ of ϕ is also found to increase with collision energy. However, ϕ $\langle p_t \rangle$ exhibits no significant variation with centralities in $Au + Au$ collisions.

Our measured yield ratio ϕ/K^- is consistent with the world measurement of this ratio at various energies and in very different systems. This ratio is also flat as a function of centrality in $Au+Au$ collisions, inconsistent with model calculations that assume ϕ production via coalescence of kaons in the final hadronic stage. The flat distribution of ϕ $\langle p_t \rangle$ as a function of centrality is also inconsistent with the predictions of kaon coalescence models. Both the ϕ/K^- yield ratio and ϕ $\langle p_t \rangle$ are predicted to increase as a function of centrality in the kaon coalescence picture. Our measurement effectively rules out kaon coalescence as the dominant production mechanism for the ϕ at RHIC.

A hydrodynamic model inspired blast wave fit to the spectra provides evidence that ϕ and Ω freeze out earlier than other ordinary hadrons such as π, K and p, consistent with speculation that multi-strange particles don't participate in hadronic rescatterings significantly. A comparison of the $\langle p_t \rangle$ distributions as a function of centrality for the ϕ and π, K and p also lends support for the earlier freeze out of ϕ, since the ϕ $\langle p_t \rangle$ is flat while the $\langle p_t \rangle$ of π, K and p increases as a function of centrality. If the ϕ does freeze out earlier than other hadrons, it will retain more information about the early stages of heavy ion collisions, being a clean probe for the hot matter produced at RHIC.

Nuclear modification factors R_{AA} and R_{CP} for ϕ meson are measured. The

R_{AA} for the ϕ is consistent with unity in the region of intermediate p_t, which indicates either that ϕ production is enhanced in $Au + Au$ collisions or that ϕ production is suppressed in $p + p$ collisions (for example, by the OZI rule). Comparison of the R_{CP} for the ϕ with that for the K_S^0 and Λ support the particle type (meson or baryon) dependence of hadron production in the intermediate p_t region as predicted by quark coalescence models. It provides direct evidence that a partonic state of matter has been produced in central $Au + Au$ collisions at RHIC.

Measurement of v_2 for the ϕ meson indicates that a significant amount of elliptic flow has been built up for the ϕ. Combined with the previous observation that the ϕ does not participate in final stage hadronic interaction, this indicated that the elliptic flow has been built up in early partonic stages. v_2 measurements for the ϕ meson will provide direct insight into the hot matter produced at RHIC.

STAR has accumulated much more data now. Systematic measurements of these data sets will provide energy and system size dependence of ϕ production and further investigate the ϕ production mechanisms in heavy ion collisions. Precise measurements of R_{AA}, R_{CP} and the elliptic flow parameter v_2 for the ϕ will ultimately pin down the scaling behavior of hadron production in the intermediate p_t region at RHIC, and provide more strict constraints for model calculations.

5.2 The search for penta-quark particles

We've searched for the Θ^{++} and Ξ^{--} pentaqurks in the STAR data. A comprehensive search for the $\Theta^{++} \to p + K^+$ pentaquark is done in available STAR data sets. It is observed that a clear peak structure is seen in $d + Au$ collisions at 200 GeV. The measured mass is 1528$\pm$2 MeV/c^2 and the Gaussian width is 6.5$\pm$0.5 MeV/c^2. Estimated significance of the peak is about 4.2 σ from a gaussian function fit. The observed peak structure is consistent with the production of pentaquark particle Θ^{++}. It seems that this peak structure is robust, that is, its existence persists when different cuts are applied. A signal for the anti-particle channel is also seen. The measured $\bar{\Theta}^{--}/\Theta^{++}$ yield ratio is found to be 0.78 ± 0.32 (stat), consistent with the anti-baryon to baryon ratio in this system.

In other collision systems, however, only weak signals are observed. The production rate of Θ^{++} across all collision systems is found to be consistent within error bars. The yield ratio $\Theta^{++}/\Lambda(1520)$ is approximately 5% in all systems.

No significant evidence for the Ξ^{--} pentaquark has been observed in $d + Au$ collisions at 200 GeV.

To either confirm or exclude the existence of such a Θ^{++} peak structure at RHIC energy, a high statistics $d + Au$ data sample is needed. A high statistics data run should help to resolve the ambiguities in the current measurements and help to resolve the puzzle of pentaquark particles.

In heavy ion collisions, overwhelming background is usually the biggest obstacle for the search of exotic particles. A better particle identification capability is desirable in STAR. The installation of a full coverage TOF detector will greatly help the PID and thus the search for pentaquarks in the future.

At this stage, the situation for the existence of pentaquark particles is not clear, from both experimental and theoretical stand points. It relies on the clarifications of different experimental results and awaits more precise measurements.

APPENDIX A

Kinematic Variables

In relativistic energies, new variables are necessary for convenience. The transverse momentum p_t is defined as

$$p_t \equiv \sqrt{p_x^2 + p_y^2}, \tag{A.1}$$

where p_x and p_y are the transverse components of the momentum.

Transverse mass/energy is defined by

$$m_t \equiv \sqrt{p_t^2 + m_0^2}, \tag{A.2}$$

where m_0 is the particle mass in its center of mass frame. So the transverse kinetic energy is $m_t - m_0$.

The dimensionless quantity rapidity (y) of a particle is defined by

$$y \equiv \frac{1}{2} \ln \left(\frac{E + p_z}{E - p_z} \right), \tag{A.3}$$

where E is the total energy of the particle. The rapidity of a particle is boost invariant, that is, it's additive by a constant under Lorentz transformations. In the non-relativistic limit, the rapidity of a particle travelling in the longitudinal direction is equal to the velocity of the particle in units of the speed of light.

The pseudo-rapidity (η) of a particle is used to characterize the emission of particle with respect to the beam direction and defined as

$$\eta \equiv -\ln[\tan(\theta/2)] = \frac{1}{2} \ln \left(\frac{|\vec{p}| + p_z}{|\vec{p}| - p_z} \right), \tag{A.4}$$

where θ is the angle between the particle momentum $\vec{p}$ and the beam axis. Note that to calculate η the particle type (mass) does not to be known. At high momentum $|\vec{p}| \approx E$ thus $\eta \approx y$.

References

[Abd04] M. Abdel-Bary et al. "Evidence for a narrow resonance at 1530 MeV/c^2 in the $K^0 p$ system of the reaction $pp \to \Sigma^+ K^0 p$ from the COSY-TOF experiment." *Phys. Lett.*, **B595**:127–134, 2004. hep-ex/0403011.

[Abe04] K. Abe et al. "Search for pentaquarks at Belle." 2004. hep-ex/0411005.

[Abe06] K. Abe et al. "Search for the $\Theta(1540)^+$ pentaquark using kaon secondary interactions at Belle." *Phys. Lett.*, **B632**:173–180, 2006. hep-ex/0507014.

[Abt04] I. Abt et al. "Limits for the central production of Θ^+ and Ξ^{--} pentaquarks in 920 GeV pA collisions." *Phys. Rev. Lett.*, **93**:212003, 2004. hep-ex/0408048.

[Ack03a] K. H. Ackermann et al. "The forward time projection chamber (FTPC) in STAR." *Nucl. Instrum. Meth.*, **A499**:713–719, 2003. nucl-ex/0211014.

[Ack03b] K. H. Ackermann et al. "STAR detector overview." *Nucl. Instrum. Meth.*, **A499**:624–632, 2003.

[Ada03] J. Adams et al. "Transverse momentum and collision energy dependence of high p_T hadron suppression in $Au + Au$ collisions at ultrarelativistic energies." *Phys. Rev. Lett.*, **91**:172302, 2003. nucl-ex/0305015.

[Ada04a] M. I. Adamovich et al. "Search for the exotic $\Xi^{--}(1860)$ resonance in 340 GeV/c $\Sigma-$nucleus interactions." *Phys. Rev.*, **C70**:022201, 2004. hep-ex/0405042.

[Ada04b] J. Adams et al. "Identified particle distributions in pp and $Au + Au$ collisions at $\sqrt{s_{NN}} = 200$ GeV." *Phys. Rev. Lett.*, **92**:112301, 2004. nucl-ex/0310004.

[Ada04c] J. Adams et al. "Multi-strange baryon production in $AuAu$ collisions at $\sqrt{s_{NN}} = 130$ GeV." *Phys. Rev. Lett.*, **92**:182301, 2004. nucl-ex/0307024.

[Ada04d] J. Adams et al. "Particle dependence of azimuthal anisotropy and nuclear modification of particle production at moderate p_T in $Au+Au$

collisions at $\sqrt{s_{NN}} = 200$ GeV." *Phys. Rev. Lett.*, **92**:052302, 2004. nucl-ex/0306007.

[Ada05a] J. Adams et al. "Azimuthal anisotropy in $Au + Au$ collisions at $\sqrt{s_{NN}} = 200$ GeV." *Phys. Rev.*, **C72**:014904, 2005. nucl-ex/0409033.

[Ada05b] J. Adams et al. "Experimental and theoretical challenges in the search for the quark gluon plasma: The STAR collaboration's critical assessment of the evidence from RHIC collisions." *Nucl. Phys.*, **A757**:102–183, 2005. nucl-ex/0501009.

[Ada05c] J. Adams et al. "Phi meson production in $Au + Au$ and $p + p$ collisions at $\sqrt{s_{NN}} = 200$ GeV." *Phys. Lett.*, **B612**:181–189, 2005. nucl-ex/0406003.

[ADK04] A. E. Asratyan, A. G. Dolgolenko, and M. A. Kubantsev. "Evidence for formation of a narrow $K^0_S p$ resonance with mass near 1533 MeV in neutrino interactions." *Phys. Atom. Nucl.*, **67**:682–687, 2004. hep-ex/0309042.

[Adl02a] C. Adler et al. "Centrality dependence of high p_T hadron suppression in $Au + Au$ collisions at $\sqrt{s_{NN}} = 130$ GeV." *Phys. Rev. Lett.*, **89**:202301, 2002. nucl-ex/0206011.

[Adl02b] C. Adler et al. "Midrapidity ϕ production in $Au + Au$ collisions at $\sqrt{s_{NN}} = 130$ GeV." *Phys. Rev.*, **C65**:041901, 2002.

[Adl03] S. S. Adler et al. "Scaling properties of proton and anti-proton production in $\sqrt{s_{NN}} = 200$ GeV $Au + Au$ collisions." *Phys. Rev. Lett.*, **91**:172301, 2003. nucl-ex/0305036.

[Adl04] C. Adler et al. "Kaon production and kaon to pion ratio in $Au + Au$ collisions at $\sqrt{s_{NN}} = 130$ GeV." *Phys. Lett.*, **B595**:143–150, 2004. nucl-ex/0206008.

[AER05] P. Zh. Aslanyan, V. N. Emelyanenko, and G. G. Rikhkvitzkaya. "Observation of $S = +1$ narrow resonances in the system $K^0_S p$ from $p + C_3H_8$ collision at 10 GeV/c." *Nucl. Phys.*, **A755**:375–378, 2005. hep-ex/0403044.

[Afa00] S. V. Afanasev et al. "Production of ϕ-mesons in $p + p$, $p + Pb$ and central $Pb + Pb$ collisions at E(beam) = 158 A GeV." *Phys. Lett.*, **B491**:59–66, 2000.

[Afa02] S. V. Afanasiev et al. "Energy dependence of pion and kaon production in central $Pb + Pb$ collisions." *Phys. Rev.*, **C66**:054902, 2002. nucl-ex/0205002.

[Ahl98] L. Ahle et al. "Kaon production in $Au + Au$ collisions at 11.6 A GeV/c." *Phys. Rev.*, **C58**:3523–3538, 1998.

[Air04] A. Airapetian et al. "Evidence for a narrow $|S| = 1$ baryon state at a mass of 1528 MeV in quasi-real photoproduction." *Phys. Lett.*, **B585**:213, 2004. hep-ex/0312044.

[Aki96] Y. Akiba et al. "Production of Phi mesons in central Si-28 + Au-196 collisions at 14.6 A GeV/c." *Phys. Rev. Lett.*, **76**:2021–2024, 1996.

[Akt04] A. Aktas et al. "Evidence for a narrow anti-charmed baryon state." *Phys. Lett.*, **B588**:17, 2004. hep-ex/0403017.

[Ale03] B. Alessandro et al. "phi production in Pb - Pb collisions at 158 GeV/c per nucleon incident momentum." *Phys. Lett.*, **B555**:147–155, 2003.

[Ale05] A. Aleev et al. "Observation of narrow baryon resonance decaying into pK^0_S in pA interactions at 70 GeV/c with SVD-2 setup." *Phys. Atom. Nucl.*, **68**:974–981, 2005. hep-ex/0401024.

[All03] C. E. Allgower et al. "The STAR endcap electromagnetic calorimeter." *Nucl. Instrum. Meth.*, **A499**:740–750, 2003.

[Alt04] C. Alt et al. "Observation of an exotic $S = -2$, $Q = -2$ baryon resonance in proton proton collisions at the CERN SPS." *Phys. Rev. Lett.*, **92**:042003, 2004. hep-ex/0310014.

[And03] M. Anderson et al. "The STAR time projection chamber: A unique tool for studying high multiplicity events at RHIC." *Nucl. Instrum. Meth.*, **A499**:659–678, 2003. nucl-ex/0301015.

[Ant04] Yu. M. Antipov et al. "Search for $\Theta(1540)^+$ in exclusive proton-induced reaction $p+C(N) \to \Theta^+\bar{K}_0+C(N)$ at the energy of 70 GeV." *Eur. Phys. J.*, **A21**:455–468, 2004. hep-ex/0407026.

[Arm05] Stephen R. Armstrong. "Pentaquark searches in electron positron annihilations and two-photon collisions at LEP." *Nucl. Phys. Proc. Suppl.*, **142**:364–369, 2005. hep-ex/0410080.

[ASW03] R. A. Arndt, I. I. Strakovsky, and R. L. Workman. "K^+ nucleon scattering and exotic $S = +1$ baryons." *Phys. Rev.*, **C68**:042201, 2003. nucl-th/0308012.

[Aub04a] B. Aubert et al. "Search for strange pentaquark production in e^+e^- annihilations at $\sqrt{s} = 10.58$ GeV and in $\Upsilon(4S)$ decays." 2004. hep-ex/0408064.

[Aub04b] B. Aubert et al. "A search for the $Theta^{*++}$ pentaquark in $B^\pm \to p\bar{p}K^\pm$." 2004. hep-ex/0408037.

[Bac04a] B. B. Back et al. "Production of Phi mesons in Au + Au collisions at 11.7 A GeV/c." *Phys. Rev.*, **C69**:054901, 2004. nucl-ex/0304017.

[Bac04b] B. B. Back et al. "Production of Phi mesons in Au + Au collisions at 11.7 A GeV/c." *Phys. Rev.*, **C69**:054901, 2004. nucl-ex/0304017.

[Bai04] J. Z. Bai et al. "Search for the pentaquark state in $\Psi(2S)$ and J/Ψ decays to $K^0_S pK^-\bar{n}$ and $K^0_S \bar{p}K^+n$." *Phys. Rev.*, **D70**:012004, 2004. hep-ex/0402012.

[Bar03a] V. V. Barmin et al. "Observation of a baryon resonance with positive strangeness in K^+ collisions with Xe nuclei." *Phys. Atom. Nucl.*, **66**:1715–1718, 2003. hep-ex/0304040.

[Bar03b] J. Barth et al. "Observation of the positive-strangeness pentaquark Θ^+ in photoproduction with the SAPHIR detector at ELSA." *Phys. Lett.*, **B572**:127–132, 2003. hep-ex/0307083.

[Bas99] S. A. Bass et al. "Hadronic freeze-out following a first order hadronization phase transition in ultrarelativistic heavy-ion collisions." *Phys. Rev.*, **C60**:021902, 1999. nucl-th/9902062.

[Bat06] M. Battaglieri et al. "Search for $\Theta(1540)^+$ pentaquark in high statistics measurement of $\gamma p \to \bar{K}_0 K^+ n$ at CLAS." *Phys. Rev. Lett.*, **96**:042001, 2006. hep-ex/0510061.

[BD00] S. A. Bass and A. Dumitru. "Dynamics of hot bulk QCD matter: From the quark-gluon plasma to hadronic freeze-out." *Phys. Rev.*, **C61**:064909, 2000. nucl-th/0001033.

[Bed03] M. Beddo et al. "The STAR barrel electromagnetic calorimeter." *Nucl. Instrum. Meth.*, **A499**:725–739, 2003.

[Bel03] R. Bellwied et al. "The STAR silicon vertex tracker: A large area silicon drift detector." *Nucl. Instrum. Meth.*, **A499**:640–651, 2003.

[BGP97] Abhijit Bhattacharyya, Sanjay K. Ghosh, S. C. Phatak, and Sibaji Raha. "In-medium effects on the phi meson." *Phys. Rev.*, **C55**:1463–1466, 1997. nucl-th/9602042.

[Bie03] F. S. Bieser et al. "The STAR trigger." *Nucl. Instrum. Meth.*, **A499**:766–777, 2003.

[Ble99] M. Bleicher et al. "Relativistic hadron hadron collisions in the ultra-relativistic quantum molecular dynamics model." *J. Phys.*, **G25**:1859–1896, 1999. hep-ph/9909407.

[Bra03] A. Braem et al. "Identification of high p_T particles with the STAR-RICH detector." *Nucl. Instrum. Meth.*, **A499**:720–724, 2003.

[Bur05] Volker D. Burkert. "Have pentaquark states been seen?" 2005. hep-ph/0510309.

[Che04] S. Chekanov et al. "Evidence for a narrow baryonic state decaying to $K^0_S p$ and $K^0_S \bar{p}$ in deep inelastic scattering at HERA." *Phys. Lett.*, **B591**:7–22, 2004. hep-ex/0403051.

[CLL03] Y. Cheng, F. Liu, Z. Liu, K. Schweda, and N. Xu. "Transverse expansion in Au-197+Au-197 collisions at RHIC." *Phys. Rev.*, **C68**:034910, 2003.

[CPR03] Simon Capstick, Philip R. Page, and Winston Roberts. "Interpretation of the Θ^+ as an isotensor resonance with weakly decaying partners." *Phys. Lett.*, **B570**:185–190, 2003. hep-ph/0307019.

[CT04] Robert N. Cahn and George H. Trilling. "Experimental limits on the width of the reported $\Theta(1540)^+$." *Phys. Rev.*, **D69**:011501, 2004. hep-ph/0311245.

[CV03] D. Cabrera and M. J. Vicente Vacas. "Phi meson mass and decay width in nuclear matter." *Phys. Rev.*, **C67**:045203, 2003. nucl-th/0205075.

[Dan05] Michael Danilov. "Experimental review on pentaquarks." 2005. hep-ex/0509012.

[DBB99] A. Dumitru, S. A. Bass, M. Bleicher, Horst Stoecker, and W. Greiner. "Direct emission of multiple strange baryons in ultrarelativistic heavy-ion collisions from the phase boundary." *Phys. Lett.*, **B460**:411–416, 1999. nucl-th/9901046.

[DFN84] D. Drijard, H. G. Fischer, and T. Nakada. "Study of event mixing and its application to the extraction of resonance signals." *Nucl. Inst. Meth. in Phys. Res.*, **A225**:367, 1984.

[DH77] K. P. Das and Rudolph C. Hwa. "QUARK - ANTI-QUARK RECOMBINATION IN THE FRAGMENTATION REGION." *Phys. Lett.*, **B68**:459, 1977.

[DPP97] Dmitri Diakonov, Victor Petrov, and Maxim V. Polyakov. "Exotic anti-decuplet of baryons: Prediction from chiral solitons." *Z. Phys.*, **A359**:305–314, 1997. hep-ph/9703373.

[Eid04] S. Eidelman et al. "Review of particle physics." *Phys. Lett.*, **B592**:1, 2004.

[FMN03a] R. J. Fries, B. Muller, C. Nonaka, and S. A. Bass. "Hadron production in heavy ion collisions: Fragmentation and recombination from a dense parton phase." *Phys. Rev.*, **C68**:044902, 2003. nucl-th/0306027.

[FMN03b] R. J. Fries, B. Muller, C. Nonaka, and S. A. Bass. "Hadronization in heavy ion collisions: Recombination and fragmentation of partons." *Phys. Rev. Lett.*, **90**:202303, 2003. nucl-th/0301087.

[GKL03] V. Greco, C. M. Ko, and P. Levai. "Parton coalescence at RHIC." *Phys. Rev.*, **C68**:034904, 2003. nucl-th/0305024.

[Gor04] Igor V. Gorelov. "Pentaquark searches at CDF." 2004. hep-ex/0408025.

[Hag05] Kevin L. Haglin. "Phi meson propagation and decay at finite temperature." *Acta Phys. Hung.*, **A24**:283–289, 2005. nucl-th/0404069.

[Hic05a] K. H. Hicks. "Search for the Θ^+ in photoproduction on the deuteron." 2005. hep-ex/0510067.

[Hic05b] Kenneth H. Hicks. "Experimental search for pentaquarks." *Prog. Part. Nucl. Phys.*, **55**:647–676, 2005. hep-ex/0504027.

[HK03] J. Haidenbauer and G. Krein. “Influence of a $Z(1540)^+$ resonance on K^+N scattering.” *Phys. Rev.*, **C68**:052201, 2003. hep-ph/0309243.

[HKH01] P. Huovinen, P. F. Kolb, Ulrich W. Heinz, P. V. Ruuskanen, and S. A. Voloshin. “Radial and elliptic flow at RHIC: Further predictions.” *Phys. Lett.*, **B503**:58–64, 2001. hep-ph/0101136.

[HM96] John W. Harris and Berndt Muller. “The search for the quark-gluon plasma.” *Ann. Rev. Nucl. Part. Sci.*, **46**:71–107, 1996. hep-ph/9602235.

[HSX98] H. van Hecke, H. Sorge, and N. Xu. “Evidence of early multi-strange hadron freezeout in high energy nuclear collisions.” *Phys. Rev. Lett.*, **81**:5764–5767, 1998. nucl-th/9804035.

[HY03] Rudolph C. Hwa and C. B. Yang. “Scaling distributions of quarks, mesons and proton for all p_T, energy and centrality.” *Phys. Rev.*, **C67**:064902, 2003. nucl-th/0302006.

[IOS66] Jugoro Iizuka, Kunihiko Okada, and Okiyasu Shito. “Systematics and phenomenology of boson mass levels. 3.” *Prog. Theor. Phys.*, **35**:1061–1073, 1966.

[JM04] Byron K. Jennings and Kim Maltman. “Z^* resonances: Phenomenology and models.” *Phys. Rev.*, **D69**:094020, 2004. hep-ph/0308286.

[Jue05] H. G. Juengst. “Search for a Θ^{++} pentaquark state.” *Nucl. Phys.*, **A754**:265–271, 2005. nucl-ex/0312019.

[JW03] Robert L. Jaffe and Frank Wilczek. “Diquarks and exotic spectroscopy.” *Phys. Rev. Lett.*, **91**:232003, 2003. hep-ph/0307341.

[Kar02] Frithjof Karsch. “Lattice QCD at high temperature and density.” *Lect. Notes Phys.*, **583**:209–249, 2002. hep-lat/0106019.

[Kar04] Uri Karshon. “Study of narrow baryonic pentaquark candidates with the ZEUS detector at HERA.” 2004. hep-ex/0410029.

[KL03] Marek Karliner and Harry J. Lipkin. “The constituent quark model revisited: Quark masses, new predictions for hadron masses and KN pentaquark.” 2003. hep-ph/0307243.

[KLP00] F. Karsch, E. Laermann, and A. Peikert. “The pressure in 2, 2+1 and 3 flavour QCD.” *Phys. Lett.*, **B478**:447–455, 2000. hep-lat/0002003.

[KMR86] P. Koch, B. Muller, and J. Rafelski. "STRANGENESS IN RELATIVISTIC HEAVY ION COLLISIONS." *Phys. Rept.*, **142**:167–262, 1986.

[Kub04] V. Kubarovsky et al. "Observation of an exotic baryon with $S = +1$ in photoproduction from the proton." *Phys. Rev. Lett.*, **92**:032001, 2004. hep-ex/0311046.

[KZZ04] K. T. Knopfle, M. Zavertyaev, and T. Zivko. "Search for Θ^+ and $\Xi(3/2)^{--}$ pentaquarks in HERA-B." *J. Phys.*, **G30**:S1363–S1366, 2004. hep-ex/0403020.

[Lan03] J. M. Landgraf et al. "An overview of the STAR DAQ system." *Nucl. Instrum. Meth.*, **A499**:762–765, 2003.

[LH94] D. L'Hote. "About resonance signal extraction from multiparticle data: combinatorics ane event mixing methods." *Nucl. Inst. Meth. in Phys. Res.*, **A337**:544, 1994.

[Lit05] Dmitry O. Litvintsev. "Pentaquark searches at CDF." *Nucl. Phys. Proc. Suppl.*, **142**:374–377, 2005. hep-ex/0410024.

[LK02] Zi-wei Lin and C. M. Ko. "Flavor ordering of elliptic flows at high transverse momentum." *Phys. Rev. Lett.*, **89**:202302, 2002. nucl-th/0207014.

[LM05] Keh-Fei Liu and Nilmani Mathur. "A review of pentaquark calculations on the lattice." 2005. hep-lat/0510036.

[Lon02] H. Long. "Mid-rapidity Lambda and Lambda-bar Production in $Au+Au$ Collisions at the Relativistic Heavy Ion Collider." *Ph.D. Thesis, University of California - Los Angeles*, 2002. unpublished.

[Lon04] M. J. Longo et al. "High statistics search for the $\Theta^+(1.54)$ pentaquark." *Phys. Rev.*, **D70**:111101, 2004. hep-ex/0410027.

[MV03] Denes Molnar and Sergei A. Voloshin. "Elliptic flow at large transverse momenta from quark coalescence." *Phys. Rev. Lett.*, **91**:092301, 2003. nucl-th/0302014.

[Nak03] T. Nakano et al. "Observation of $S = +1$ baryon resonance in photoproduction from neutron." *Phys. Rev. Lett.*, **91**:012002, 2003. hep-ex/0301020.

[NCW04] J. Napolitano, J. Cummings, and M. Witkowski. "Search for $\Theta(1540)^+$ in the reaction $K^+p \to K^+n\pi^+$ at 11 GeV/c." 2004. hep-ex/0412031.

[NFB04] Chiho Nonaka, Rainer J. Fries, and Steffen A. Bass. "Elliptic flow of multi-strange particles: Fragmentation, recombination and hydrodynamics." *Phys. Lett.*, **B583**:73–78, 2004. nucl-th/0308051.

[Nus03] S. Nussinov. "Some comments on the putative $\Theta^+(1543)$ exotic state." 2003. hep-ph/0307357.

[Oka04] Makoto Oka. "Theoretical overview of the pentaquark baryons." *Prog. Theor. Phys.*, **112**:1–19, 2004. hep-ph/0406211.

[Oku63] S. Okubo. "Phi meson and unitary symmetry model." *Phys. Lett.*, **5**:165–168, 1963.

[Pin04] Christopher Pinkenburg. "Search for the $\bar{\Theta}^- \to K^-\bar{n}$ with PHENIX." *J. Phys.*, **G30**:S1201–S1206, 2004. nucl-ex/0404001.

[PKL02] Subrata Pal, C. M. Ko, and Zi-wei Lin. "Phi meson production in relativistic heavy ion collisions." *Nucl. Phys.*, **A707**:525–539, 2002. nucl-th/0202086.

[PV98] Arthur M. Poskanzer and S. A. Voloshin. "Methods for analyzing anisotropic flow in relativistic nuclear collisions." *Phys. Rev.*, **C58**:1671–1678, 1998. nucl-ex/9805001.

[Raf84] Johann Rafelski. "STRANGENESS PRODUCTION IN THE QUARK GLUON PLASMA." *Nucl. Phys.*, **A418**:215c–235c, 1984.

[RHI] For more information, visit http://www.bnl.gov/rhic.

[RM82] Johann Rafelski and Berndt Muller. "STRANGENESS PRODUCTION IN THE QUARK - GLUON PLASMA." *Phys. Rev. Lett.*, **48**:1066, 1982.

[Sch96] Michael Schmelling. "Status of the strong coupling constant." 1996. hep-ex/9701002.

[Sch04] S. Schael et al. "Search for pentaquark states in Z decays." *Phys. Lett.*, **B599**:1–16, 2004.

[Sho85] A. Shor. "PHI MESON PRODUCTION AS A PROBE OF THE QUARK GLUON PLASMA." *Phys. Rev. Lett.*, **54**:1122–1125, 1985.

[Sor95] H. Sorge. "Flavor Production in Pb(160 A GeV) on Pb Collisions: Effect of Color Ropes and Hadronic Rescattering." *Phys. Rev.*, **C52**:3291–3314, 1995. nucl-th/9509007.

[Sor99] H. Sorge. "Highly sensitive centrality dependence of elliptic flow: A novel signature of the phase transition in QCD." *Phys. Rev. Lett.*, **82**:2048–2051, 1999. nucl-th/9812057.

[SR03] Fl. Stancu and D. O. Riska. "Stable $uudd\bar{s}$ pentaquarks in the constituent quark model." *Phys. Lett.*, **B575**:242–248, 2003. hep-ph/0307010.

[STA] STAR internal communication.

[Ste03] S. Stepanyan et al. "Observation of an exotic $S = +1$ baryon in exclusive photoproduction from the deuteron." *Phys. Rev. Lett.*, **91**:252001, 2003. hep-ex/0307018.

[Ste05] Kevin Stenson. "Pentaquark searches at FOCUS." *Int. J. Mod. Phys.*, **A20**:3745–3748, 2005. hep-ex/0412021.

[Sto82] Horst Stocker et al. "JETS OF NUCLEAR MATTER FROM HIGH-ENERGY HEAVY ION COLLISIONS." *Phys. Rev.*, **C25**:1873–1876, 1982.

[Tro] Yu. A. Troyan et al. "The search and study of the baryonic resonances with the strangeness $S = +1$ in the system of nK^+ from the reaction $np \to npK^+K^-$ at the momentum of incident neutrons $P_n = (5.20 \pm 0.12)$ GeV/c." hep-ex/0404003.

[Wil00] Frank Wilczek. "QCD made simple." *Phys. Today*, **53N8**:22–28, 2000.

[Yam01] E. Yamamoto. "Phi Meson Production in Au+Au collisions at the Relativistic Heavy Ion Collider." *Ph.D. Thesis, University of California - Los Angeles*, 2001. unpublished.

[Zhu03] Shi-Lin Zhu. "Understanding pentaquark states in QCD." *Phys. Rev. Lett.*, **91**:232002, 2003. hep-ph/0307345.

[Zhu04] Shi-Lin Zhu. "Pentaquarks." *Int. J. Mod. Phys.*, **A19**:3439–3469, 2004. hep-ph/0406204.

[Zwe64] G. Zweig. *CERN Report Nos. TH-401 and TH-412*, 1964. unpublished.